



Massachusetts
Institute of
Technology



POLITECNICO DI TORINO

MASTER'S THESIS

**Development of a 3D-bioprinted
Neuronal Network as a Reliable In Vitro
Platform for the Study of
Neurodegenerative Diseases**

Author:

Giulio ZORZI

Supervisors:

Prof. Fabrizio PIRRI

Dr. Giancarlo CANAVESE

Advisors:

Prof. Ali KHADEMHOSEINI

Dr. Su Ryon SHIN

Collaborator:

Dr. Marie Engelene OBIEN

*A thesis submitted in fulfillment of the requirements
for the degree of Master of Science*

in

Nanotechnologies for ICTs
Department of Electronics and Telecommunications

February 26, 2018

Politecnico di Torino

Abstract

Faculty of Engineering
Department of Electronics and Telecommunications

Master of Science

Development of a 3D-bioprinted Neuronal Network as a Reliable In Vitro Platform for the Study of Neurodegenerative Diseases

by Giulio ZORZI

Reproducing the important features of the three-dimension (3D) brain environments such as cell-cell contact and interactions *in vitro* is important to provide a reliable drug testing platform for brain diseases. In this work, a 3D artificial brain construct with neural cellular features is developed with embedded printing technology. Bio-compatible materials are used as a supporting gel and a bioink, and free-standing astrocyte- and neuron-laden structures with brain-like stiffness, neurite structures, and astrocyte-neuron interactions are printed. The brain-like construct not only can reproduce the neurotransmitter synthetic mechanism between astrocyte and neuron (i.e. Glutamate synthesis) but also recapitulate the transition of neurotransmitter by synaptic functions of neuron. Finally, the potential use of this brain-like construct as an *in vitro* model for drug testing that can achieve the goal of providing a reliable and highly-reproducible platform for drug screening for the treatment of brain diseases is discussed.

Politecnico di Torino

Sommario

Faculty of Engineering
Department of Electronics and Telecommunications

Master of Science

Development of a 3D-bioprinted Neuronal Network as a Reliable In Vitro Platform for the Study of Neurodegenerative Diseases

by Giulio ZORZI

La riproduzione accurata *in vitro* delle caratteristiche fondamentali dell'ambiente tridimensionale (3D) del cervello, come il contatto e le interazioni tra cellule, è importante per fornire una piattaforma affidabile per la sperimentazione dei farmaci per le malattie neurodegenerative. In questo lavoro viene sviluppato un costrutto artificiale 3D riprodotto le funzioni delle cellule neurali mediante tecnologia di stampa incorporata. Materiali biocompatibili vengono utilizzati come gel di supporto e per la creazione di inchiostri contenenti cellule, e con essi vengono stampate strutture in grado di auto-sostenersi contenenti astrociti e neuroni, replicanti in modo accurato la rigidità cerebrale, le strutture delle neuriti, e le interazioni astrociti-neuroni. Questa struttura replicante il cervello non solo può riprodurre il meccanismo di neurotrasmissione tra astrociti e neuroni (per esempio, la sintesi di glutammato), ma anche ricapitolare i meccanismi regolanti le funzioni sinaptiche (regolamentazione dell'ambiente extracellulare durante la neurotrasmissione). Infine, viene discusso il potenziale utilizzo di questa piattaforma come un modello *in vitro* affidabile e altamente riproducibile per il test di medicinali per il trattamento delle malattie cerebrali.

Politecnico di Torino

Résumé

Faculty of Engineering
Department of Electronics and Telecommunications

Master of Science

Development of a 3D-bioprinted Neuronal Network as a Reliable In Vitro Platform for the Study of Neurodegenerative Diseases

by Giulio ZORZI

La reproduction *in vitro* des caractéristiques importantes des environnements cérébrales à trois dimensions (3D) tels que le contact cellulaire et les interactions est importante pour fournir une plate-forme de test de drogue fiable pour les maladies du cerveau. Dans ce travail, une construction de cerveau artificiel 3D avec des fonctions neuronales cellulaires par une technologie d'impression intégrée est développée. Des matériaux biocompatibles sont utilisés comme gel de support et bioink, et des structures d'astrocytes et de cellules neuronales avec une rigidité, des structures de neurites et des interactions astrocytes-neurones semblable à cela cérébrale sont imprimées. La construction non seulement peut reproduire le mécanisme synthétique des neurotransmetteurs entre les astrocytes et le neurone (c'est-à-dire la synthèse du glutamate), mais aussi récapituler la transition du neurotransmetteur par les fonctions synaptiques du neurone. Enfin, on discute de l'utilisation potentielle de cette construction semblable au cerveau en tant que modèle *in vitro* pour les tests de dépistage de drogues qui peut atteindre l'objectif de fournir une plate-forme fiable et hautement reproductible pour le dépistage de médicaments pour le traitement des maladies cérébrales.

Acknowledgements

Foremost, I would like to thank Prof. Ali Khademhosseini, head of Khademhosseini lab, for giving me the opportunity of working in the stimulating environment of the Harvard-MIT Division of Health Sciences and Technology, and most of all on a project I deeply cared about.

I am very thankful to my instructor, Dr. Su Ryon Shin, who was always a true support and helped me throughout all the difficult steps of the project, to Dr. Yi-Chen Li, for being the mentor everyone would want to have and for letting me discover yet another wonderful aspect of Neuroscience, and to Roya, for sharing the joys and the trivial parts of the project with me and for being a constant support.

I am also extremely grateful for the collaboration with Dr. Marie Engelen Obien from the Bio Engineering laboratory of ETH-Zurich, who always gave valuable advices for the development of the project and, together with Dr. Michele Fiscella, took the time off of their extremely busy schedule to perform the electrical characterization of our 3D neuronal network.

My very special thanks go to Shirin, for sharing with me all the crazy early morning and late night shifts in the lab, the scavenger hunts around the shelves looking for syringe pumps, a dangerously high number of coffees, and all the good times in and around Boston; to Anne-Marie and Victoria, for all the fun experiences, the unforgettable moments together, and for always being "presibene"; to Chiara, Amir, Maik, Melvin, Edoardo, Andrea, Alessandro, Sasha, Brett, and Wesley, for being the best friends and colleagues one could wish for; to Marcello and Marco, the most amazing roommates Boston has ever had the pleasure to host.

Finally, I would like to thank my family and Chiara. None of this could have been possible without all your love and support.

Contents

Acknowledgements	ix
1 Introduction	1
1.1 Cell cultures: 2D models vs 3D models	2
1.1.1 Morphology	3
1.1.2 Differentiation	3
1.1.3 Viability	4
1.1.4 Response to stimuli	4
1.1.5 Drug metabolism	4
1.1.6 Gene expression and protein synthesis	4
1.1.7 <i>In vivo</i> relevance	5
1.1.8 Proliferation	5
1.2 Current methods for 3D cell culturing	5
1.2.1 Hanging-drop method	5
1.2.2 Forced-floating method	6
1.2.3 Matrices and scaffolds	6
1.2.4 Agitation-based approaches	7
1.2.5 Limitations	7
1.3 3D bioprinting	8
1.3.1 3D bioprinting approaches	8
Biomimicry	8
Autonomous self-assembly	8
Mini-tissues	8
1.3.2 Bioprinting techniques	9
Extrusion-based	9
Droplet-based	9
Laser-based	10
1.3.3 Materials	10
Printability	11
Biocompatibility	11
Degradation kinetics and byproducts	12
Structural and mechanical properties	12
Material biomimicry	12
1.3.4 Cell sources	13
1.4 Co-culture systems	15

2	Theory	17
2.1	Neurons and glial cells	17
2.2	Synapses and neurotransmission	19
2.2.1	Chemical transmission	19
2.2.2	Electrical transmission	20
2.2.3	Extracellular recordings: Multi-electrode arrays	21
2.3	Astrocytes as neurotransmission regulators	21
2.4	Neural stem cells differentiation	22
3	Materials and methods	25
3.1	Gelatin Methacrylate (GelMA) synthesis	25
3.2	Cell culturing protocols	26
3.2.1	3T3, MCF-7	26
3.2.2	PC12	28
3.2.3	Astrocytes	28
3.2.4	NE-4C	29
3.3	GelMA solution and supporting bath	30
3.4	Biopinks	30
3.4.1	5%wt gelatine, 2%wt alginate	31
3.4.2	1%wt alginate	31
3.4.3	7%wt GelMA High Methacrylation (MA), 5mg/ml multi-walled carboxylic acid functionalized carbon nanotubes (MWCNT-COOH), 0.5%wt PI	31
	Synthesis of MWCNT stock solution (4 ml)	32
	Ink synthesis	32
3.5	Bioprinting	32
3.5.1	Printing strategy	32
3.6	Samples culturing protocols	34
3.7	Imaging	34
3.7.1	Fluorescence microscopy	36
3.7.2	Confocal microscopy	36
	Immunostaining: Alexa Fluor 488 phalloidin [®] /Alexa Fluor 594 phalloidin [®] / 4',6-Diamidino-2-phenylindole di- hydrochloride (DAPI)	36
	Ethidium homodimer-1 (EthD-1)/Calcein acetoxymethyl ester (Calcein/ acetoxymethyl (AM))	38
	Localization of glial fibrillary acidic protein (GFAP) and beta- III tubulin	38
3.8	Samples and processes characterization	39
3.8.1	Mechanical tests	39
3.8.2	Cell viability assays	40
	Live/Dead [™]	40

3.8.3	Cell proliferation assays	40
	PrestoBlue™	40
3.8.4	Electrical characterization	41
4	Results	43
4.1	Tests for 2D cultures	43
4.1.1	Astrocytes expression	43
4.1.2	PC12 differentiation	44
4.1.3	NE-4C differentiation	44
4.2	Recreating the brain environment	45
4.2.1	Optimization of mechanical properties and printability	45
	GelMA concentration in the bath	46
4.2.2	Self-healing and shear-thinning behavior	47
	Degradation tests	49
	Bioinks printability tests	49
	Optimization of printed fibers	50
4.2.3	3T3 and MCF-7: fine-tuning for cell encapsulation	51
4.2.4	Astrocytes encapsulation	52
4.2.5	3T3: fine-tuning of bioink	54
4.2.6	Full structure development	55
4.3	Electrical mapping of a 3D neuronal network	56
4.3.1	Preliminary results	56
5	Conclusion and future work	65
5.1	Future work	65
A	Supporting information	69
A.1	GelMA concentration	69
A.2	The effect of CaCl ₂ on shear-thinning behavior	69
A.3	Bioink testing	70
A.4	Astrocytes viability for different UV exposure times	70
	Bibliography	77

List of Figures

1.1	A Astrocytes-neurons interaction at the synapses level in the brain. B Astrocytes as regulators of the glutamate-glutamine cycle: during neurotransmission, glutamate produced by the pre-synaptic cell (1) is secreted into the synaptic cleft and interacts with the post-synaptic cell receptors (2). Astrocytes rapidly remove synaptically released glutamate, converting it into the amino acid glutamine by the enzyme glutamine synthetase (3a), and avoid excitotoxic damage of the cells. Glutamate uptake increases the calcium (Ca^{2+}) intracellular concentration in astrocytes (3b), which triggers the release of glutamine into the extracellular space (4). Glutamine is then taken up by neurons, providing the necessary substrate for the synthesis of glutamate (5). C The engineered 3D co-cultured brain like tissue construct. Astrocytes (green) and neurons (purple) interact at the interface of the printed fibers.	2
1.2	Current methods for 3D cell culturing. (Adapted from [32])	6
2.1	Structure of a neuron and glial cells. (Credit: NIH/National Institute of Neurological Disorders and Stroke (NINDS))	17
2.2	Schematic layout depicting the spatial relationship between the neuronal cell and the substrate-integrated electrode. (Adapted from [98])	21
2.3	Differentiation of neural stem cells into neurons, astrocytes, and oligodendrocytes. (Credit: Sigma-Aldrich)	23
3.1	The final product: 50 Falcon tubes of GelMA were produced. The same batch of GelMA was used throughout the six months of experiments to minimize variability in the results.	27
3.2	PDMS molds containing the uncured GelMA solution.	33
3.3	One of the structures after removal from the mold: in this particular case, full crosslinking could not be obtained, as it can be evinced by the dark-purple color that characterize the middle section of the cube.	35
3.4	A fully-cured structure, distinguishable by the full transparency of its texture.	36
3.5	The setup for mechanical testing. The structures were loaded between the two sections, and compressive tests were carried out.	40
3.6	The HD-MEAs provided by Maxwell Biosystems.	42

4.1	GFAP-staining of astrocytes isolated from 1-day-old rat brains (P1) at confluency.	43
4.2	PC12 cultured on fibronectin-coated TCPS after 7 days of incubation. Green: neuron-specific mouse anti-beta-III tubulin; blue: DAPI. The long strands are neurites extending out of the cell bodies.	44
4.3	Evolution of NE-4C culture exposed to MEM (Day 4, 7, 10, 13).	45
4.4	Evolution of NE-4C culture exposed to DMEM (Day 4, 7, 10, 13).	45
4.5	Evolution of NE-4C culture exposed to DMEM + 10% FBS (Day 4, 7, 10, 13).	45
4.6	Evolution of NE-4C culture exposed to MEM + retinoic acid (Day 4, 7, 10, 13).	46
4.7	Evolution of NE-4C culture exposed to DMEM + retinoic acid (Day 4, 7, 10, 13).	46
4.8	Evolution of NE-4C culture exposed to MEM + 10% FBS + retinoic acid (Day 4, 7, 10, 13).	46
4.9	Evolution of NE-4C culture exposed to DMEM + 10% FBS + retinoic acid (Day 4, 7, 10, 13).	46
4.10	NE-4C differentiation: astrocytes star-like shape on day 7 after introduction of FBS.	47
4.11	NE-4C differentiation: neurites outgrowth on day 10 after exposure to retinoic acid in DMEM.	48
4.12	The chemical GelMA gel formation behaviors of GelMA solutions with different concentrations by treatment with various UV exposure times.	49
4.13	Compressive modulus of GelMA for different GelMA concentration.	50
4.14	Oscillatory stress model shows the storage modulus (G') of the 5%wt GelMA bath is higher than that of the bioinks. This property is what allows to maintain the fiber structure after printing.	51
4.15	Fluorescence pictures of bioinks with fluorescent dye. The constructs (three, six, eight, and twelve branches) show the printing ability of the bioprinter.	52
4.16	Self-healing behavior of GelMA: after scratching the surface of the printed bath with the bioprinter needle, the structure was left in the incubator for 24 hours, taking pictures at precise time-points. As it can be observed, full recovery from the scratch was obtained, proving the self-healing properties of the material.	52
4.17	The samples were scratched with a needle, performing a horizontal cut with the bioprinter nozzle.	53
4.18	The continuous flow ramp model shows that 5%wt physical GelMA hydrogels have a rapid hydrogel transition from gel-like to fluid-like behavior, with a shear-thinning ability for nozzle moving.	54

4.19	Oscillatory strain sweep between low (1%) and high (250%) strain shows the rapid self-healing ability of 5%wt physical GelMA hydrogel during the printing process.	55
4.20	The degradation behaviors of 5%wt GelMA supporting hydrogel after 7 and 14 days of incubation.	56
4.21	Oscillatory strain sweep between low (1%) and high (250%) strain shows a rapid transition of bioink from gel-like to fluid-like behavior, necessary for localization of extruded bioinks. It indicates that the 5%wt gelatin/2%wt alginate-based bioinks were printable.	57
4.22	Visualization of the fiber continuity and quantification of the fiber diameter and the circularity of printed fibers for 27G nozzle.	58
4.23	Visualization of the fiber continuity and quantification of the fiber diameter and the circularity of printed fibers for 30G nozzle. The fibers printed by 30 G nozzle at a printing rate of 3 μ l/min and with a nozzle moving rate of 2 mm/s could get the minimal diameter and obtain a fiber cross-section aspect ratio close to the one of a circle.	59
4.24	3T3 cells spreading in the supporting bath. 5%wt GelMA, 0.25%wt PI , 800 mW/cm ² UV power, 5 cm distance from source, 60s total UV exposure time, 8 million/ml cells (day 7). From the left: only Alexa Fluor 594 phalloidin [®] staining to observe cellular strands more accurately, then Alexa Fluor 594 phalloidin [®] / DAPI staining to include visualization of cell nuclei.	59
4.25	MCF-7 cells forming colonies in the supporting bath. 5%wt GelMA, 0.25%wt PI , 800 mW/cm ² UV power, 5 cm distance from source, 60s total UV exposure time, 8 million/ml cells (day 7). Alexa Fluor 488 phalloidin [®] / DAPI staining. The first two images are taken at different planes of focus to stress the fact that the cells were not in a 2D flat surface, but encapsulated in a 3D environment.	60
4.26	The morphologies of astrocyte in the 3.5%wt, 5%wt, and 7%wt GelMA gel with different UV exposed time after 14 days of incubation. It shows that the astrocytes could fully migrate and extend in 5%wt chemical GelMA hydrogel under 80 second of UV exposure time. . . .	60
4.27	Live/Dead [™] assay for 80 s UV exposure time and cell viability of astrocytes in the 5%wt GelMA supporting gel after UV treatment. . . .	61
4.28	The cell viability and morphologies of astrocytes in the 5% GelMA supporting gel after 7 and 14 days of incubation. Figure shows that astrocytes could maintain a high viability, extend and form a network in the 5%wt GelMA supporting gel.	61
4.29	3T3 cells encapsulated in 5%wt gelatin/2%wt alginate ink at treatment of 70 s UV after 7 days of incubation.	62
4.30	3T3 cells encapsulated in 5%wt gelatin/2%wt alginate ink at treatment of 80 s UV after 7 days of incubation.	62

4.31	3T3 cells encapsulated in 5%wt gelatin/2%wt alginate ink at treatment of 70 s UV after 14 days of incubation.	63
4.32	3T3 cells encapsulated in 5%wt gelatin/2%wt alginate ink at treatment of 80 s UV after 14 days of incubation.	63
4.33	From top to bottom: co-cultures of astrocytes and PC12 cells in the absence (top) and presence (middle) of MWCNT, day 7. Imaging of PC12 aggregations (bottom), day 7.	64
4.34	Axonal signal recorded through the HD-MEA.	64
5.1	Astrocytes as regulators of the glutamate-glutamine cycle: during neurotransmission, glutamate produced by the pre-synaptic cell (1) is secreted into the synaptic cleft and interacts with the post-synaptic cell receptors (2). Astrocytes rapidly remove synaptically released glutamate, converting it into the amino acid glutamine by the enzyme glutamine synthetase (3a), and avoid excitotoxic damage of the cells. Glutamate uptake increases the calcium (Ca^{2+}) intracellular concentration in astrocytes (3b), which triggers the release of glutamine into the extracellular space (4). Glutamine is then taken up by neurons, providing the necessary substrate for the synthesis of glutamate (5).	66
5.2	Effect of dexamethasone on the glutamate-glutamine cycle: rate of glutamate conversion to glutamine by astrocytes (3a) and glutamine release into the extracellular space (4) increase significantly. Increased glutamate uptake provokes a detectable increase in the Ca^{2+} intracellular concentration (3b).	67
5.3	Glutamate assay with/without astrocytes (expected figure).	67
A.1	Formation of a fully-crosslinked gel for different concentration of GelMA at 60 s UV exposure time.	69
A.2	Shear-thinning behavior for different concentrations of GelMA in the presence of CaCl_2	71
A.3	Shear-thinning behavior for different concentrations of GelMA in the absence of CaCl_2	71
A.4	Oscillatory strain sweep between low (1%) and high (250%) strain shows the rapid self-healing ability of 3% gelatin/ 2% alginate bioinks during the printing process.	72
A.5	Oscillatory strain sweep between low (1%) and high (250%) strain shows the rapid self-healing ability of 3.5% gelatin/ 2% alginate bioinks during the printing process.	73
A.6	Oscillatory strain sweep between low (1%) and high (250%) strain shows the rapid self-healing ability of 7% gelatin/ 2% alginate bioinks during the printing process.	74

A.7 The Live/Dead™ assay of astrocyte-laden 5% GelMA gel after different UV exposure times. It shows that astrocyte mortality will increase following the increase of UV exposure time.	75
---	----

Chapter 1

Introduction

Each year, over 1 million patients in the world suffer from brain diseases such as Alzheimer's, Parkinson's, ischemia stroke, and brain tumor [1, 2, 3]. Brain disorders have an estimated annual economical burden of almost \$7.2 billion [4, 5, 6, 7, 8] worldwide and are usually cause of high mortality rate in patients. Pre-clinical pharmaceutical treatment therapies have been typically performed with two-dimensional (2D) cell culture and animal models. However, these existing models do not necessarily recapitulate the important features of the three-dimension (3D) brain environment such as cell-cell contact and interactions, leading to a loss of understanding of the global synchronous activity. The high costs, uncertain translation to human patients, and ethical concerns also limited the use of animal models. Current models to study brain diseases rely on oversimplified 2D *in vitro* cell cultures and genetically different pre-clinical animal models to predict human responses to pharmaceutical compounds. Human organotypic cultures may be the closest representation of *in vivo* human brain tissue outside of live patients [9]; however, the preparation of organotypic cultures for human tissues are extremely rare and expensive due to limited specimen availability [10, 11]. Therefore, there is a strong need for a 3D biomimetic human brain model containing both neurons and astrocytes, to precisely replicate the astrocyte-neuron interactions in the human brain. Bioprinting has emerged as a versatile technology that allows for the fabrication of 3D tissue constructs of high complexity at extremely high spatial precision and reproducibility. To date, a variety of different techniques for bioprinting have been proposed, such as extrusion [12, 13, 14, 15], injection [16, 17, 18, 19], magnetic [20], and laser-based approaches [21, 22, 23]. However, current strategies are all limited in their abilities to bioprint soft and self-supporting materials able to mimic the anisotropic directional neural network in the brain, which extends across a large scale in a 3D space. Recently, a novel 3D bioprinting strategy based on direct extrusion of a shear-thinning bioink into a self-healing supporting hydrogel matrix has allowed for embedded bioprinting of freeform biological structures [24, 25, 26]. By combining this strategy with the engineered hydrogels/bioinks, it was possible to bioprint an aligned neural network directly within an astrocyte-laden matrix to facilitate axonal extension and neural signaling. Therefore, in this study, the development of an innovative 3D bioprinted neural tissue model will be investigated. It features an astrocyte-laden

hydrogel with brain-like stiffness, aligned neurite structures, astrocyte-neuron interactions, and neurotransmitter synthetic functions such as glutamate synthesis, and is obtained through the use of a unique bioprinting technology, which allows for the development of a co-culture of astrocytes and neurons to construct a biomimetic 3D human brain model (See Figure 1.1).

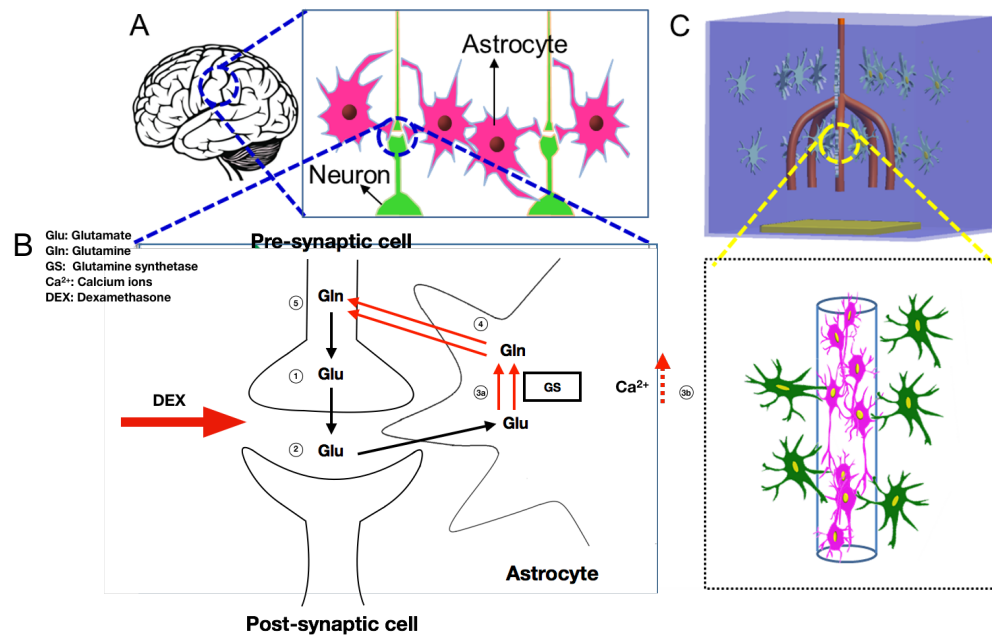


Figure 1.1: **A** Astrocytes-neurons interaction at the synapses level in the brain. **B** Astrocytes as regulators of the glutamate-glutamine cycle: during neurotransmission, glutamate produced by the pre-synaptic cell (1) is secreted into the synaptic cleft and interacts with the post-synaptic cell receptors (2). Astrocytes rapidly remove synaptically released glutamate, converting it into the amino acid glutamine by the enzyme glutamine synthetase (3a), and avoid excitotoxic damage of the cells. Glutamate uptake increases the calcium (Ca^{2+}) intracellular concentration in astrocytes (3b), which triggers the release of glutamine into the extracellular space (4). Glutamine is then taken up by neurons, providing the necessary substrate for the synthesis of glutamate (5). **C** The engineered 3D co-cultured brain like tissue construct. Astrocytes (green) and neurons (purple) interact at the interface of the printed fibers.

In the following paragraphs, an introductory discussion on 2D and 3D cell cultures, current 3D bioprinting techniques, and on co-cultures of different cell types, which portrays the literature research done in order to decide the approaches to be taken during the project, will be carried out.

1.1 Cell cultures: 2D models vs 3D models

The development of new drugs, together with many other ongoing studies in the biomedical field, has massively relied on cell-based assays during the testing phases

as easily reproducible, highly accessible and cost-effective investigation tools to obtain essential data before moving to further testing on animal models [27]. Although being able to give important insights into cell-based studies, two-dimensional (2D) models have some major limitations that hinder the value of the obtained results. Cells in 2D cultures exhibit behaviors in response to external stimuli that can be significantly different from those *in vivo*. First of all, 2D cultures are mostly studied on flat, rigid substrates. This situation does not take into account the complexity of the *in vivo* environment, in which cells are surrounded by neighboring cells and extracellular matrix (ECM). This often leads to misleading results and unreliable data when moving to *in vivo* models [28]: to date, in drug discovery, only 10% of the compounds tested in 2D cell culture-based assays go through animal model testing and, eventually, clinical trials without being proven unsuccessful [29]. Part of the failures during clinical trials are to be attributed to a lack of understanding of how to properly culture cells *in vitro* in order to extrapolate phenotypically relevant data for *in vivo* applications [30]. Recent studies suggest that three-dimensional (3D) cell culture systems, exhibiting substantial differences in terms of cell morphology, phenotype, physiology and functionality if compared to 2D cell culture systems, reproduce with higher accuracy the actual tissue environment in which cells grow, being therefore more reliable as models for translational studies to *in vivo* models [31, 32]. 2D and 3D cultures can be compared in terms of several features including, but not limited to cell response to stimuli, drug metabolism, and *in vivo* relevance.

1.1.1 Morphology

Cells grown in 2D cultures usually exhibit a flat morphology with an average thickness of approximately 3 μm , whilst in 3D cultures they develop in ellipsoids with dimensions ranging from 10 to 30 μm . Monolayers of cells do not show alterations in morphology due to diseased conditions [33], and usually express a series of distinctive traits less prominently (i.e. neurite extension for human retinal cells[34]). On the contrary, 3D cultures of the same cells strongly express differences in terms of alignment (important for controlling their biological functions and replicate the conditions of highly organized native tissues [35]), integrity and polarization (fundamental for signal transmission in neurons [36]). 3D cultures therefore offer a deeper understanding of cellular responses associated to changes in their structure.

1.1.2 Differentiation

Differentiation of cells in 3D cultures is widely characterized, whilst 2D cultures do not efficiently show the same behavior. For example, osteogenesis of rat mesenchymal stem cells can be observed in 3D cultures but not in 2D cultures [37]. Moreover, parameters as duration, phenotypic modifications and states of non-differentiation can be easily visualized in 3D cultures. Gene expression in undifferentiated mouse embryonic stem cells shows that they can retain this state better than in 2D cultures,

together with their normal viability and morphology [38]. The progression of cellular differentiation is therefore best understood when the cells are cultured in a 3D environment, giving a powerful tool for understanding *in vivo* models.

1.1.3 Viability

Cells in 2D cultures undergo apoptosis more easily than in 3D cultures. This has to be attributed to the more conspicuous cell-to-cell interactions in 3D that, even when the cells are subjected to sub-optimal conditions (i.e. depletion of nutrients), allows for a higher viability [39]. In the framework of this study, this becomes of major importance when it comes to understanding the effect of drugs on cancer cells death, which was observed to be significantly different in 2D and 3D cultures [40].

1.1.4 Response to stimuli

Cells respond differently to stimuli provoked by adjacent cells or external inputs according to the way they are cultured. For example, effects of radiation exposure on morphology and sensitivity of non-tumorigenic epithelial cells was shown to be null in 3D cultures, while the same cell line was observed to be affected when cultured in 2D [41]. The effect of some growth factors is also proven to be different, affecting the proliferation of cells in radically different ways [42]. Studying the development of cells in 3D cultures allows to distinguish more easily between the different responses of cells, i.e. those that have to be attributed to their normal functionality and those triggered by diverse stimuli.

1.1.5 Drug metabolism

The way cells metabolize drugs and secrete metabolic products can change drastically in 3D cultures. Studies conducted on the activity of well known cancer drugs such as Paclitaxel, Doxorubicin, Alimta, Zactima, and Vinorelbine show a different cytotoxicity in cells cultured in 3D systems with respect to 2D [43, 44]. Chemosensitivity in 3D cell cultures varies substantially for cancer cell lines such as MCF-7, Lovo and PC-3, suggesting cell architecture, phenotype variations and extracellular matrix (ECM) play a significant role and should be carefully taken into account when a drug transport model has to be developed [45].

1.1.6 Gene expression and protein synthesis

SH-SY5Y human neuroblastoma cells grown in 3D cultures express altered differential expression of more than 1,700 genes. Among these, also those relevant to cytoskeleton, ECM, and neurite outgrowth are affected. These substantial differences are attributed to the influence that culture material has on gene expression, cell spreading, and neurite growth. Increased and decreased gene expression was observed in vascular smooth muscle cells and attributed to a diminishing of stress

fibers formation and focal adhesion in the 3D matrix [34]. MCF-7 cells showed increased expression of a series of proteins, together with collagen synthesis, attributed to a different state of cellular adhesion and intercellular adhesion molecules expression in a 3D environment [46].

1.1.7 *In vivo* relevance

Cells *in vivo* naturally grow in a 3D pattern and, in addition to interacting with the ECM, they interact with other cell types that affect their functions. 3D cell cultures allow for the expression of cell characteristics that resemble more closely the *in vivo* environment. For example, tumors characterized with polarized epithelial structures or spheroids are more prominent thanks to the enhanced cell-to-cell contact [47]. Human endothelial cells demonstrate an increased ability of mimicking angiogenesis [42]. The generation and maintenance in time of functional and healthy neural tissue on 3D scaffolds, in addition to provide a lower mortality rate, showed a higher neurons/astrocytes ratio with respect to 2D cultures, and allowed for cell survival even in total absence of supporting substrates of poly-D-lysine and laminin, essential to avoid cell death in 2D cultures [48]. Histology, morphology and functional phenotypes are also proven to resemble more closely the *in vivo* models [49].

1.1.8 Proliferation

Mesenchymal stem cells, osteosarcoma cells, human umbilical vein endothelial cells (HUVEC), human glioblastoma cells and tumor epithelial cells (TEC) cells show an higher growth rate in 3D culture models. Moreover, even cells subjected to unfavorable conditions (i.e. nutrient depletion) showed lower apoptosis in conditions where they were more protected from shear stress [38, 50]. On the other hand, human neuroblastoma, sheep bone marrow, breast cancer, and other types of cells express an inferior growth rate due to differences in morphology, lower contractile protein expression and basal proliferation in a 3D environment [51, 52].

1.2 Current methods for 3D cell culturing

3D cell cultures can be developed in several ways, which include hanging-drop method, forced-floating method, use of matrices and scaffolds, use of hydrogels, agitation-based approaches, and exploitation of microfluidic systems (which will not be treated in this work).

1.2.1 Hanging-drop method

This method, proven to be simple and 100% reproducible, allows for the production of 3D spheroids (one per drop) for a wide range of cell lines. Small volumes (ranging between 20 and 50 μl) of single cell suspension at a density of 50-500 cells/drop is

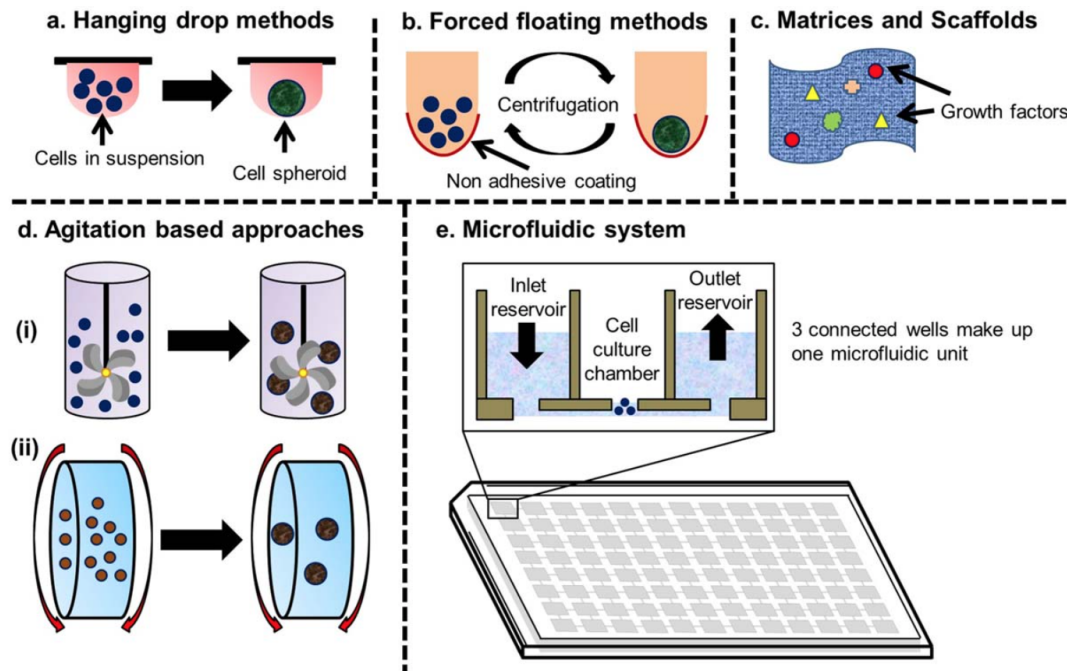


Figure 1.2: Current methods for 3D cell culturing. (Adapted from [32])

pipetted into the wells of a well plate, which is then turned upside down in order to create hanging droplets of cells, which concentrate at the bottom of the droplet and are kept in place by surface tension. This method allows for the creation of tightly packed and morphologically homogeneous spheroids [53]. The main disadvantage is that the volume of the droplet must be limited below $50 \mu\text{l}$, as surface tension is not sufficient to withhold the droplet if the volume overcomes this limit.

1.2.2 Forced-floating method

The forced-floating method consists mainly in the surface modification of the wells in which cells are seeded. Poly-hydroxyethylmethacrylate (poly- HEMA) coating prevents the adhesion of the cells to the surface, whilst the addition of reconstituted basement membrane to the suspension enhances the generation of spheroids over loose aggregates. Differently from the hanging-drop method, spheroids size can be easily manipulated by changing the amount of seeded cells [54]. Agarose can also be introduced to enable for long-term culturing (over 20 days) [55]. The main disadvantage of this method is the time consumption during the coating process, which may take multiple days.

1.2.3 Matrices and scaffolds

Extracellular matrix (ECM) is composed of extracellular molecules secreted by cells which help providing biochemical and structural support to the cells embedded in it or growth on its top. It is proven to enhance the cell-to-cell communication and to be

fundamental for proper cellular functioning. An ECM made commercially available by BD Biosciences, Matrigel, is widely used in 3D tumor cells culturing, and contains tumor-derived basement membrane proteins and growth factors fundamental for cell differentiation and cellular signaling [56]. The main disadvantages include scarce reproducibility in terms of spheroids uniformity, variability between batches and high costs for large-scale production. In scaffold-based 3D cultures alginate, laminin, collagen and other hydrogels are used to construct scaffolds, consisting in networks of fibers and porous structures through which cells easily migrate and proliferate in a 3D fashion, filling the interstices. These porous constructs allow for long-term nutrient and drugs perfusion, oxygen availability and wastes removal. Moreover, cells have better mobility and general organization. The disadvantages are mainly related to the special equipment needed to synthesize these types of cultures [57].

1.2.4 Agitation-based approaches

In agitation-based approaches, cell suspension is placed in a container and kept in motion through stirring, which prevents cells adhesion to the walls. The main setups are spinner flask bioreactors (in which a stirring element keeps the cell solution in continuous motion), and rotating cell culture bioreactors (in which the whole container is kept in rotation). Spheroids of different dimensions can be obtained, and the motion of culture fluids helps in nutrient provision and waste removal. The main drawbacks are associated with the sheer stress exerted on the cells (for spinner flask bioreactors) and the shape inconsistency of spheroids produced (for both setups) [32].

1.2.5 Limitations

Although being a promising approach, 3D cell culture systems still present some issues that need to be addressed [32], mainly:

- Reproducibility from batch to batch.
- Need of a system with higher resemblance to true biological systems (also for what concerns modifications through time).
- Interaction of drugs and molecules with the scaffold constituent materials, which can sensibly modify the outcomes.
- Need of modification of inert synthetic scaffolds before cell embedding.
- Nutrients and drug perfusion uniformity through the whole 3D culture, which can lead to significant variations in cell viability, proliferation and functionality.

1.3 3D bioprinting

3D bioprinting is a field gaining more and more attention from a wide range of academic disciplines. In tissue engineering, in particular, its potential of addressing major issues as functional tissue and organ fabrication is regarded as a promising approach to mitigate organ shortage for transplantation. Moreover, it allows for the creation of constructs that replicate more closely the *in vivo* environment and allow for useful models for drug discovery and testing *in vitro*. It differs from normal 3D printing as it involves printing living cells with great spatial precision in the placement of cells, proteins, and growth factors to control tissue formation [58].

1.3.1 3D bioprinting approaches

3D bioprinting is based on three main approaches: biomimicry, autonomous self-assembly and mini-tissues.

Biomimicry

Engineering reproductions of functional cellular and extracellular components at the microscale allows to recreate physiologically accurate biomaterials, which mimic the real biological tissue and have various uses in many fields of research. For this to be achieved, it is necessary to understand the cells arrangement in the real tissue, the gradients of soluble and insoluble factors, the composition of the ECM surrounding the cells and the nature of the biological forces involved [58].

Autonomous self-assembly

An alternative approach is to replicate biological tissues using the cellular components of the tissue early developing stages as a guide for tissue generation. During these stages, the cellular components produce their own ECM components, and give way to an appropriate cells organization and patterning to obtain the desired micro-architecture. Autonomous self-assembly relies on cells ability of being the primary drivers for histogenesis, directing all the desired properties of the desired developing tissue [59]. For this approach to be successful it is necessary to have a deep knowledge of embryonic tissue genesis and organogenesis and of the diverse methods for manipulating the surrounding environment to drive correctly these embryonic mechanisms [58].

Mini-tissues

The last concept is important for both of the previous approaches. Tissues and organs are made of smaller structural and functional blocks, or mini-tissues. These blocks can be fabricated and aggregated into larger structures through both the previously mentioned approaches. The main strategies to obtain this are the following [60]:

- assemble cell spheres into a macro-tissue in a biologically inspired way.
- recreate high-resolution reproductions of the micro-tissue and allow them to self-assemble into a structurally accurate and functional macro-tissue.

Among the possible applications, the self-assembly of vascular micro-tissues and functional tissue units for "organs-on-a-chip" applications should be remembered.

1.3.2 Bioprinting techniques

The main technologies used for patterning and depositing biological materials can be divided into three major groups, according to their working principles: extrusion-based, droplet-based, and laser-based bioprinting [58].

Extrusion-based

Extrusion-based bioprinting (EBB) as a viable approach for printing living cells is regarded as one of the more versatile and affordable bioprinting approaches. It allows for the bioprinting of cells [61], tissues [62], organ modules [63], organs-on-chip, and is regarded as one of the most promising approaches for printing functional organs [64]. EBB combines fluid dispensing and a robotic system for automatic extrusion and bioprinting. During the process, a bioink is dispensed in a controlled way. Encapsulated cells are therefore deposited in cylindrical filaments or fibers in the desired 3D structures. The continuous deposition of filaments allows for good structural integrity, even if the process is quite rapid. Moreover, computer-aided design (CAD) software can be easily incorporated in this method, allowing for the bioprinting of previously obtained medical images or design on-demand [65]. It is therefore regarded as the most convenient technique for the fabrication of 3D porous cell-laden structures. The 3D EBB dispensing system can be driven by a pneumatic-, mechanical- (piston or screw driven), or solenoid-based system.

Droplet-based

Droplet-based bioprinting (DBB) originates from inkjet printing technology, firstly developed in the 1950s. To apply the same technologies used in nonbiological applications to biocompatible materials, these need to be modified to minimize the risk of compromising cell viability. Instead of dispensing ink, the commercially available inkjet printers were modified to print proteins and cell solutions [66]. DBB offers several advantages related to its intrinsic simplicity, versatility and precise control over the pattern of deposition, allowing for the creation of heterocellular constructs with high spatial resolution [67] and high throughput. The main limitation is that it is a technology still limited to 2D tissue constructs. However, this limitation could be overcome printing successive layers of cellular aggregates using thermosensitive gels and eventually generating 3D constructs [68]. This group comprises inkjet

-divided in continuous inkjet (CIJ) and drop-on-demand (DOD) bioprinting-, electrohydrodynamic (EHD) jet, acoustic-droplet-ejection, and microvalve bioprinting. CIJ bioprinting takes advantages of Rayleigh-Plateau instability to divide bioink jets into droplets; DOD bioprinting uses actuators (thermal or piezoelectric) to produce droplets. Acoustic bioprinting uses acoustic waves, whilst microvalve bioprinting exploits a solenoid pump to produce the same effect.

Laser-based

Laser-based bioprinting (LBB) techniques can be classified into two major subgroups according to their working principle: processes involving photopolymerization and processes based on cell transfer. The first group includes Stereolithography (SLA), dynamic optical projection stereolithography (DOPsL), and two-photon polymerization (2PP); the second group includes laser-guidance direct writing (LGDW), matrix-assisted pulsed laser evaporation-direct write (MAPLE-DW), and laser-induced forward transfer (LIFT). The first transfer of living cells using a laser-assisted technology was first introduced to facilitate two-dimensional (2D) patterning of cells. This enabled the rapid formation of cell patterns within cell media. Although 2D patterning of cells was the first use of LGDW, the introduction of laser-assisted bioprinting as an extension of MAPLE eventually allowed for the fabrication of 3D tissue constructs. LBB has the major advantage of offering high accuracy and resolution in biofabrication. However, its complicate setup limited its use in bioprinting if compared to EBB or DBB. Moreover, the use of toxic photoinitiators for decreasing the curing time of tissue scaffolds limits the applications of SLA and its modifications in the field of bioprinting. Nonetheless, the introduction of two-photon polymerization (2PP) and dynamic projection printing, especially in the field of tissue engineering, has allowed for the fabrication of tissue scaffolds with unprecedented resolution and high speed, leading to the introduction of these particular technologies in the bioprinting arena [58].

1.3.3 Materials

3D printing technologies were initially conceived for nonbiological applications (i.e. deposition of metals, ceramics and thermo-plastic polymers) and involved the use of organic solvents, high temperatures processes or non-biocompatible crosslinking agents. One of the main challenges of 3D bioprinting was hence to find biocompatible materials which could be not only efficiently printed, but also could meet the desired set of functional and mechanical properties [58]. Nowadays, these materials are mainly:

- **naturally derived polymers**, obtained from animal or human tissues, like alginate, gelatin, collagen, chitosan, fibrin, and hyaluronic acid.
- **synthetic molecules**, like polyethylene glycol (PEG).

Naturally derived polymers have the advantages of a composition similar to the human ECM, and of being bioactive. Synthetic molecules, on the other hand, can be synthesized with specific physical properties to meet particular needs; however, they exhibit poor biocompatibility, and generation of toxic products and loss of mechanical properties during degradation. Nonetheless, synthetic hydrogels, whose physical properties are easily controllable during synthesis, are being widely used in 3D bioprinting for regenerative medicine applications. The set of desirable properties for printable materials increases together with the complexity of their possible applications: materials should have proper crosslinking mechanisms for optimal printability, must be biocompatible for long-term implantation *in vivo*; they should meet both short-term stability (to maintain initial mechanical properties and avoid collapsing of the developed microstructures) and remodeling (to allow for the formation of structures imposed by cellular and physiological drivers); cellular adhesion, proliferation, and functionality should also be fully supported [67]. These main characteristics, namely printability, biocompatibility, degradation kinetics and byproducts, structural and mechanical properties, and material biomimicry will be discussed more in detail in the following paragraphs.

Printability

A material suitable for 3D bioprinting should allow for accurate and precise deposition, together with the desired spatial and temporal control of the process. Inkjet bioprinting has some limitations on material viscosity, whilst microextrusion bioprinting may impose strict requirements on the crosslinking mechanisms or shear-thinning properties of the material. Some of the parameters involved in the process strongly affect the printability: nozzle gauge determines both the shear stress to which cells are exposed as well as the time required for material deposition when developing a 3D structure [69, 70]. Rapid crosslinking time is required in inkjet bioprinting to allow for layering of a complex 3D structure. On the contrary, the highly viscous materials used in microextrusion bioprinting are able to maintain a 3D shape after deposition, therefore allowing the final crosslinking to happen well after fabrication. Attention should also be given to the ability of the material to preserve cell viability and functionality during printing: processes that involve localized heating (inkjet, LAB) should involve materials with low thermal conductivity or with the ability to protect locally the cells during delivery [71, 72, 73, 74] in order to increase post-printing cell viability.

Biocompatibility

In the bioprinting field, biocompatibility refers not only to the need of avoiding undesirable effects when the material is implanted *in vivo*, but also to the expectation that the implanted material will actively and controllably contribute to the biological

functionalities. This may involve interactions with the surrounding tissue, and support of cellular activity and molecular signaling to allow for efficient implantation *in vivo* [75].

Degradation kinetics and byproducts

During the degradation of a material scaffold, the embedded cells start secreting proteases and producing ECM proteins that modify the characteristics of the new tissue [76]. These processes should be fully understood to avoid undesired effects. They can be summarized as follows [67]:

- **control of degradation rates:** degradation of the material should ideally match the ability of cells to substitute the degraded materials with their own specific ECM proteins.
- **biocompatibility of degradation byproducts:** they should be nontoxic, easy to metabolize and expel from the body. Attention should be devoted to proteins and molecules (even inert ones that can break into oligomers and provoke inflammation), non-physiological pH, and temperature increases as the result of reactions
- **swelling and contractile characteristics:** overly-swelling materials can absorb fluid from the surrounding tissues, overly-contractile materials can clog pores and vessels and hinder cell migration and nutrient perfusion. Special attention should also be dedicated to cases in which materials with different swelling or contractile properties are put one close to the other, as their interaction can affect the integrity of the final construct.

Structural and mechanical properties

Materials selection should be done carefully considering the required mechanical properties of the construct. Fine-tuning of the mechanical properties should be carried out on the basis of the desired application and the different structural requirements, which radically change according to the diverse applications (i.e. skin, liver, cartilage, bone [70, 77, 78]). The use of sacrificial materials to address this limitation and provide the desired structural and mechanical properties has been widely investigated: it either allows for enhanced crosslinking mechanisms at the time of printing or as a supporting material which gradually degrades, giving enough time to the supporting material to fully develop the desired functions [79].

Material biomimicry

The possibility of incorporating biomimetic components during bioprinting affects cells in terms of attachment, proliferation, migration and functionality. The choice of material strongly influences cell attachment [80], shape, and size [81], therefore

allowing for a fine control of proliferation, differentiation and cytoskeletal assembly. Surface modifications through the use of ligands [80] or through the introduction of nanometric features (i.e. steps, grooves, general roughness) can further affect these properties. Cell adhesion, orientation, motility, display of surface antigen, modulation of intracellular signaling pathways that regulate gene expression and transcriptional activity, and condensation of cytoskeleton are also strongly affected by nanoscale variation of the material surface [82]. The biomimicry approach involves engineering the materials in order to obtain specific physiological functions, and therefore requires a deep understanding of the ECM components in the target tissue. More than 300 ECM proteins, multiple ECM-modifying enzymes and ECM-binding growth factors can be found in mammals [83], among which the most studied and well-understood are collagens, proteoglycans, and glycoproteins, which provide strength and space-filling functions, binding of growth factors, protein complexes regulation, cell adhesion promotion, and participate in cellular signaling [67]. There are two main approaches to biomimicry which involve ECM components:

- **ECM scaffolds:** Ideally, the ability of reproducing identical ECM scaffolds through bioprinting would give way to great advances in tissue engineering and regenerative medicine. Tissue decellularization methods, which involve the lysis and removal of the cellular components of a tissue via perfusion with deionized water, could provide intact ECM scaffolds for an in-depth analysis of ECM composition. The main challenges of this approach are related to the difficulty of removing cellular components while maintaining the fine vascular structures, and to the toxicity provoked in cells when grown on decellularized tissue scaffolds [84].
- **scaffold-free ECM:** a scaffold-free approach can be an interesting direction to pursue to address the issues that arise during decellularization. The concept is the following: while cells produce and deposit the tissue ECM, bioprinted cellular spheroids produce an ECM environment that best meets their function, giving a dynamic ECM mechanism and, therefore, control over cell behavior. The main challenge is to incorporate efficiently these materials into constructs using bioprinting.

1.3.4 Cell sources

One crucial aspect for 3D bioprinting of functional tissues and organs is the choice of cells. They comprise multiple primary functional cell types with specific biological functions that have to be recapitulated in the transplanted tissue. In addition to that, most tissues contain cell types whose functions are mainly supportive, structural or as barriers, and are involved in processes of vascularization or of stem cells maintenance and differentiation. Printing cells currently involve either the direct deposition of multiple **primary cells** or the use of **stem cells** that proliferate and

differentiate into the desired cell types. In both approaches, the following aspects should be considered:

- cells should mimic as much as possible the physiological state of cells *in vivo*, maintaining their functions over time.
- cells should be able to expand into sufficiently high numbers for printing.
- cells should be robust enough to withstand the whole bioprinting process, including physical forces (shear stress, pressure), biological stress (presence of toxins, non-physiological pH, enzymes).
- proliferation should be precisely controlled: too little proliferation will result in loss of viability when the structure is transplanted, whilst too much proliferation may result in cellular apoptosis. It is also essential to achieve a proper ratio of functional and supporting cells.
- proliferation rate and timing should also be considered: ideally, the perfect condition would be an initially high proliferation rate to populate the construct, whilst over the long term the rate should be suitable to achieve tissue homeostasis and avoid hyperplasia (enlargement of the tissue caused by the increase of the reproduction rate of its cells).

In general, for bioprinted constructs maintained over long-term, the correct functionality requires the tissues to be able to maintain cellular homeostasis, respond to tissue damage and renew itself. The advancements in understanding the nature of stem cells will surely improve these aspects, together with addressing the issues related to the isolation and culturing of some types of primary cell types. Stem cells are promising cell types for bioprinting applications as they efficiently proliferate in an undifferentiated but multipotent state (i.e. they have the ability to develop into more than one cell type), and they can generate multiple functional tissue-specific cell phenotypes [85]. Embryonic stem cells and induced pluripotent stem cells can self-renew for an indefinite time and can maintain their undifferentiated state for over 80 passages [86]. The possibility of generating large number of cells from pluripotent cells makes them promising candidates for bioprinting, especially in therapeutic applications, but thorough studies on their safety for clinical transplantation is still to be conducted. Another promising cell source is represented by mesenchymal stromal cells (MSCs), whose protocols for isolation, expansion and differentiation are well established [67]. Current bioprinting studies often involve cell lines which are very robust and capable of substantial proliferation (i.e. fibroblasts), but are incapable of dealing with cell types more sensitive to physical stress and biological conditions. Cellular direct differentiation and reprogramming are therefore important fields of study to finally achieve cell types highly adapted for bioprinting, which at the same time meet the desired requirements as *in vitro* models or for implantation [67].

1.4 Co-culture systems

As mentioned in the previous section, 3D bioprinting offers enormous advantages in terms of precise cell patterning and spatial disposition. This technique is particularly useful in the case of **co-culture systems**. These systems have been widely used to study cell-cell interaction of any kind, and there is a growing interest in engineering multicellular synthetic systems with higher and higher levels of complexity. Co-cultures are, at their simplest form, cell cultivations in which two or more cell types are grown together with some degree of contact [87]. The motivations for developing such a set-up include:

- **studying natural interactions between populations:** this includes infection studies, creation of experimental models, development of biomimetic environments [88], representative human *in vivo*-like tissue models for drug research [89].
- **improving culturing success for certain populations:** some cell types are either not easily monocultured or do not exhibit a physiological behavior resembling the *in vivo* situation [90]. The presence of another co-cultured cell type may improve both aspects [87].
- **establishing synthetic interactions between populations:** development of complex systems with industrial, medical, and environmental applications is gaining more and more interest for the proven advantages over monocultured systems [91, 92].

Chapter 2

Theory

2.1 Neurons and glial cells

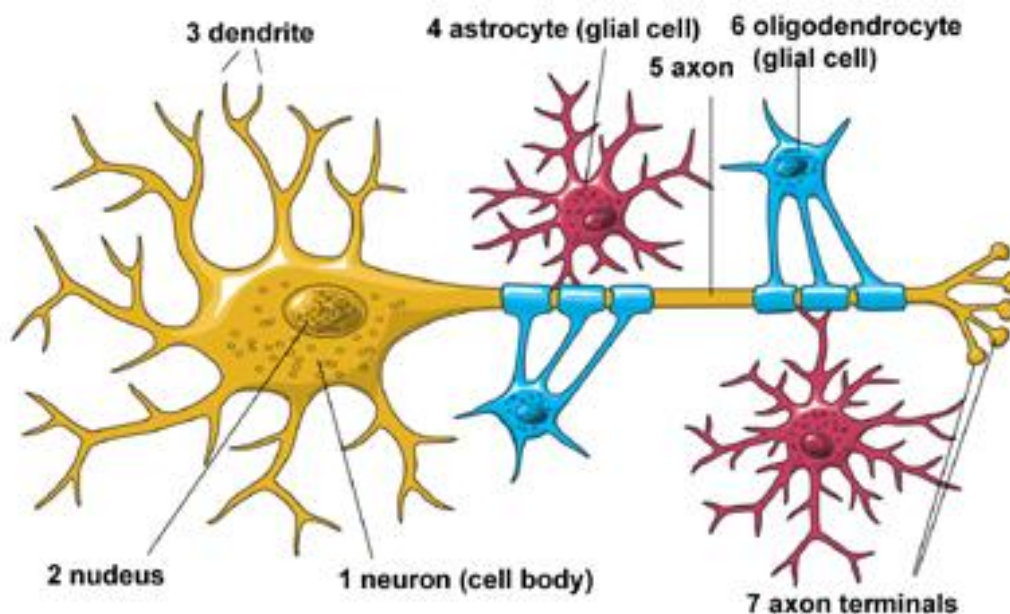


Figure 2.1: Structure of a neuron and glial cells. (Credit: NIH/National Institute of Neurological Disorders and Stroke (NINDS))

Neurons are highly specialized cell types and the essential cellular elements in the central nervous system (CNS). Complex cell–cell interactions among single neurons or groups of related neurons are responsible for all neurological processes. Neurons can be categorized in terms of their size, shape, neurochemical characteristics, location, and connectivity, which determine their specific functional role in the brain. Neurons can be categorized in five general groups:

- **inhibitory neurons involved in local contacts**, as GABAergic interneurons in the cerebral and cerebellar cortex;
- **inhibitory neurons involved in distant contacts**, as Purkinje cells of the cerebellar cortex and medium spiny neurons of the basal ganglia;

- **excitatory neurons involved in local contacts**, as the spiny stellate cells of the cerebral cortex;
- **excitatory neurons involved in distant contacts**, as the pyramidal neurons in the cerebral cortex;
- **neuromodulatory neurons** that affect neurotransmission (usually long-distance interactions).

A further division within these classes, based on the anatomic features of the neurons (chandelier, double-bouquet, bipolar cells etc.), can be carried out, allowing for a connection between the cell characteristics and their specific functional roles. Neurons develop distinct subcellular domains that are devoted to different functions. A typical neuron can be divided in three morphologically distinct regions:

- **the cell body (soma or perikaryon)**: contains the nucleus and most of the cytoplasmic organelles;
- **the dendrites**: they can be in variable number, emanate from the soma, ramify over a volume of gray matter and differ in size and shape depending on the different neuronal type. They can be spiny (for example in pyramidal cells) or non-spiny (in most interneurons). They play a crucial role in providing an extended receptive area on the neuronal surface, receiving external afferents;
- **the axon**: each neuron has only a single axon, which usually extends much further than the dendrites. In opposition to the dendrites, it is usually smooth, with a variable number of branches emitting from itself called collaterals. In vertebrates, axons are usually covered by an insulating myelin sheath, which allows for rapid impulse conduction. It is responsible for transmitting neural information (primary, in the case of a sensory receptor, or processed, if it has already been modified by a series of integrative steps). The axon departs from the soma from a small swelling called the *axon hillock*.

Glial cells, on the other hand, support and maintain neuronal physiology through highly diverse (and not completely understood) functions, which include myelination, trophic factors secretion, and extracellular milieu maintenance. These supporting cells greatly outnumber neurons in the CNS, and can be divided in three types:

- **oligodendrocytes**: they are myelin-producing cells. Myelin insulates axonal segments bioelectrically and accelerates the speed of action potential conduction;
- **astrocytes**: they play a wide variety of metabolic support roles, including providing energy intermediates and removing the excessive extracellular neurotransmitter secretions;

- **microglia:** they are relatively uncharacterized cells which, in addition of providing support, are believed to have a major role in recruiting macrophages and other white blood cells to remove necrotic tissue and defend against microbial infection during infection, traumatic injuries, and degenerative diseases [93].

2.2 Synapses and neurotransmission

Neurons naturally form circuits, which constitute the structural basis for brain functioning. These circuits can either involve a set of neurons projecting from one brain region to another (macrocircuits), or refer to local cell-cell interactions within a given brain region (microcircuits). Neurons in these circuits communicate chemically and electrically through specialized contact zones called **synapses** (in the CNS), which are active zones for the release and reception of specific transmitters, called **neurotransmitters** (chemical synapses) or for the transmission of electrical signals (electrical synapses). The active zone is characterized by the presence of voltage gated calcium channels and of an accumulation of organelles called synaptic vesicles, which contain proteins having fundamental roles in transmitter storage, voltage- and Ca^{2+} -dependent secretion, and scavenging and recycling of previously released molecules. Synapses consist of a pre-synaptic (axonal) element, a synaptic cleft, and a post-synaptic element (somedendritic membrane). Both pre-synaptic and post-synaptic elements are characterized by a thickening: when these thickenings are symmetric the synapses tend to be inhibitory, whilst if they are asymmetric they tend to be excitatory [94]. The synaptic cleft is a gap of approximately $20\ \mu\text{m}$ in which each vesicle releases its content, and therefore the space in which the highest concentration of neurotransmitters is found.

2.2.1 Chemical transmission

Neurotransmitters are considered to be endogenous substances released from neurons, that act on receptor sites typically present on membranes of post-synaptic cells, and provoke a functional change in the target cell. For a substance to be qualified as a neurotransmitter, several criteria should be met:

- A neurotransmitter must be synthesized by and released from neurons, either in the axonal terminal or in the cell body (i.e. the pre-synaptic neuron should contain a transmitter and the enzymes required to synthesize that specific neurotransmitter).
- The transmitter should be released from nerve terminals in a chemically identifiable form.
- The released substance should reproduce at the post-synaptic level the specific events that are observed after stimulation of the pre-synaptic cell.

- The effects of a neurotransmitter should be inhibited by competitive antagonists of the receptor in a way that is exclusively dose-dependent. Moreover, treatments that hinder the synthesis of the transmitter should block the effects of pre-synaptic stimulation.
- Active mechanisms to terminate the action of the neurotransmitter should be present (i.e. uptake of the transmitter by either the pre-synaptic neuron or the glial cells through specific transporter molecules, or enzymatic inactivation of the chemical messenger).

The Process of Chemical Neurotransmission consists of a number of steps, which can be summarized as the following:

- Synthesis of the neurotransmitter in the pre-synaptic cell. It requires proper precursor(s), enzymes, and cofactors necessary for enzyme activity. Drugs that affect the synthesis of neurotransmitters have been widely used in medicine;
- Storage of the neurotransmitter (and/or its precursor) in the pre-synaptic nerve terminal, where they are protected from enzymatic degradation and remain ready for rapid release;
- Release of the neurotransmitter into the synaptic cleft;
- Interaction and recognition of the neurotransmitter by receptors on target cell;
- Termination of the released neurotransmitter effect. If this last step does not happen, major dysfunctions can occur: the unstoppped activation of post-synaptic targets can result in seizures (in the brain) or tetanus (in muscles). Termination can happen both actively (i.e. pre-synaptic re-uptake of the neurotransmitter or enzymatic degradation to inert substances) and passively (diffusion of neurotransmitter from synaptic region) [93].

2.2.2 Electrical transmission

On the other hand, long distance, rapid communication is achieved by neurons thanks to their ability to send electrical signals (**action potentials**) along axons, through a mechanism called conduction. Action potentials (APs) are generated close to the cell body, in a section of the axon called axon initial segment (AIS) [95], and propagate through the axon. They occur due to ions movement across the cell membrane through ion channels, that open or close due to neurotransmitters presence. In normal conditions, the cell membrane is at around -70 mV (resting potential), and it is said to be polarized. During APs, an influx of sodium ions (Na^+) makes the inside of the neuron more positive. When a threshold for this process is reached, a negative spike in the membrane external action potential is generated (membrane depolarization). This is then followed by a smaller positive spike generated by an outflux of potassium ions (K^+), which brings the membrane back to its polarized state (membrane repolarization).

2.2.3 Extracellular recordings: Multi-electrode arrays

APs can be detected through extracellular recordings. In 2D, direct culture of neuronal cells on arrays of electrodes allows for the analysis of the culture both at the network and at the single cell level [96], revealing the electrical dynamics behind neurotransmission. Electrophysiological analyses have also been proven to be extremely efficient in detecting the effect of external factors (e.g. drugs, electrical and chemical stimuli) on neuronal cells, and in giving reliable models for the investigation of neurodegenerative diseases. Recent advances in the field [97] brought to the creation of very sophisticated devices, comprising more than 26,400 electrodes in less than $3.85 \times 2.10 \text{ mm}^2$, which allow for the investigation of large neuronal cultures at the network, cellular, and sub-cellular level.

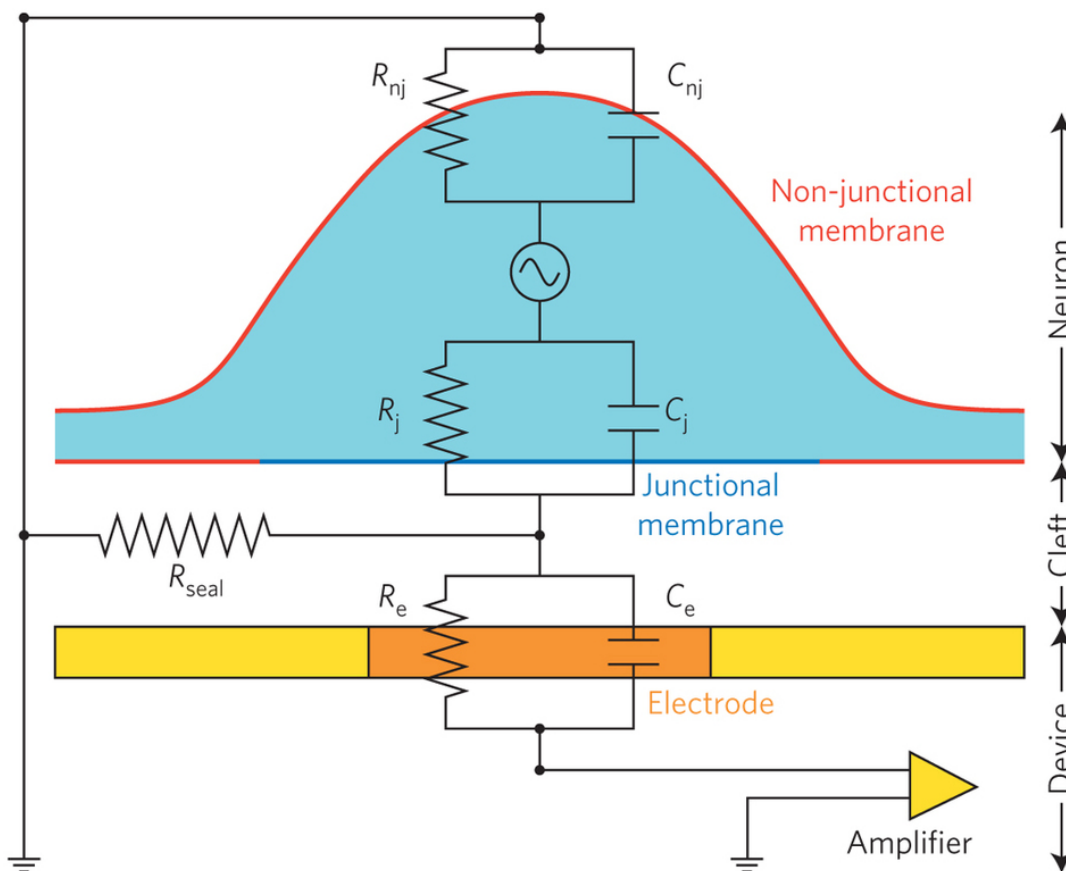


Figure 2.2: Schematic layout depicting the spatial relationship between the neuronal cell and the substrate-integrated electrode. (Adapted from [98])

2.3 Astrocytes as neurotransmission regulators

Although in the past years neuron loss in neurodegenerative diseases has been considered as a completely cell-autonomous process, recent studies investigated the role

that other CNS cells have in these disorders [99, 100, 101, 102, 103]. Astrocytes, especially, are necessary for neuronal homeostasis and are responsible for a range of fundamental regulatory functions, among which support of neuronal metabolic functions [104], clearance of neurotransmitters from the synaptic cleft following neuronal excitation [105], and axonal guidance and synaptogenesis regulation [106, 107], are of particular interest to drug discovery studies. If any of these functions incur into a malfunctioning, neuronal homeostasis can be profoundly disrupted, as well observable in acute and chronic neurodegenerative diseases [108, 109, 110]. The regulatory role of astrocytes on neuronal functions within a 3D in vitro neuronal network has to be considered to obtain a reliable model for translational studies. In particular, the ability of astrocytes to regulate glutamate metabolism and avoid excitotoxic damage to neuronal cells is fundamental for neuronal network homeostasis. As mentioned in the previous paragraph, in the process of neurotransmission, neurotransmitters are secreted into the synaptic cleft and interact with the target cell receptors. Eventually, neurotransmitters actions have to be terminated to avoid cell dysfunctions. They may be terminated passively (diffusion of the transmitter away from the synaptic region) or actively (uptake into the postsynaptic compartment, re-uptake of neurotransmitter via specific transporter proteins either on the pre-synaptic neuron or on glial cells). This is where the role of astrocytes becomes fundamental: they present transport systems for many neurotransmitters and, in particular, they are responsible of synaptically released glutamate removal. Astrocytes convert glutamate into the amino acid glutamine by the enzyme glutamine synthetase. Glutamine is released, together with ATP and D-serine, into the extracellular space (gliotransmitters release), and is then taken up by neurons, providing the necessary substrate for the synthesis of glutamate and γ -aminobutyric acid (GABA), respectively excitatory and inhibitory neurotransmitters. It has been shown that the calcium (Ca^{2+}) concentration increases in astrocytes are to be attributed only to metabotropic neurotransmitters (such as glutamate), which are, as mentioned above, released by the synaptic terminals during neuronal depolarization. These Ca^{2+} increases are what activates the gliotransmitters release [111, 112].

2.4 Neural stem cells differentiation

The examination of single neural progenitor cells brought to the discovery of neural stem cells, which are a subtype of progenitor cells (immature cells) in the nervous system that have the ability of self-renewing and generate glia and neurons [113]. The first studies brought to the isolation of stem-like cells from the embryonic mammalian CNS [114], but stem cells isolation was discovered to be possible from many regions of the embryonic nervous system. After the isolation in the embryo, stem-like cells were also obtained from the adult brain [115], being found in the two principal adult neurogenic regions, the hippocampus and the sub-ventricular zone (SVZ),

as well as in some non-neurogenic zones [116]. After isolation, the tissue is disaggregated and the dissociated cells are exposed to a high concentration of mitogens (e.g. fibroblast growth factor-2 (FGF-2) or epidermal growth factor (EGF)) in media. After a certain time in which cells proliferate, cells are either induced to differentiate by interrupting the exposure to the mitogens or by introducing another factor that induces cell development into specific lineages. In adherent cultures, stem cells isolated from the CNS produce large clones containing glia, neurons, and more stem cells. In non-adherent cultures, they can be cultured as multicellular floating neurospheres [117]. Differentiation is analyzed through staining with antibodies that interact with antigens specific for neurons, astrocytes, and oligodendrocytes. Studies on cells plated at low density allow to determine if a single cell can differentiate into the three phenotypes if exposed to different conditions [118, 119].

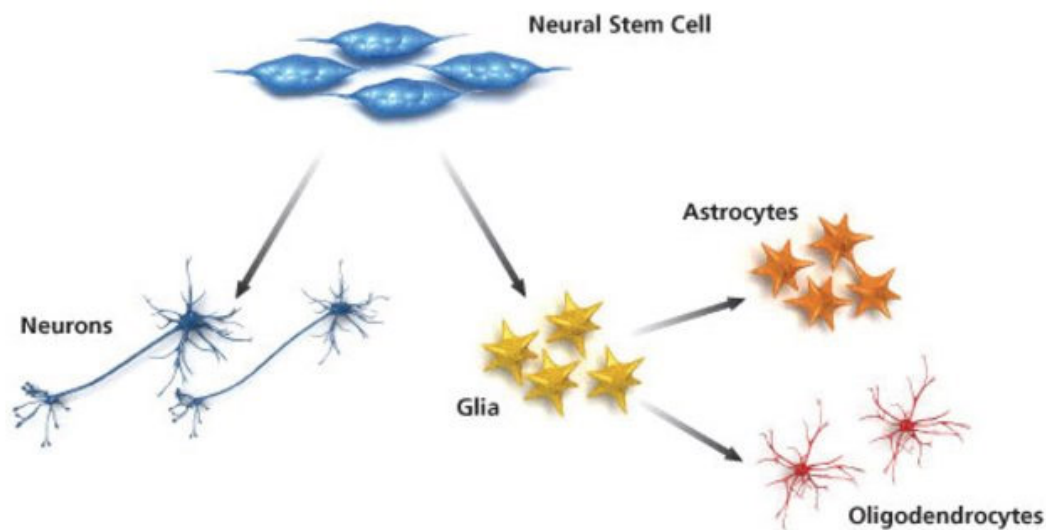


Figure 2.3: Differentiation of neural stem cells into neurons, astrocytes, and oligodendrocytes. (Credit: Sigma-Aldrich)

Chapter 3

Materials and methods

3.1 Gelatin Methacrylate (GelMA) synthesis

The medium level methacrylation GelMA was synthesized according to the procedure described in the following [120].

Day 0:

- Take 10 g Gelatin Porcine Skin, add 100 ml Dulbecco's phosphate buffered saline (D-PBS) (sterile) in a cleaned Erlenmeyer flask with magnet stirrer.
- Set undissolved mixture on heating plate, let it rotate (240rpm) at 50°C until gelatin is melted. Cover Erlenmeyer flask with aluminum foil for approximately 1 hour. Check every 15 minutes for temperature with a mercury thermometer to find exact calibration of the heating plate.
- When gelatin is melted (uniform solution, no more visible granula), add 1.25 ml Methacrylic Anhydride (MA) very slowly and drop-wisely (using a 1000 μ l pipette) and let emulsion rotate (240rpm) at 50°C for 2 hours, covered. In the meanwhile, prepare next step.
- Preheat 100ml of sterile D-PBS in Erlenmeyer to 50°C. Use this preheated D-PBS to dilute GelMA solution produced in the previous step (total final volume of the solution should be 200 ml). After mixing D-PBS with concentrated solution, leave the whole solution for 10 minutes at 50°C. In the meanwhile, prepare next step.
- Prepare dialysis membrane (Spectra/Por molecular porous membrane tubing, MWCO 12-14,000, Fisher Scientific) by cutting them in proper size (20-30cm). Immerse them into distilled water to soften them. Close one side by twisting the membrane end and making a knot. Examine by distilled water the membranes for any hole or defect.
- Transfer diluted GelMA with a funnel into the membranes. Close the second end of the membrane remembering to leave some extra space for air: this will allow better dialysis. Place the membranes into distilled water in 5 l plastic beaker.

- Let dialysis run at 40°C for at least 5 days with magnetic stirrer (approximately 500 rpm if possible), covering the beaker. Change water 2 times a day. Each time turn/flip upside down 5-6 times the membranes to homogenize the content. This step removes the toxic unreacted MA.

Day 5-7:

- Add 200 ml of ultrapure water (same amount as the gel in membranes) in an empty conical flask and add GelMA. Heat the solution for 15 minutes covered at 40°C.
- Prepare adequate number of 50 ml Falcon tubes, each will contain 25 ml of the solution.
- Optional step, if solution does not seem clean enough: first filtration step through a coffee filter (maintaining 40°C temperature is really important) and put the diluted GelMA back on heating plate before second filtration.
- Use sterile vacuum Express Plus (0.22 μm) Milipore filtration cup to filter the liquid.
- Transfer sterilized polymer into 50ml Falcon tubes. Store Falcons horizontally at -80°C for at least 2 days to make sure the whole gel is at the same temperature and have an optimal repartition in tube when gel will be lyophilized.
- The frozen GelMA is freeze-dried for 5 days. When the process is finished, remove caps and cover the Falcon tubes' opening with Kimwips secured with a rubber band.

3.2 Cell culturing protocols

All cell types described in the following were either purchased from the American Type Culture Collection (ATCC) or directly isolated. All cell culture flasks were incubated at 37°C in 5% CO₂.

3.2.1 3T3, MCF-7

The **3-day transfer, inoculum 3×10^5 cells (3T3)** is one of the standard fibroblast cell lines. These cells become confluent at a density of approximately 40,000-50,000 cells/cm². However, when cultured, complete confluency¹ should be avoided as this results in cells becoming senescent. They have a doubling time of 20-26 hours

¹Confluency is a term used to describe a relative measure of how many cells are attached to a flask bottom. For example, 50% confluency means that, when the culture is observed under the microscope, approximately half of the space contains growing cells. A confluent culture will exhibit very packed cells, with little or no space between them. At full confluency, cellular stress becomes excessive and inhibits growth. To avoid this, cell cultures should be sub-cultured at 80-90% confluency.

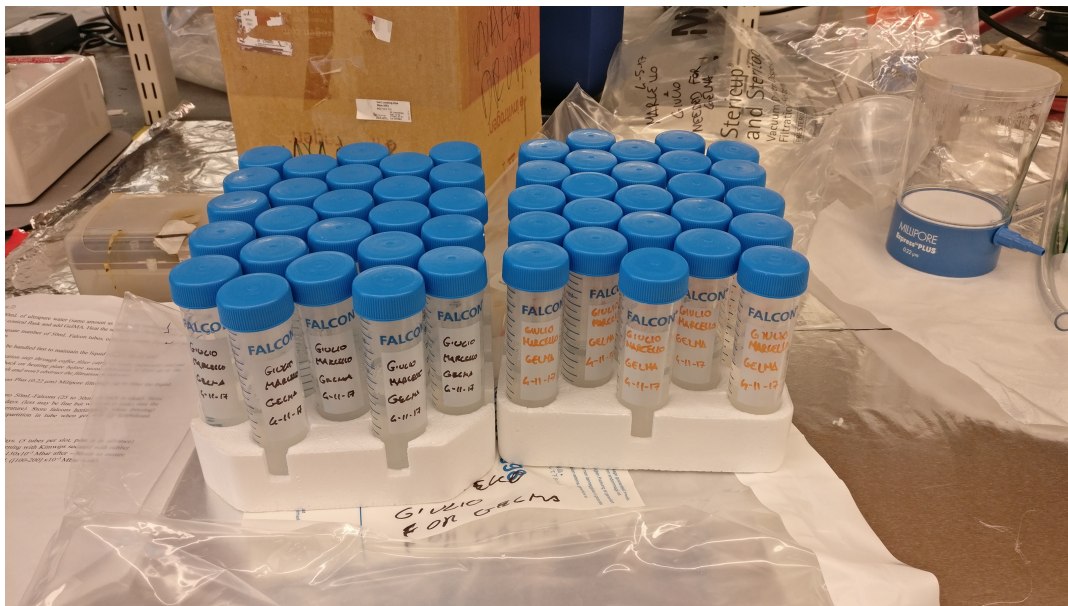


Figure 3.1: The final product: 50 Falcon tubes of GelMA were produced. The same batch of GelMA was used throughout the six months of experiments to minimize variability in the results.

and should be cultured in a plastic flask (Corning[®] T-25, T-75 or T-175 were used according to the different needs), as their adherence is not optimal to certain types of glass. The medium used for culturing 3T3 cells was Dulbecco's Modified Eagle Medium (DMEM) formulated with the addition of 10% Fetal bovine serum (FBS) and 1% penicillin/streptomycin (P/S).

The **Michigan Cancer Foundation-7 (MCF-7)** is a breast cancer cell line isolated in 1970, and it is the first mammary cell line that could be cultured for more than a few months [121]. Cell confluency should be maintained between 30-90%, as exceeding concentrations will decrease proliferation rates. The doubling time of MCF-7 cells is 30-40 hours. The medium used for culturing MCF-7 cells was Eagle's Modified Eagle Medium (EMEM), supplemented with 10% FBS, and 1% P/S.

The protocol for passaging (i.e. dividing in sub-cultures) these two cell types is the same, and was performed every 3 days:

- Remove medium, wash once with D-PBS to remove traces of serum from the cells, which contains proteins and divalent cations that can inhibit trypsin.
- Aspirate D-PBS, rinse cells with trypsin-Ethylenediaminetetraacetic acid (EDTA) (0.5% trypsin, 0.2% EDTA). EDTA is a calcium chelator which will remove the remaining divalent cations. Shake the flask gently to distribute uniformly the trypsin-EDTA.
- Incubate flask at 37°C for 1-5 minutes, checking for cell detachment. Shaking or tapping gently the flask favors the process.

- When cells are floating: add medium (2-3 times the volume of trypsin-EDTA) to neutralize the trypsin, avoiding damaging to the cells and viability reduction.
- Collect the suspension, put in a Falcon tube and centrifuge for 5 minutes at 1000 rpm.
- Aspirate the supernatant, carefully avoiding to touch the pellet of cells at the bottom of the Falcon tube.
- Add medium to the Falcon tube, mix well and split the solution in 3 new flasks of the same dimension.

3.2.2 PC12

The **adrenal phaeochromocytoma (PC12)** is a cell line originally isolated from a tumor in a rat's adrenal medulla in 1976 [122]. In the experiments, confluency was maintained at a maximum of 80%. PC12 were cultured in complete Roswell Park Memorial Institute (RPMI) 1640 medium supplemented with 10% horse serum (HS), 5% FBS, and 1% P/S. Murine Nerve Growth Factor (NGF), 2.5S, purified from male mouse submaxillary glands purchased from Promega was added (100 ng/ml) during the experiments to induce PC12 differentiation and neurite outgrowth [123]. PC12 are floating cells, therefore the passaging protocol differs from the one of 3T3 and MCF-7 as no trypsinisation is needed. Cells are centrifuged, old medium is aspirated, new medium is added, and the cell suspension is subdivided into 3 new flasks of the same dimension.

3.2.3 Astrocytes

Astrocytes were isolated from Day 1 mice according to the following protocol [124]:

- Prewarm 30 ml of astrocyte culture media (DMEM, high glucose + 10% FBS + 1% P/S to 37°C.
- Coat one T-75 flask with 20 ml of poly-D-lysine (PDL) at a concentration of 50 $\mu\text{g}/\text{ml}$ for 1 hr at 37°C in the 5% CO₂ incubator.
- Prepare surgical scissors, smooth fine forceps, flat tip forceps, paper towels, waste bag, 70% ethanol and 2 dissecting dishes (3.5 cm diameter) on ice filled with 2 ml of Hank's Balanced Salt Solution (HBSS) each.
- Reveal the skull through a mid-line incision along the scalp, and cut the cranium from neck to nose to allow access to the brain. Disconnect the cranium from the skull base.
- Using the flat tip forceps, the brain is extracted and put into the first dish, kept on ice.

- Under a stereomicroscope: remove olfactory bulbs and the cerebellum using the fine dissecting forceps. Retrieve the cortices grabbing the back of the brain with fine forceps, performing a mid-line incision between the hemispheres, and peeling away the plate-like structure of the cortex. Dissect the meninges from the cortex hemispheres with the fine forceps to avoid future contamination of astrocytes by fibroblasts and meningeal cells.
- Transfer the cortex hemispheres into the second dish, kept on ice.
- Cut the cortex hemisphere into small pieces using sharp blades.
- Under a sterile hood: transfer cortex pieces into a Falcon tube and add HBSS.
- Add 2.5% trypsin, and incubate the tissue in a water bath at 37°C for 30 minutes. Shake the Falcon every 10 minutes.
- Centrifuge for 5 minutes at 1000 rpm to obtain a pellet of cortex tissue pieces, and remove supernatant by decantation.
- Dissociate the tissue into a single cell suspension: add astrocyte plating medium and pipette vigorously using a 10 ml plastic pipette until the tissue is dissociated into single cells. Approximately $2-4 \times 10^6$ cells per brain should be obtained.
- Aspirate PDL from the T-75 flask and plate the cell suspension.
- Incubate at 37°C in the 5% CO₂ incubator.

Astrocytes were cultured in DMEM with the addition of 10% FBS and 1% P/S. The passaging protocol is the same as for 3T3 and MCF-7 cell types, with the exception that astrocytes grow quite slowly in comparison. Sub-culturing was therefore performed every 7-8 days, based on the observation of the confluency of the culture. Medium, on the other hand, was regularly changed every 3 days, simply aspirating the old one and replacing it with new medium.

3.2.4 NE-4C

The **neuroepithelial cell line (NE-4C)** is a neural stem cell line obtained from cerebral vesicles of 9-day-old mice embryos lacking the functional p53 genes². The population doubling time was observed to be approximately 12 hours. NE-4C were cultured undifferentiated in Minimum Essential Medium Eagle (MEM) with 10% FBS

²P53 (or TP53) is a tumor suppression gene. In the healthy cell, p53 correctly behaves as a DNA-binding protein, and has the effect of stimulating another gene to produce the p21 protein, which interacts with a protein (cdk2) responsible for stimulating cell division. When p21 associates with cdk2 the cell cannot pass through to the next stage of cell division. On the other hand, mutant p53 does not carry out its DNA-binding functions correctly, and therefore the p21 protein is not made available to inhibit cell division. Thus cells divide uncontrollably, and form tumors.

and 1% P/S, whilst differentiation to astrocytes and neurons was obtained culturing them in DMEM, 10% FBS, 1% P/S and DMEM, 10% FBS, 1% P/S, 1 μ M retinoic acid [125, 126, 127]. Passaging of undifferentiated cells was conducted in a peculiar way, as this cell type can be either floating or attach to the flask. The supernatant, containing a portion of the cells, was removed and kept in a Falcon tube. The cells attached were treated following the same standard protocol used for 3T3, MCF-7 and astrocytes. The final cell suspension was added to the one containing the floating cells and initially transferred into the Falcon tube, and the complete suspension was then sub-divided between the new flask to maintain culture uniformity. Passaging of differentiated cells followed the standard aforementioned protocol.

3.3 GelMA solution and supporting bath

The supporting bath was synthesized following these steps:

- Get two 15 ml Falcon tubes and cover one in aluminum foil.
- Calculate right amount of Calcium chloride (CaCl_2) (22 mM), photo-initiator (PI)³ (0.5%wt) and GelMA(10%wt) for stock solution. It will be diluted to the desired amounts of 11 mM CaCl_2 , 0.25%wt PI and 5%wt GelMA when mixed with the cell suspension.
- Put CaCl_2 in the uncovered Falcon tube.
- Put GelMA and PI in the covered Falcon tube.
- Add right amount of media to uncovered Falcon tube under the hood, mix well, than transfer it to the covered one with a 5 ml syringe, filtering it with a sterile filter. Lights should be kept switched off to avoid initiating an unwanted crosslinking of the solution.
- Vortex for 2 minutes.
- Put in 80 degrees oven for 55 minutes.
- Take solution out of the oven and either use it straight away or put directly in the fridge to avoid material degradation. The solution can be used up to two days after synthesis.

3.4 Bioinks

Different inks were tested in order to obtain the best results in terms of cell viability and proliferation. Moreover, additional recipes were tried to obtain conductive inks for carrying out an electrical analysis of the developed neuronal network. For all the bioinks tested the concentration was 15×10^6 cells/ml.

³2-hydroxy-1-[4-(2-hydroxyethoxy)phenyl]-2-methyl-1-propanone (Irgacure 2959, Sigma-Aldrich): it is added to allow for Ultra-Violet (UV) curing of the GelMA solution.

3.4.1 5%wt gelatine, 2%wt alginate

Gelatin from porcine skin and alginic acid from brown algae were both obtained from Sigma-Aldrich. Bioink was synthesized through the following steps:

- Put 1 ml HBSS, 10% FBS, 5%wt gelatin, 2%wt alginic acid in a sterile eppendorf tube under a sterile hood.
- Put 1 ml DMEM, 5%wt Gelatin, 2%wt Alginic acid in a second sterile eppendorf tube under a sterile hood.
- Leave both eppendorfs at 80°C for 2 hr, checking every 30 minutes for dissolution of alginic acid and gelatin.
- When dissolution is completed: suspend desired amount of cells in 50 μ l of DMEM in an eppendorf tube.
- Add to cell suspension 500 μ l from each eppendorf to obtain 1 ml of bioink in total.

This bioink was used for all cell types, with the following modifications:

- For 3T3 and MCF-7: no modifications.
- For PC12: DMEM was substituted with RPMI 1640, and 1 μ l/ml of NGF was added to the final solution to induce PC12 differentiation and neurites outgrowth.
- For NE-4C: DMEM was substituted with MEM, and 1 μ M of retinoic acid was added to induce differentiation into neurons.

3.4.2 1%wt alginate

A similar bioink, based on a recent study by R. Dreher and B. Starly [128], was tailored for PC12 cells through the following steps:

- put 1 ml DMEM, 1%wt alginic acid in a sterile eppendorf tube and leave it at 80°C for at least 2 hr, always checking on Alginic acid dissolution.
- Suspend cells in 50 μ l DMEM in an eppendorf tube and mix it with the alginate solution.
- Add 1 μ l of NGF to the final solution.

3.4.3 7%wt GelMA High Methacrylation (MA), 5mg/ml multi-walled carboxylic acid functionalized carbon nanotubes (MWCNT-COOH), 0.5%wt PI

This bioink was specifically developed to obtain electrically conductive bioprinted fibers and characterize electrically the developed neuronal network. MWCNT were

purchased from Sigma-Aldrich. The bioink development can be divided in two steps:

Synthesis of MWCNT stock solution (4 ml)

- Put 20 mg of MWCNT, 80 mg of GelMA (7%wt, high MA), 100 μ l deionized water (DI) in a vial and add 4 ml D-PBS (everything should be done under the chemical hood).
- Vortex until solution is uniform.
- Leave at 80°C for 10-15 minutes.
- After having cleaned thoroughly the Ultrasonicator with ethanol 70% (15 minutes) and DI (15 minutes), ultrasonicate the MWCNT stock solution for 1 hr at 25% amplitude with 2 s pulses and pauses of 1 s between each pulse until the solution does not show any aggregations.

Ink synthesis

- Move desired volume of stock solution to an eppendorf tube covered in aluminum foil.
- Add 0.5%wt PI to the solution.
- Vortex until PI is dissolved.
- Leave bioink at 80°C for 1 hr.
- Suspend cells in 50 μ l DMEM in an eppendorf tube and mix it with the MWCNT bioink.

3.5 Bioprinting

For all the experiments, a modified version of a commercially available bioprinter (Organovo) was used.

3.5.1 Printing strategy

Polydimethylsiloxane (PDMS) molds (See Figure 3.2) with a hollow chamber of 10x10x5 mm³ in size were made to host the GelMA solution during printing. 24 hr before the experiment they were put in 70% ethanol and left overnight in a petri dish under a sterile hood to assure a sterile condition.

On the day of the experiment, the PDMS molds were thoroughly washed with sterile D-PBS (at least 3 times) and left in sterile D-PBS until the experiment was ready to start. The experiment followed the subsequent steps:

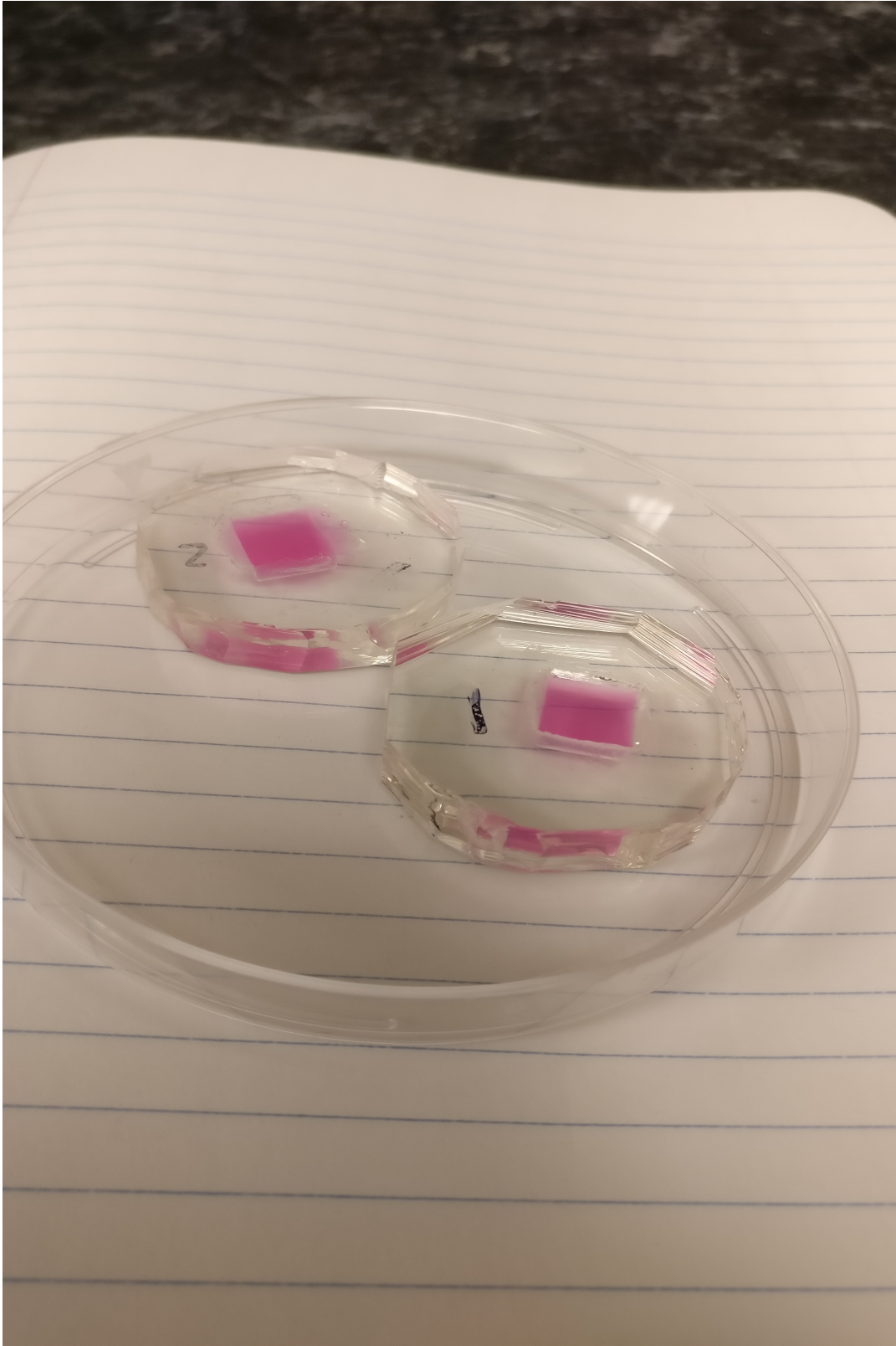


Figure 3.2: PDMS molds containing the uncured GelMA solution.

- UV machine was calibrated and warmed up, letting it run at the desired power for at least 15 minutes.

- Cells were detached from culture flasks and a suspension with the desired concentration was obtained.
- Bioinks were kept at 80°C in the oven.
- GelMA solution was taken out of the fridge and put for 10 minutes at 80°C in the oven.
- GelMA was taken out of the oven, cooled down and rapidly added to the cell suspension to obtain the final concentration desired (8×10^6 cells/ml).
- After gentle mixing to avoid damage to the cells, 500 μ l of the final solution were added to each mold.
- Molds were put in petri dishes and kept at 4°C for 15-20 minutes.
- Bioinks were taken out of the oven, cooled down, and mixed with the cell suspension.
- Bioprinting needles and microtubes were washed 3 times with 70% ethanol and 3 times with D-PBS.
- Bioinks were transferred to a 1 ml syringe and kept at 37°C through a small heated case. Proper flow rate and printing velocity were set.
- Molds were taken to the bioprinter and bioinks were injected into the GelMA bath.
- Structures were crosslinked under UV light.
- Once proper curing was obtained (For comparison, see Figures 3.3, 3.4), the structures were extracted from the molds under a sterile hood and put into a 24 well plate, washed with D-PBS and covered with media.
- On the following day: media was removed, the structures were washed with D-PBS, and new media was added.

3.6 Samples culturing protocols

Samples were cultured for 14 days, changing media regularly every 2 days, adding NGF in cultures containing PC12 and retinoic acid in those containing NE-4C.

3.7 Imaging

In order to monitor culture development, a series of imaging techniques was employed. For both fluorescence and confocal microscopy a series of staining protocols were adopted, which will be treated in the following paragraphs.

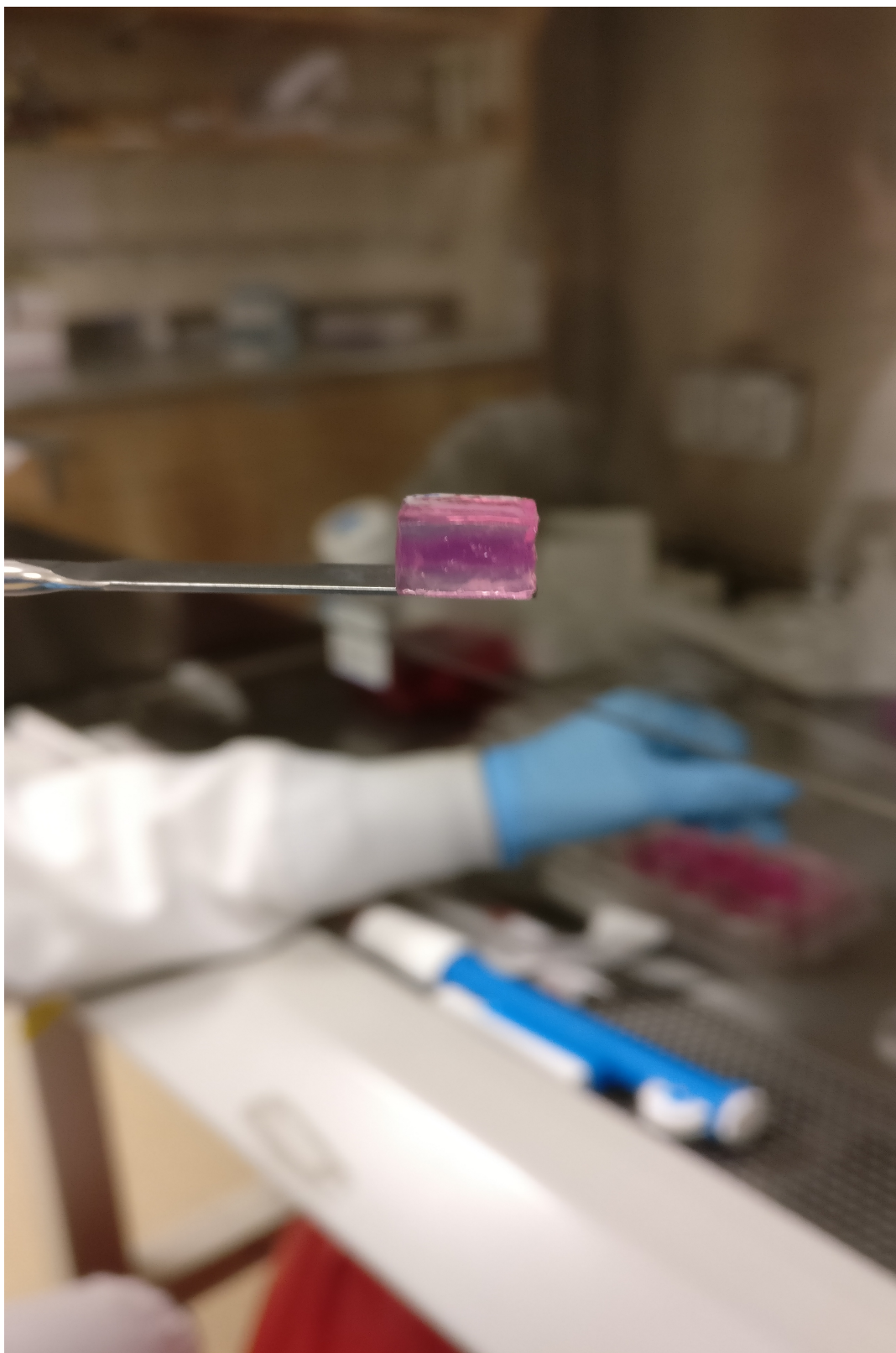


Figure 3.3: One of the structures after removal from the mold: in this particular case, full crosslinking could not be obtained, as it can be evinced by the dark-purple color that characterize the middle section of the cube.

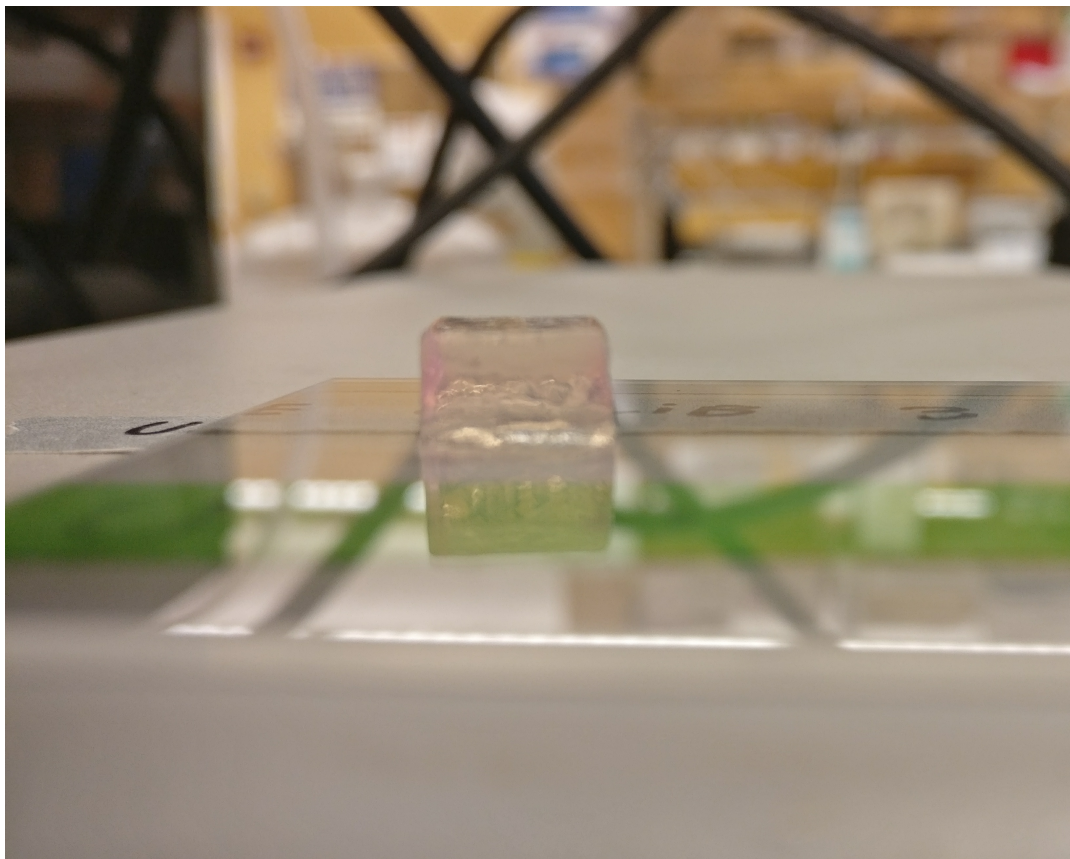


Figure 3.4: A fully-cured structure, distinguishable by the full transparency of its texture.

3.7.1 Fluorescence microscopy

The benchtop microscope of choice for imaging was a Zeiss Axio Observer D1 microscope, equipped with an AxioCam MRm Rev.3 camera (Carl Zeiss), a Long working Distance (LD) A-Plan 10X objective with a 0.25 Numerical Aperture (NA), and an LD Plan-Neofluar 20X objective with a 0.4 NA. Apart from normal bright field, fluorescent imaging was carried out on the samples to obtain data on cell morphology and viability, and to check on neurite extension in the case of neuronal cells.

3.7.2 Confocal microscopy

The confocal microscope was CSU-X1 (Yokogawa) equipped with a Zyla 5.5 camera (Andor) and a 20X objective with an NA of 1.15. It was used to obtain 3D imaging of the samples developed and assess the goodness of the printing strategies.

Immunostaining: Alexa Fluor 488 phalloidin[®]/Alexa Fluor 594 phalloidin[®]/ 4',6-Diamidino-2-phenylindole dihydrochloride (DAPI)

Cell morphology for 3T3 and MCF-7 was studied through immunostaining. Phalloidin is a bicyclic peptide, and belongs to a family of toxins isolated from the *Amanita phalloides* mushroom. It is commonly used in imaging applications to selectively

label filamentous-actin (F-actin). F-actin is usually stained using one of the two different most common stains: Alexa Fluor 488 phalloidin[®] (green) and Alexa Fluor 594 phalloidin[®] (red). The excitation and emission wavelengths are 495 and 518 nm respectively for the first one, 581 nm and 609 nm for the second one. DAPI is a blue-fluorescent DNA stain that shows an approximate 20-fold fluorescence enhancement when binding to AT regions of double-stranded DNA (dsDNA). The excitation and emission wavelengths are 358 and 461 nm respectively. It is commonly used as a nuclear counterstain in fluorescence microscopy. The staining protocol was the following:

- Remove the media.
- Wash by D-PBS 1 time, enough to have coverage of the sample.
- Add 4% Paraformaldehyde (PAF)⁴ solution in D-PBS, check for good coverage of the sample. Wait for 20 minutes.
- Remove PAF and wash by D-PBS 1 time.
- Add 0.1% Triton-X 100⁵ in D-PBS for 10 minutes.
- Remove Triton-X 100 and wash by D-PBS 3 times for 5-10 minutes each.
- Prepare in a darkroom a solution of Alexa Fluor 488 phalloidin[®] or Alexa Fluor 594 phalloidin[®] (1:40) and DAPI (1:500) + 1%wt Bovine Serum Albumine (BSA)⁶ solution in D-PBS. Vortex to make BSA dissolve.
- Add the solution on the sample covered with aluminum foil and incubate at room temperature for 1hr - 1.5 hr.
- Remove and wash by D-PBS 3 times, 5 minutes each.
- Add fresh D-PBS.

⁴This step is done to fix cells. Fixation stops any biochemical reactions, increases the mechanical strength and the stability of the tissue under examination, and therefore allows to preserve cells and tissue components. PAF is widely used for this purposes in cell immunostaining: it generates covalent cross-links between cells molecules, creating an insoluble mesh. Moreover, cells fixed with PAF become permeabilized, allowing the antibodies necessary for staining to access the intracellular structures. Without this step, the intracellular structures would diffuse away before the end of the antibody incubation.

⁵Triton-X 100 is a detergent used to improve the penetration of the antibody. It solvates cellular membranes without disturbing protein-protein interactions.

⁶BSA addition is optional when only one cell type is present. It is used to avoid non-specific binding: when antibodies are added, they bind to the protein of interest, but also to other non-specific proteins. This could lead to undesired background staining. BSA blocking saturates the non-specific proteins and allows for a more precise staining and a clearer imaging.

Ethidium homodimer-1 (EthD-1)/Calcein acetoxymethyl ester (Calcein/ acetoxymethyl (AM))

Cell viability was investigated through staining with EthD-1 and Calcein/AM (Live/Dead™ assay). The cell-impermeant viability indicator EthD-1 is a high-affinity nucleic acid stain. It is weakly fluorescent until bound to DNA. It emits red fluorescence, with excitation and emission wavelengths of 528 and 617 nm respectively. Calcein AM is a cell-permeant dye used to determine cell viability in eukaryotic cells. If alive cells are exposed to non-fluorescent calcein AM, acetoxymethyl ester hydrolysis by intracellular esterases converts the non-fluorescent calcein to a green-fluorescent calcein. The excitation and emission wavelengths are 495 and 515 nm respectively. The steps are the following:

- Switch off the light in the sterile hood and prepare a solution of 2 $\mu\text{l}/\text{ml}$ of EthD-1 and 0.5 $\mu\text{l}/\text{ml}$ of calcein/AM in a Falcon tube covered with aluminum foil.
- Remove media and wash samples with D-PBS.
- Add EthD-1 and calcein/AM solution to the samples, wrap aluminum foil around the well plate to protect it from direct light, and incubate for 25 minutes.
- Aspirate solution and wash samples with D-PBS for 2 times.
- Add enough fresh D-PBS to have coverage of the samples.
- For imaging: first, excite with blue wavelength to obtain imaging of live cells (green). Then, excite with green wavelength to obtain imaging of dead cells (red). Finally, superimpose the two images to count live and dead cells.

Localization of glial fibrillary acidic protein (GFAP) and beta-III tubulin

This particular staining involves detection of specific markers for astrocytes (GFAP) and neuronal cells (beta-III tubulin). GFAP can be found in glial cells such as astrocytes and ependymal cells. The gene GFAP encodes an intermediate filament protein (50kDa) of mature astrocytes, which may be used as a marker for distinguishing astrocytes from other glial cells. Immunohistochemical staining for GFAP is a standard procedure for visualizing reactive astrocytes. Beta-III tubulin is a microtubule element of the tubulin family. It is found almost exclusively in neurons, and plays a vital role in nervous system development and axon guidance. The staining protocol is slightly more complicated than the ones previously mentioned, as it involves the use of a primary antibodies (PA), rabbit anti-rat and rabbit anti-mouse, which allow for the localization of GFAP and beta-III tubulin respectively. After incubation, secondary antibodies (SA), goat anti-rabbit (Invitrogen Alexa Fluor® 594, Thermo

Fisher) and goat anti-rabbit (Invitrogen Alexa Fluor[®] 488, Thermo Fisher), are introduced. The SA binds with the PA and allows for fluorescence imaging. The protocol is the following:

- Remove the media.
- Wash by D-PBS 1 time, enough to have coverage of the sample.
- Add 4% PAF solution in D-PBS, check for good coverage of the sample. Wait for 20 minutes.
- Remove PAF and wash by D-PBS 1 time.
- Add 0.1% Triton-X 100 in D-PBS for 10 minutes.
- Remove Triton-X 100 and wash by D-PBS 3 times for 5-10 minutes each.
- Prepare in a darkroom a solution of primary antibodies (1:250) and 10%wt BSA⁷ solution in D-PBS. Vortex to make BSA dissolve.
- Add the solution on the sample covered with aluminum foil and incubate overnight at 4°C.
- Prepare SA solution: secondary antibodies (1:100), DAPI (1:200) in D-PBS.
- Remove PA solution and wash by D-PBS 3 times, 5 minutes each.
- Add SA solution and incubate for 1.5-2 hr at 4°C.
- Remove SA solution and wash by D-PBS 3 times, 5 minutes each.
- Add fresh D-PBS.

3.8 Samples and processes characterization

The developed structures were characterized on the basis of the mechanical properties, the viability and proliferation of the encapsulated cells. The printing processes were tested in order to develop optimal printed constructs and minimize damaging to the cells.

3.8.1 Mechanical tests

Mechanical tests were carried out with a 5940 Series Single Column Table Top Systems for Low-Force Mechanical Testing (Instron[®]). Compressive tests were run to analyze the structures in terms of stiffness and extrapolate the compressive modulus.

⁷The higher concentration of BSA is needed to limit as much as possible non-specific staining, as multiple antibodies are involved in this process.

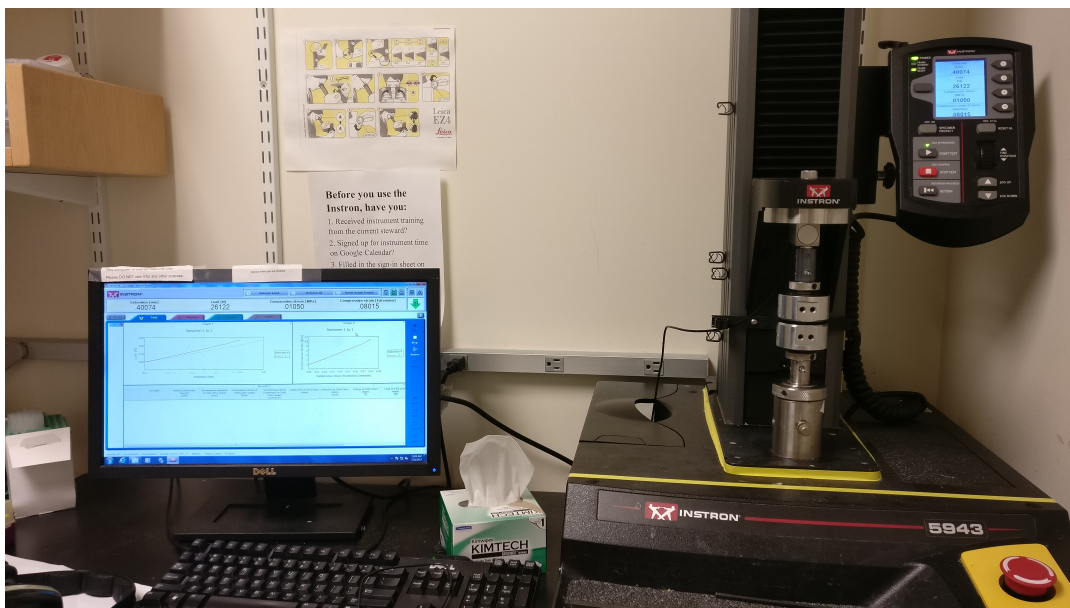


Figure 3.5: The setup for mechanical testing. The structures were loaded between the two sections, and compressive tests were carried out.

3.8.2 Cell viability assays

Live/Dead™

As mentioned above 3.7.2, Live/Dead™ assay was carried out on the samples to quantify cell viability during the culturing process.

3.8.3 Cell proliferation assays

PrestoBlue™

PrestoBlue™ cell viability reagent (purchased from Thermo Fisher) was used for testing cell proliferation in the developed structures. Viable cells maintain a reducing environment within their cytosol. PrestoBlue™ cell viability reagent uses this reducing ability to measure quantitatively cell proliferation, therefore being a valuable assay for cell relative viability during culture. PrestoBlue™ reagent is a resazurin-based solution. It works as a cell viability indicator, using the reducing power of living cells to give quantitative data on the proliferation of cells. It contains a cell-permeant compound, blue in color, which does not express fluorescence. When added to cells, the reagent is modified by the viable cells reducing environment, turning red and becoming highly fluorescent. The magnitude of this change can be detected using fluorescence or absorbance measurements. For the experiments, the protocol adopted was the following:

- The 10X stock solution is diluted in ratio 1:9 in D-PBS.
- Media is removed from the well plate.

- Diluted solution is added to the wells without exposing it to direct light.
- Well plate is incubated for 2 hr, covered in aluminum foil to avoid illumination of the samples.
- Well plate is taken out of the incubator and solution is transferred into a 96 well plate.
- Absorbance is analyzed through a plate reader (BioTek Instruments).

3.8.4 Electrical characterization

For electrical characterization, the structures were printed following the same protocols mentioned above 3.5, with the only difference that cells were encapsulated in thin (approximately 100 μm) layers of hydrogel. These thin layers were then clamped (in order to promote the connection between the fibers and the array) on top of a High Density Multi Electrode Array (HD-MEA) (See Figure 3.6) provided by Maxwell Biosystems, a spin-off company of ETH-Zurich, , and cultured for 7 days. Electrophysiology analysis of the developed network was carried out. Unfortunately, this experiment could only be run once, as it was part of a demo recording which envisaged a future collaboration. Nonetheless, the results obtained will be presented in the following chapter, whilst the future work will be discussed in the final one.

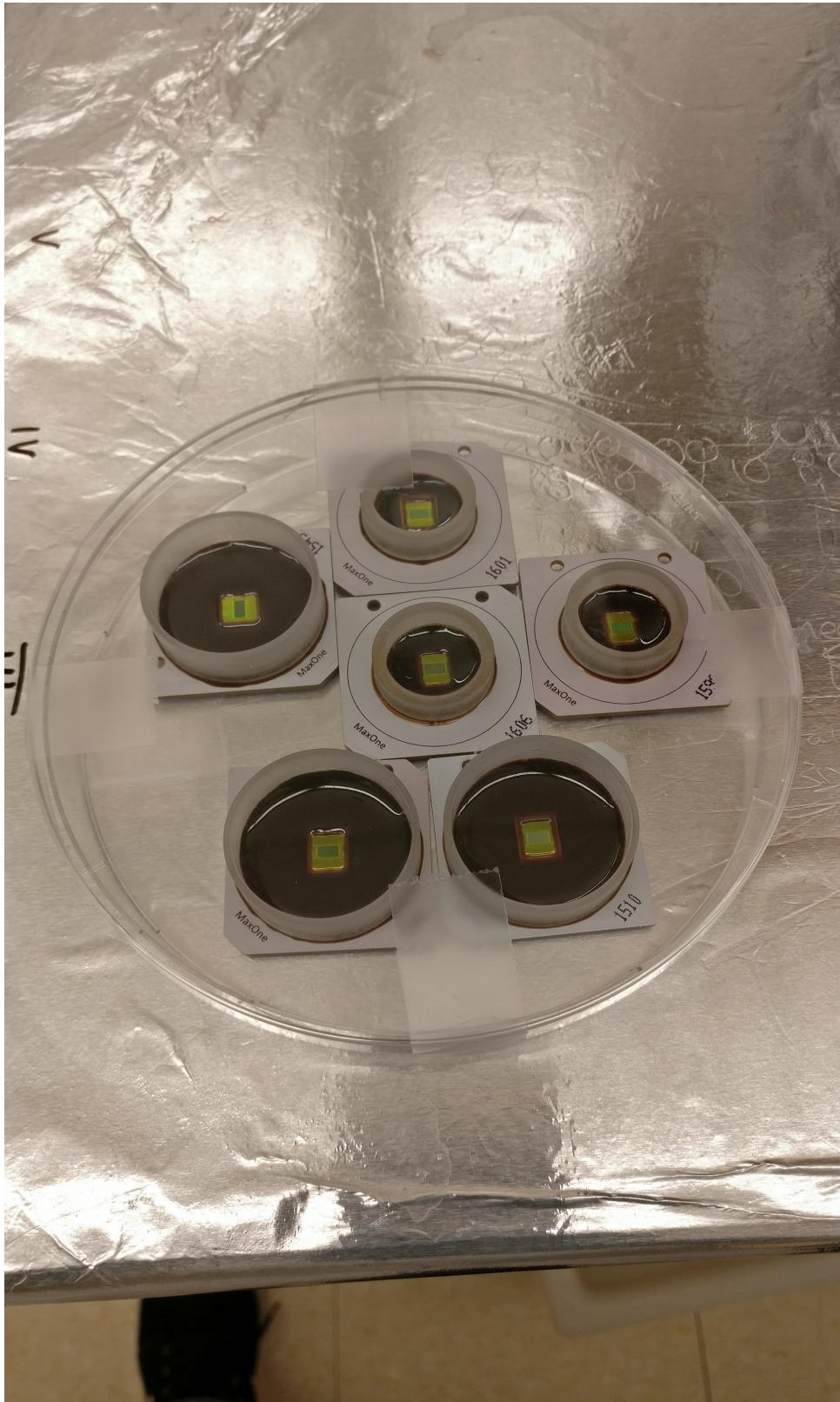


Figure 3.6: The HD-MEAs provided by Maxwell Biosystems.

Chapter 4

Results

4.1 Tests for 2D cultures

4.1.1 Astrocytes expression

Astrocytes isolated from 1-day-old rat brains were cultured in DMEM + 10% FBS + 1% PS and checked for correct development. Figure 4.1 shows passage 1 (P1) astrocytes at confluency in the well, stained for a specific marker (GFAP). Their characteristic star-like shape can be clearly observed, proving the success of the culturing protocol.

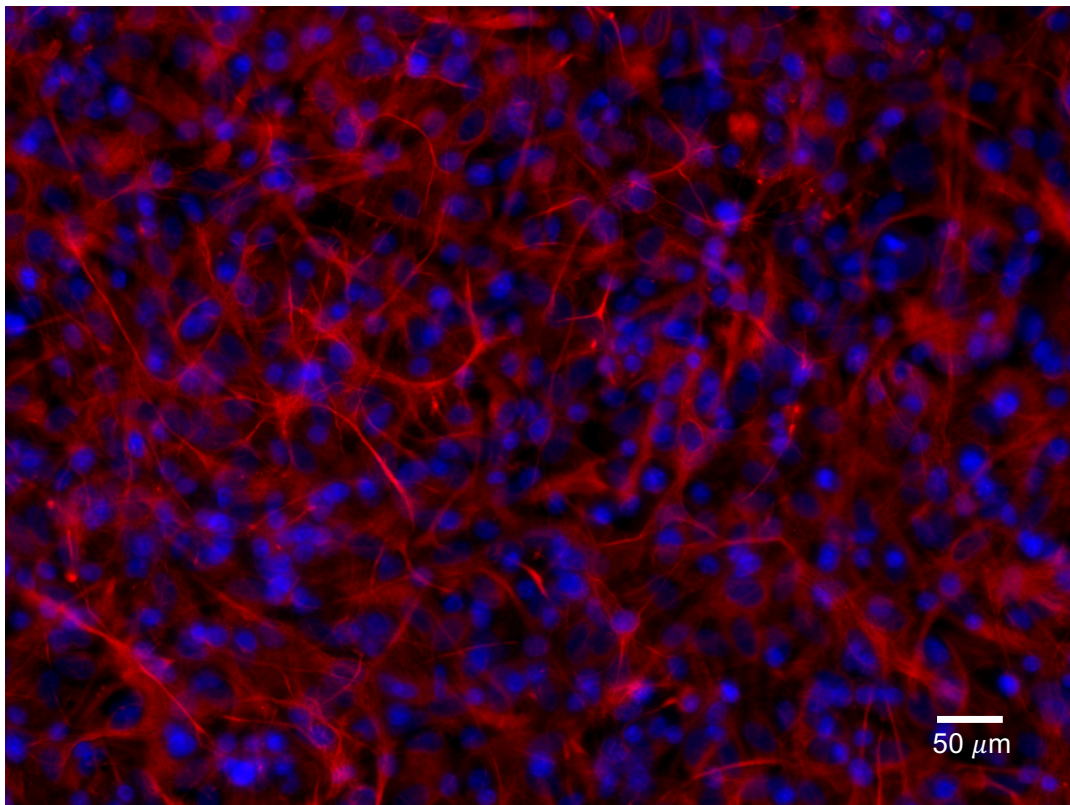


Figure 4.1: GFAP-staining of astrocytes isolated from 1-day-old rat brains (P1) at confluency.

4.1.2 PC12 differentiation

PC12 were tested for differentiation through the exposure to NGF. The medium used for differentiation was DMEM containing 1% horse serum, 1% P/S and 100ng/ml NGF. Cells were cultured on fibronectin-coated tissue culture polystyrene (TCPS) and checked for neurite outgrowth. Figure 4.2 shows the results after 7 days of culturing. Differentiated neuron-like cells were labeled with neuron-specific mouse anti-beta-III tubulin (green) and DAPI (blue).

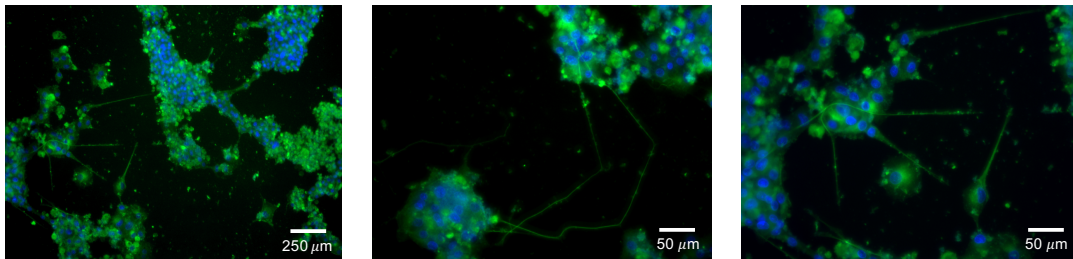


Figure 4.2: PC12 cultured on fibronectin-coated TCPS after 7 days of incubation. Green: neuron-specific mouse anti-beta-III tubulin; blue: DAPI. The long strands are neurites extending out of the cell bodies.

4.1.3 NE-4C differentiation

NE-4C cells were tested for differentiation under different conditions in order to understand their ability to give rise to astrocytes and neurons. Differentiation into astrocytes was tested with the following conditions:

- MEM + 1% P/S
- DMEM + 1% P/S
- DMEM + 10% FBS + 1% P/S

Differentiation into neurons was tested with the following conditions:

- MEM + 1% P/S + 1 μ M retinoic acid
- DMEM + 1% P/S + 1 μ M retinoic acid
- MEM + 10% FBS + 1% P/S + 1 μ M retinoic acid
- DMEM + 10% FBS + 1% P/S + 1 μ M retinoic acid

Figures 4.3, 4.4, 4.5, 4.6, 4.7, 4.8, 4.9 show how the cultures under test developed throughout the days. It can be observed that the lack of FBS led to a significant decrease in cell viability in all the cultures under test, regardless of the variation in the main medium used (See Figures 4.3, 4.4, 4.6, 4.7). The introduction of FBS in DMEM led to differentiation into astrocytes (see Figure 4.5), whilst the presence of retinoic acid in MEM and DMEM led to differentiation into neuron cells (see Figure 4.8,

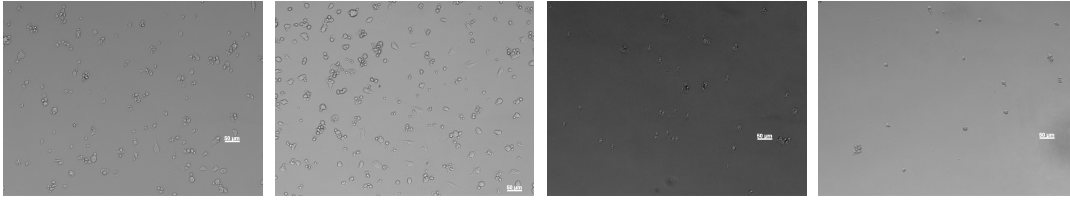


Figure 4.3: Evolution of NE-4C culture exposed to MEM (Day 4, 7, 10, 13).

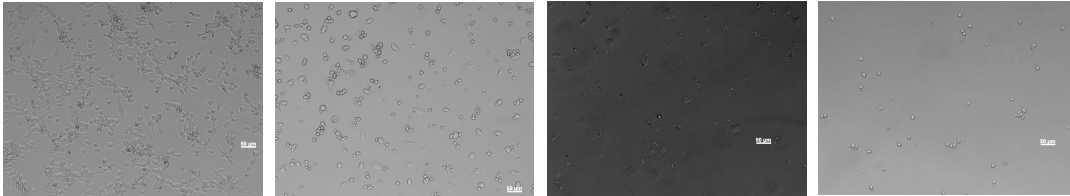


Figure 4.4: Evolution of NE-4C culture exposed to DMEM (Day 4, 7, 10, 13).

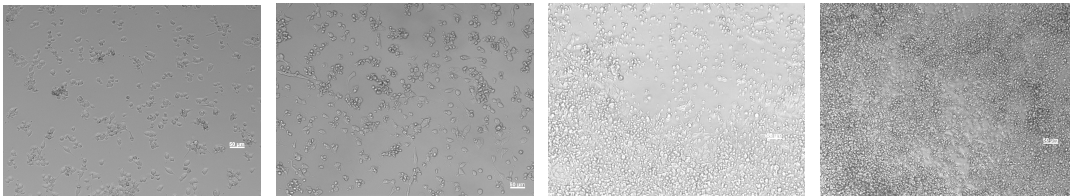


Figure 4.5: Evolution of NE-4C culture exposed to DMEM + 10% FBS (Day 4, 7, 10, 13).

4.9). Unfortunately, the presence of FBS made the cultures overconfluent before the end of the experiment, making it impossible to distinguish cells on day 13.

Nonetheless, until day 10 the characteristic star-like shape of astrocytes was fully recognizable (See details in Figure 4.10), whilst the presence of neurites was detected for the cells differentiated into neurons (See details in Figure 4.11).

These preliminary data were considered sufficient for trying to differentiate the cells while encapsulated in a 3D environment, as the supporting literature also confirmed the goodness of the procedure.

4.2 Recreating the brain environment

4.2.1 Optimization of mechanical properties and printability

The development of a hydrogel-based 3D bioprinting approach that allows for the printing of shear-thinning hydrogel bioinks directly into self-healing supporting baths was achieved through a series of optimization steps, which will be discussed in the following paragraphs.

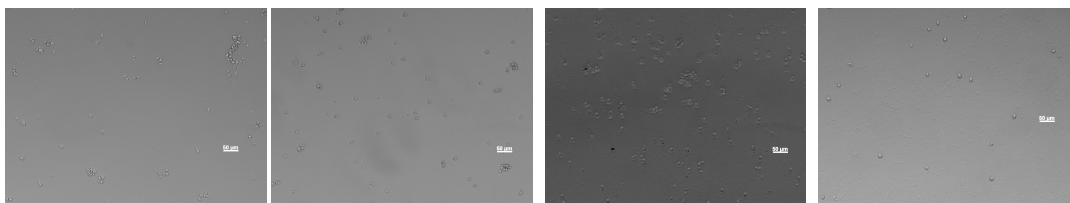


Figure 4.6: Evolution of NE-4C culture exposed to MEM + retinoic acid (Day 4, 7, 10, 13).

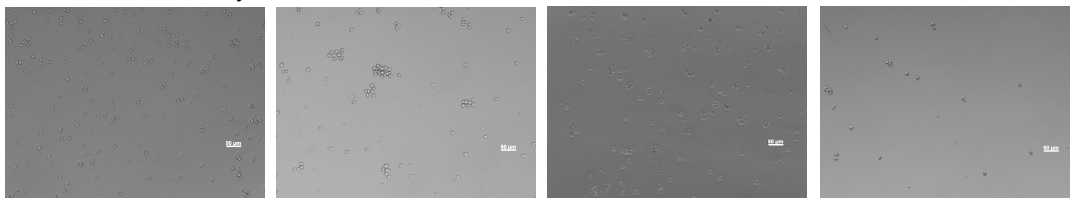


Figure 4.7: Evolution of NE-4C culture exposed to DMEM + retinoic acid (Day 4, 7, 10, 13).

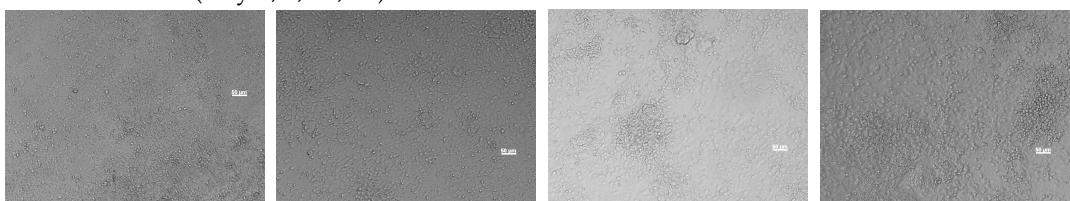


Figure 4.8: Evolution of NE-4C culture exposed to MEM + 10% FBS + retinoic acid (Day 4, 7, 10, 13).

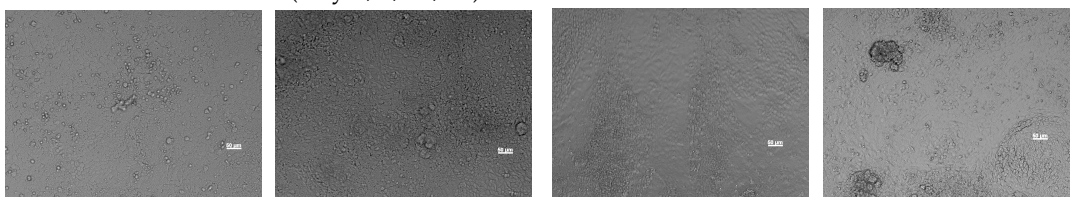


Figure 4.9: Evolution of NE-4C culture exposed to DMEM + 10% FBS + retinoic acid (Day 4, 7, 10, 13).

GelMA concentration in the bath

The hydrogel formulation used for the bath was selected from a set of possible options¹ that, according to the degree of polymer modification and concentration in the solution, exhibit the desired mechanical properties (stiffness, shear- thinning and self-healing behavior). The final concentration of GelMA in the solution was selected on the basis of a set tests on intercorrelated parameters, which will be here discussed. Since the structure is crosslinked through UV exposure, a series of tests on gel crosslinking for different exposure times and distances from the source was carried out. As it can be observed in Figure 4.12, at a fixed power of 800 mW/cm^2 ² and at a distance of 5 cm from the light source, it was found that 60 s was the minimum exposure time to induce chemical GelMA gel formation of solutions with 3 - 5%wt GelMA (for samples of dimension $10 \times 10 \times 5 \text{ mm}^3$).

¹A.1

²This low UV power was chosen in order to avoid excessive cell damaging during crosslinking.

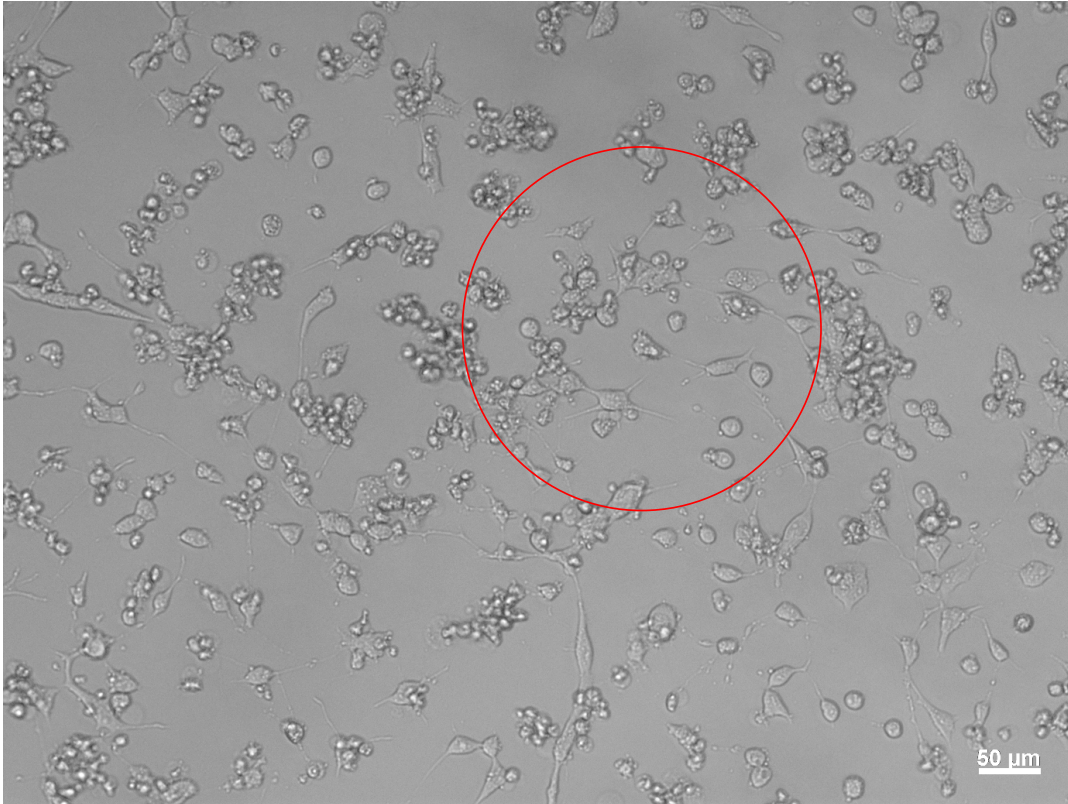


Figure 4.10: NE-4C differentiation: astrocytes star-like shape on day 7 after introduction of FBS.

Compressive tests were then carried out on fully crosslinked samples in order to extrapolate their compressive modulus. As shown in Figure 4.13, the compressive modulus of samples made with 5%wt GelMA is comparable with that of the actual human brain, whilst the other concentrations are well below that range. 5%wt GelMA was therefore chosen as the ideal concentration on which the following tests were to be performed, as it was assumed that astrocytes and neuronal cells would express more reliable phenotypes, morphology, and behavior in an environment whose mechanical characteristics were as close as possible to those of the actual brain.

4.2.2 Self-healing and shear-thinning behavior

The direct writing of hydrogels was possible because of their non-covalent, reversible bonds: they can be disrupted applying a physical stimulus such as shear stress, and are restored rapidly upon removal of the stimulus. These properties allowed for their use as injectable hydrogels, therefore being exploitable as bioinks in extrusion-based bioprinting [129, 130], but also as supporting baths: the hydrogel forming the supporting bath deformed when the syringe needle connected to the bioprinter was inserted to inject the bioink, allowing to accommodate the extruded material, and self-healed within a short time, therefore allowing to maintain material localization (See Figure 4.14).



Figure 4.11: NE-4C differentiation: neurites outgrowth on day 10 after exposure to retinoic acid in DMEM.

In figure 4.14, the oscillatory stress model shows the storage modulus (G') of the 5%wt bath as much higher than those of the printed bioinks, suggesting that the 5%wt GelMA as a bath has the ability to maintain the fiber structure after printing. Likewise, the printed ink maintained the printed structure within the support gel (See Figure 4.15).

Therefore, this writing process allowed for the printing of bioinks into any position within a 3D space initially occupied by the supporting hydrogel bath. These self healing and shear-thinning behaviors were assessed through mechanical testing (See Figures 4.16, 4.17)

Figure 4.16 shows the result of a scratch assay, whilst 4.19 shows the results of oscillatory strain sweeps on the bath. These two assays prove the self-healing behavior of GelMA.

In Figure 4.18 the curve depicts the usual behavior of shear-thinning materials subjected to mechanical stress, therefore validating the hypothesis. The same test was run on all the other concentrations (2.5-4.5%wt) of GelMA, and in presence and in absence of CaCl_2 ³ to assess substantial differences.

³A.2

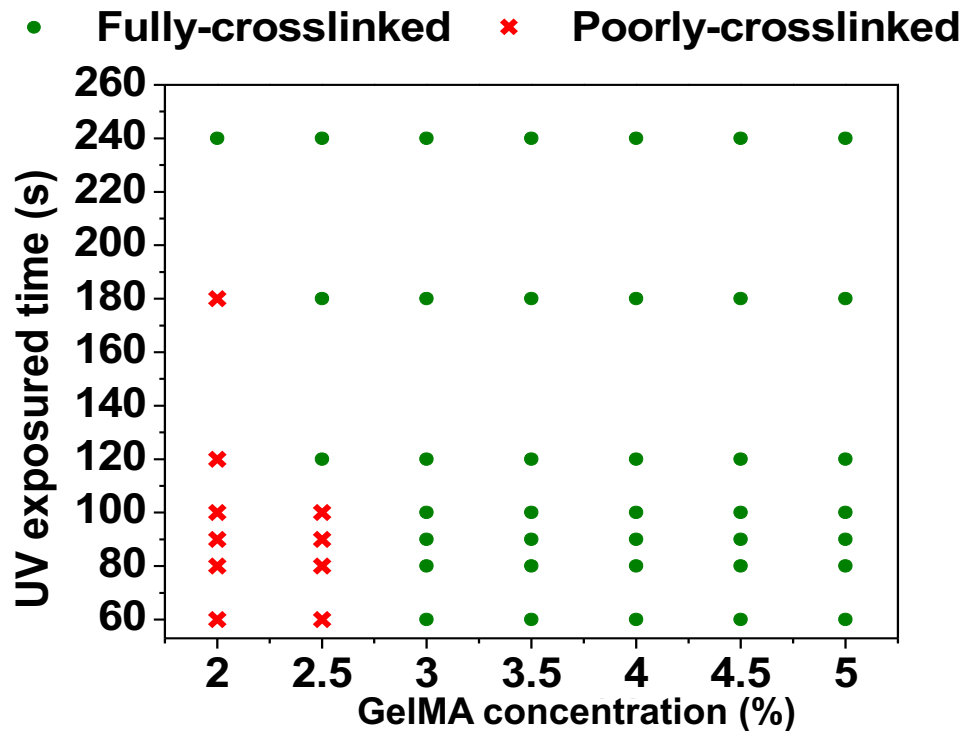


Figure 4.12: The chemical GelMA gel formation behaviors of GelMA solutions with different concentrations by treatment with various UV exposure times.

Degradation tests

Degradation tests were carried out on samples obtained with different exposure times (60 - 90 s). Samples were characterized in terms of weight percentage at day 0, 7, and 14 to assess their stability (See Figure 4.20).

Moreover, mechanical testing to monitor variations in compressive modulus, and visual observation to evaluate substantial modifications in the structure profile were carried out. Conditions obtained with 70 s and 80 s exposure times were found to be the most stable.

Bioinks printability tests

A series of bioink recipes were tested to obtain the best properties in terms of printing localization precision. Bioinks were subjected to rapid variations of applied stress. As it can be observed in Figure 4.21, the oscillatory strain sweep between low (1%) and high (250%) strain shows a rapid bioink transition from gel-like to fluid-like behavior, necessary condition for localization of extruded bioinks.

This test, performed on different conditions ⁴, indicated that the 5%wt gelatin/2%wt alginate-based bioink offered the best conditions for printing.

⁴A.3

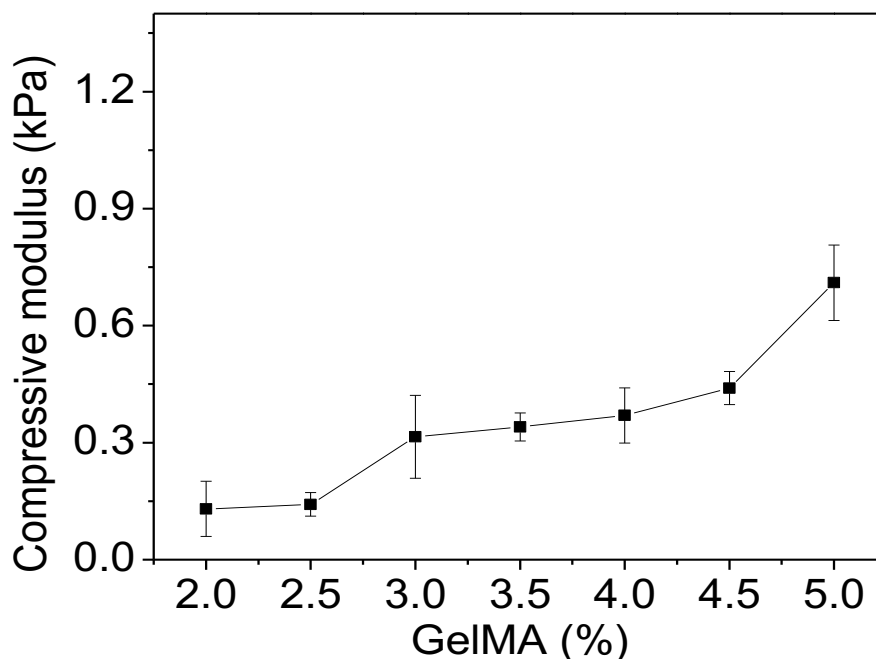


Figure 4.13: Compressive modulus of GelMA for different GelMA concentration.

Optimization of printed fibers

The viscoelastic properties of the selected composition enabled extrusion through a variety of needle gages. Nonetheless, to assure the best print fidelity after dispensation into the supporting bath, speed of needle motion and bioink extrusion rate were investigated, together with the effect of variations of needle diameter on the bioprinted structures (See Figures 4.22, 4.23).

Fibers containing a fluorescent dye dissolved in the 5%wt gelatin/2%wt alginate solution were printed with different extrusion rates (3 $\mu\text{l}/\text{min}$, 5 $\mu\text{l}/\text{min}$, 10 $\mu\text{l}/\text{min}$), and different nozzle velocities (2 mm/s, 6 mm/s, 10 mm/s) with 27G and 30G needles (210 μm and 159 μm of inner diameter respectively). Fibers were then evaluated in terms of diameter and uniformity using a fluorescence microscope. The condition which gave the best results was 3 $\mu\text{l}/\text{min}$ extrusion rate, 2 mm/s nozzle speed, 30G gage: it minimized the diameter of the printed fiber, which remained similar to those of the internal diameter of the needle, without excessive smearing of the bioink; Moreover, the aspect ratio of the cross-section of the fiber was the closest to the one of a perfect circle, assuring the best structural uniformity among all the tested conditions.

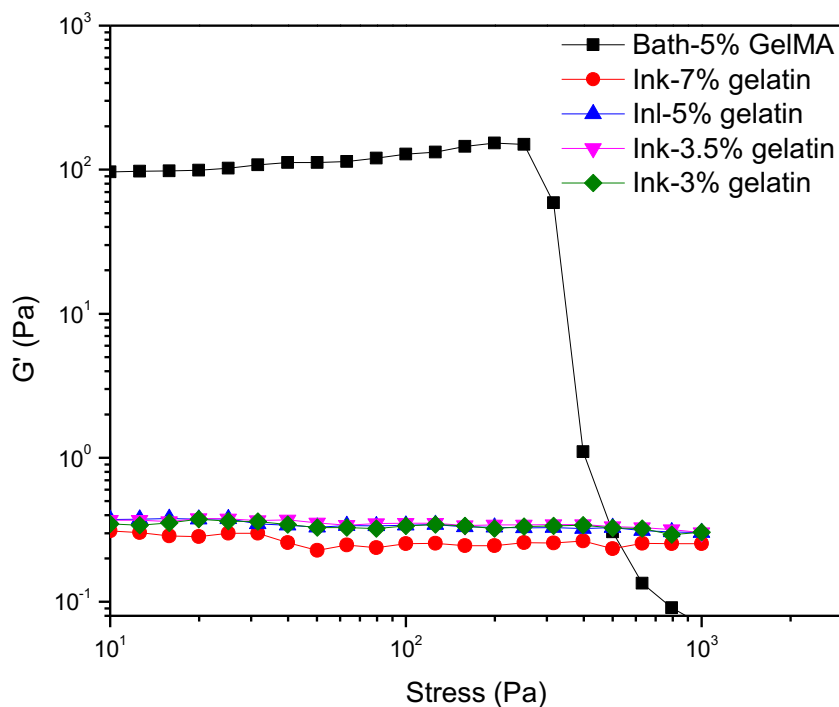


Figure 4.14: Oscillatory stress model shows the storage modulus (G') of the 5%wt GelMA bath is higher than that of the bioinks. This property is what allows to maintain the fiber structure after printing.

4.2.3 3T3 and MCF-7: fine-tuning for cell encapsulation

The effects of the printing process on cell viability were also investigated. Since astrocytes were obtained only through direct isolation from mouse brains, and since astrocytes cultures expand slowly, the first cellular experiments were carried out with different and more easily expandable cell types (3T3 and MCF-7) to limit the range of viable conditions. The two cell types were used in combination in order to exploit their particular behaviors as a model for astrocytes. 3T3 are cells that, when encapsulated in hydrogels, form several branched protrusions and extend throughout the gel. This particular behavior was used to model a hydrogel which could allow cell spreading, a major requirement in the formation of the astrocytes network. 3T3, however, are proven to prefer a stiff substrate [131]⁵, which exhibits a certain degree of micro-roughness, whilst astrocytes grow better on a much softer substrate. Knowing this, the same conditions were tested with MCF-7. These breast cancer cells exhibit a completely different behavior if compared to 3T3 cells: they do

⁵This always holds true in 2D flat cultures. However, recent studies [132] found opposite results for 3T3 cells cultured in 3D stiff hydrogels. Nonetheless, these results were found for values of stiffness (2 kPa - 10 kPa) well exceeding those of the experiment here conducted (around 1 kPa). Moreover, these results were attributed more to the easiness with which cells could degrade the surrounding microenvironment through metalloproteinase (a proteolytic enzyme) -which was much higher in softer substrates- than to the micro-features of the hydrogels itself.

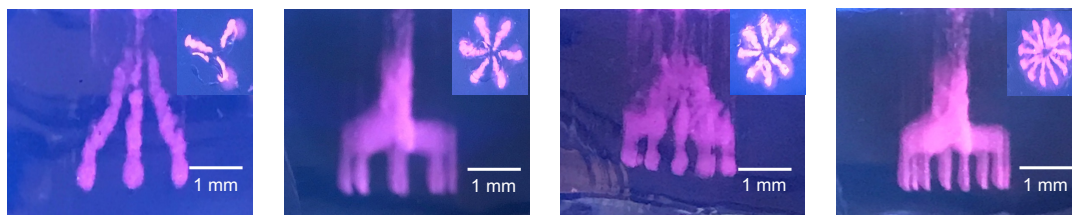


Figure 4.15: Fluorescence pictures of bioinks with fluorescent dye. The constructs (three, six, eight, and twelve branches) show the printing ability of the bioprinter.

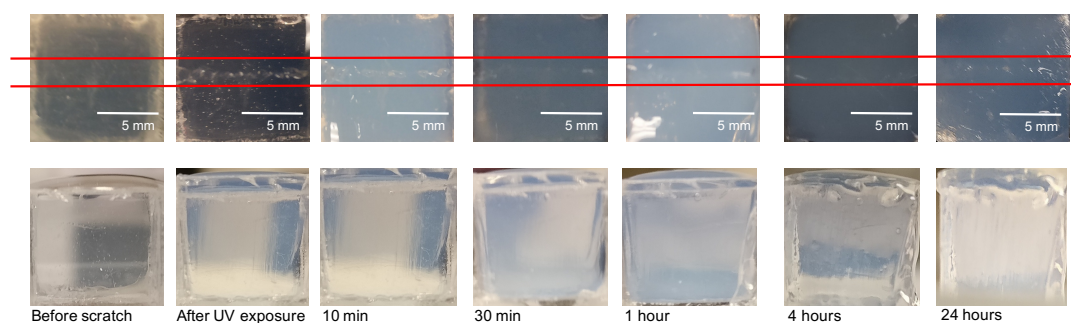


Figure 4.16: Self-healing behavior of GelMA: after scratching the surface of the printed bath with the bioprinter needle, the structure was left in the incubator for 24 hours, taking pictures at precise time-points. As it can be observed, full recovery from the scratch was obtained, proving the self-healing properties of the material.

not spread out, but instead migrate and aggregate to form colonies. Moreover, they prefer very soft substrates, therefore being an excellent test model for astrocytes.

Figures 4.24 and 4.25 show 3T3 spreading and colonies of MCF-7 in 5%wt GelMA for 60 s UV exposure time respectively. Thanks to these preliminary tests, the viable exposure times were narrowed down to the 60 s - 80 s range.

4.2.4 Astrocytes encapsulation

In order to understand astrocytes development in GelMA, they were encapsulated in thin (approximately 100 μm) layers of hydrogel. Tests were run for different concentrations (3.5%wt - 7%wt) and different exposure times (50 s - 240 s). It can be observed in Figure 4.26 that the condition in which the best expression of astrocytes morphology was obtained after 14 days was at 60 s.

Viability of astrocytes was observed to drop considerably after 100 s of UV exposure (See Figure 4.27 and supporting material⁶).

The selected exposure times for full structure testing were therefore 70 s and 80 s. Confocal imaging of the samples revealed that 80 s gave the best results in terms of cells spreading, proliferation, and viability (See Figures 4.28).

⁶A.4

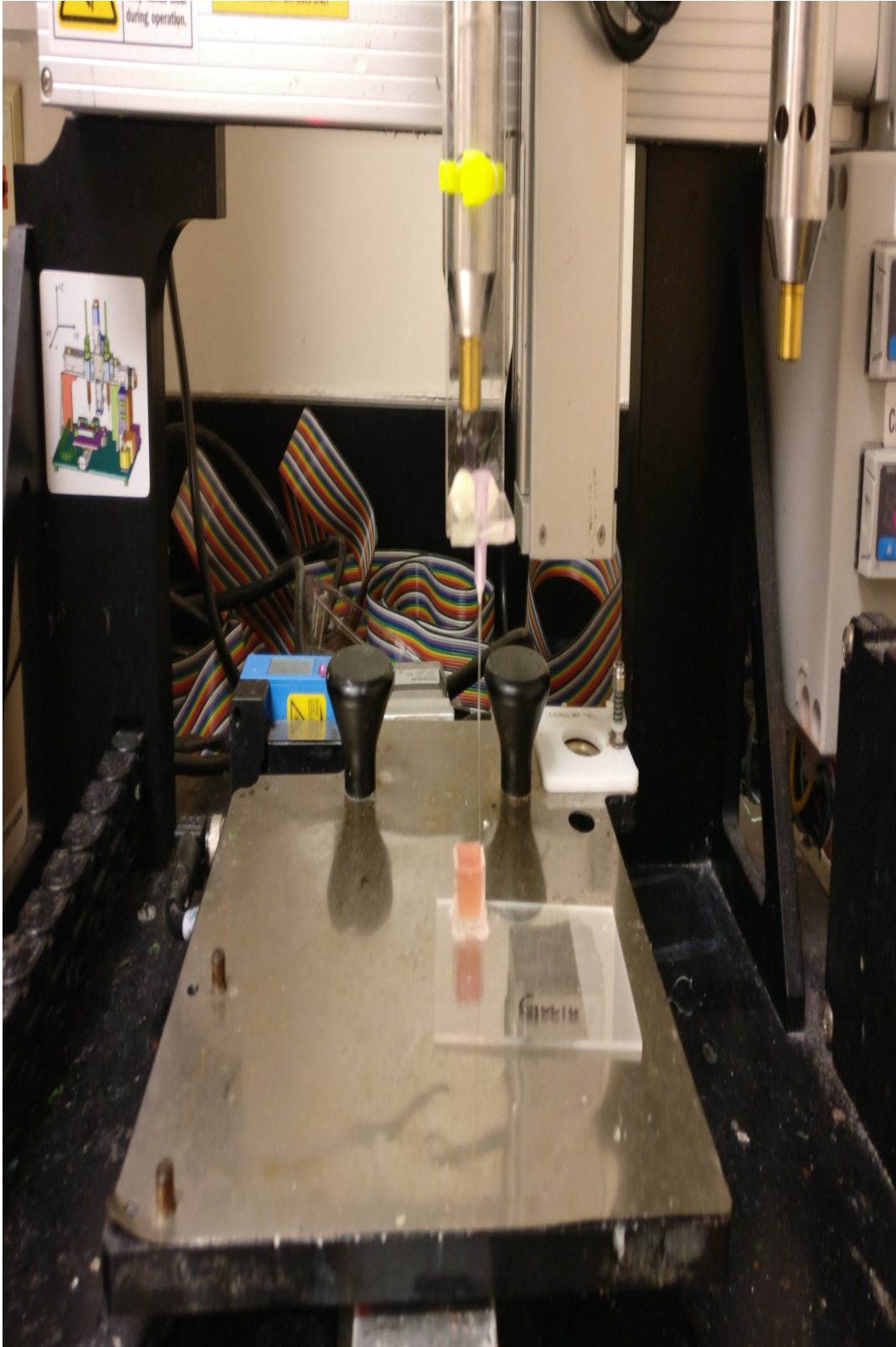


Figure 4.17: The samples were scratched with a needle, performing a horizontal cut with the bioprinter nozzle.

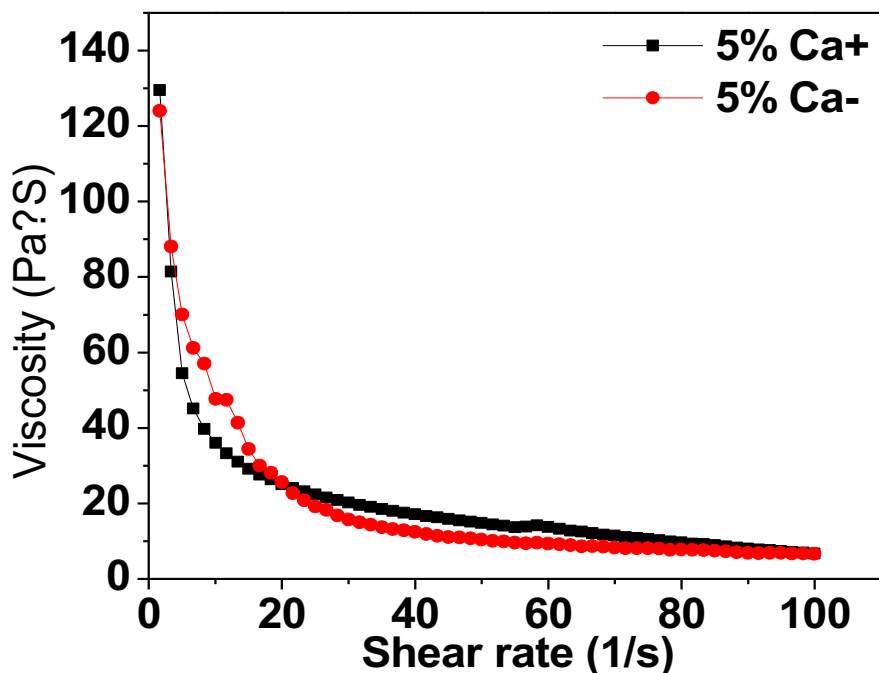


Figure 4.18: The continuous flow ramp model shows that 5%wt physical GelMA hydrogels have a rapid hydrogel transition from gel-like to fluid-like behavior, with a shear-thinning ability for nozzle moving.

4.2.5 3T3: fine-tuning of bioink

Similarly to what regarded the use of astrocytes, the use of PC12 and NE-4C was problematic for the difficulties related to obtaining a number of cells large enough to carry out wide-spectrum testing. To overcome this issue, cell survival, expression, and proliferation in the different recipes was tested with 3T3.

In Figures 4.29, 4.30, 4.31, and 4.32 are shown results for 70 s and 80 s exposure times: it can be observed that, at day 14, cells were starting to flow out of the fibers in the 70 s condition. This was attributed to the fact that a very thin layer in the middle of the sample was not fully crosslinked -even if the structure as a whole appeared to be- therefore allowing the undesired outflow of cells from the fibers to the supporting bath. The 80 s condition, on the other hand, showed optimal fiber containment, only allowing some branching out of the cells. This was actually the envisaged situation, as in the final structure the neurons contained in the fibers should extend their neurites outside of the fibers and interact with the astrocytes, although without fully exiting the fibers. The 80 s condition was therefore as optimal as it could be.

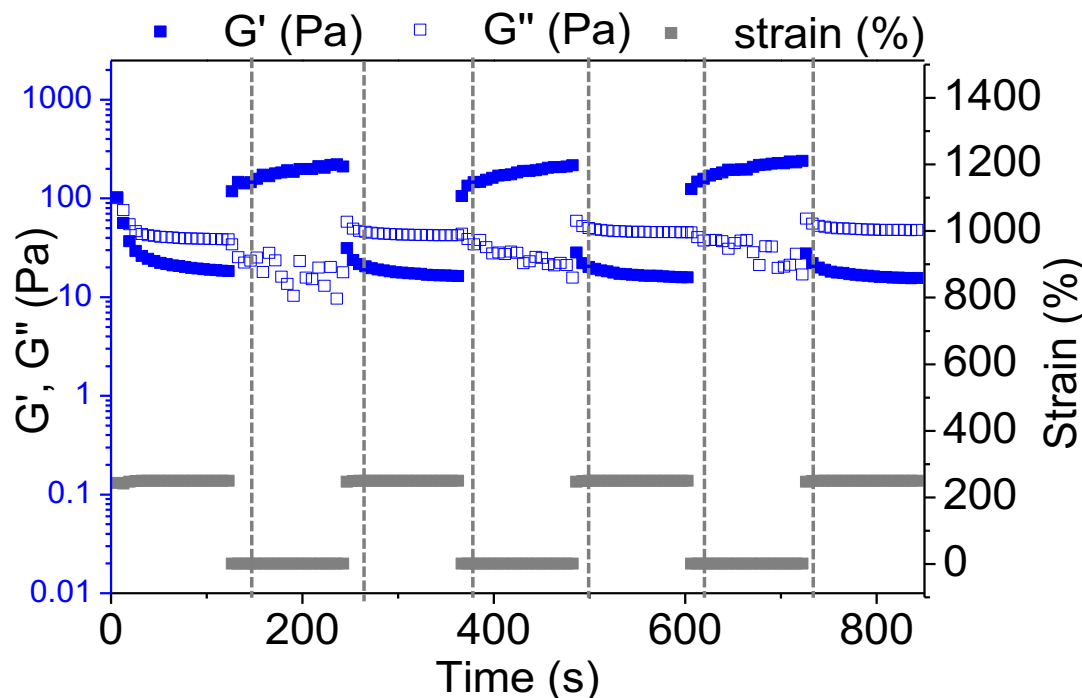


Figure 4.19: Oscillatory strain sweep between low (1%) and high (250%) strain shows the rapid self-healing ability of 5%wt physical GelMA hydrogel during the printing process.

4.2.6 Full structure development

The full 3D astrocytes-neuronal cells co-culture was finally developed. In the end, only two of the previously mentioned ⁷ bioinks were used, the 5%wt gelatin/2%wt alginate and the 7%wt GelMA High Methacrylation (MA), 5mg/ml MWCNT-COOH, 0.5%wt PI.

As it can be observed in Figure 4.33, confocal images at day 7 show a complete development of astrocytes, with good extension and spreading throughout the gel, whilst PC12 show only the extension of a limited number of neurites (especially in the case with CNT) and the tendency to form aggregations. Nonetheless, this result was considered promising, as the cells responded to neuron-specific staining (localization of beta-III tubulin), therefore confirming the initiation of the differentiation process. Moreover, cell viability was found to be high (more than 90%) in all the sections of the structure: this result shows how this structure overcomes one of the major limitation of 3D cultures in spheroids, the non-uniformity of nutrient perfusion throughout the culture, which leads to increased cell mortality in the center of the culture. The developed structure, on the other hand, provides excellent nutrient perfusion, thanks both to the porosity of the low-stiffness hydrogel bath and to the bioprinted fibers themselves, which provide additional inlets for nutrients inflows.

⁷3.4

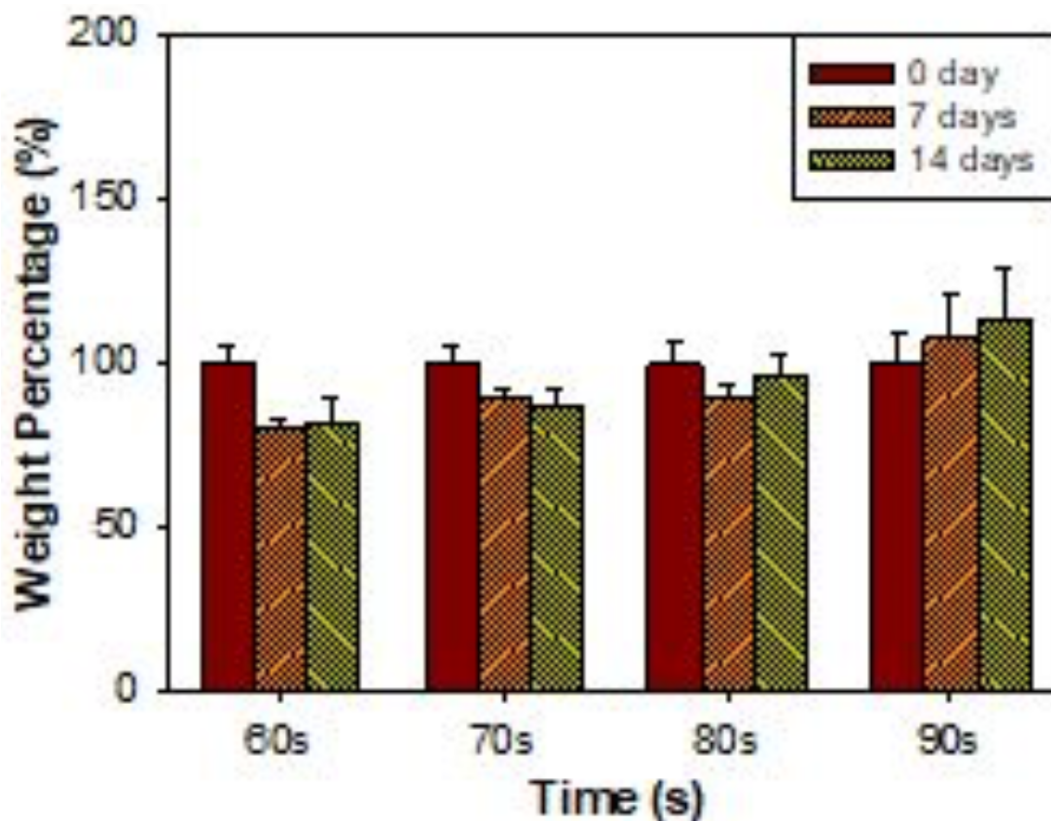


Figure 4.20: The degradation behaviors of 5%wt GelMA supporting hydrogel after 7 and 14 days of incubation.

4.3 Electrical mapping of a 3D neuronal network

4.3.1 Preliminary results

The attempt of recording electrical signals produced by the 3D neuronal network and propagated through a conductive hydrogel was unfortunately tried only once. As previously mentioned, the equipment for the recordings, produced by Maxwell Biosystems, was brought to the Khademhosseini lab for a one-day trial experiment by Dr. Marie Engelen Obien and Dr. Michele Fiscella from ETH-Z, with which the experiment was originally conceived.

Figure 4.34 shows an axonal signal recorded from one of the 26,400 microelectrodes of the HD-MEA, suggesting part of the signal was able to be transmitted from the hydrogel to the array. Unfortunately the cells were probably in too early a stage of development, therefore being unable to express a great deal of activity. Moreover, the setup was not optimized, therefore hindering the possibility of a reliable analysis at this stage of the process. Nonetheless, this results opens promising paths for the electrical investigation of 3D cell cultures, something that could still not be achieved with high precision, nor in a network fashion. These possibilities will be discussed in the conclusive chapter.

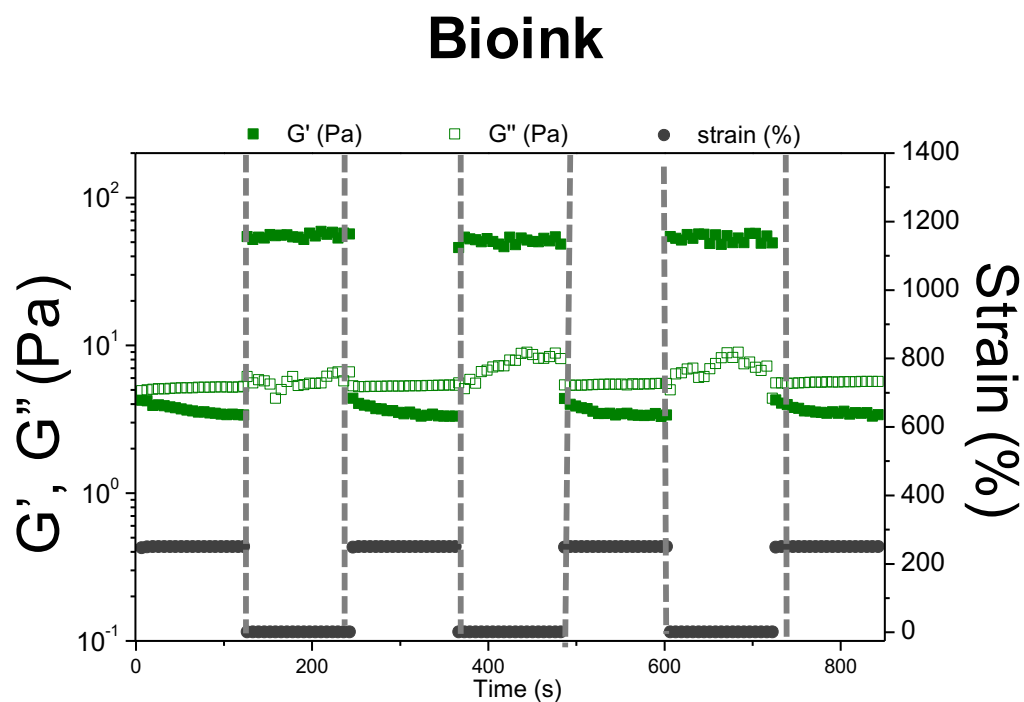


Figure 4.21: Oscillatory strain sweep between low (1%) and high (250%) strain shows a rapid transition of bioink from gel-like to fluid-like behavior, necessary for localization of extruded bioinks. It indicates that the 5%wt gelatin/2%wt alginate-based bioinks were printable.

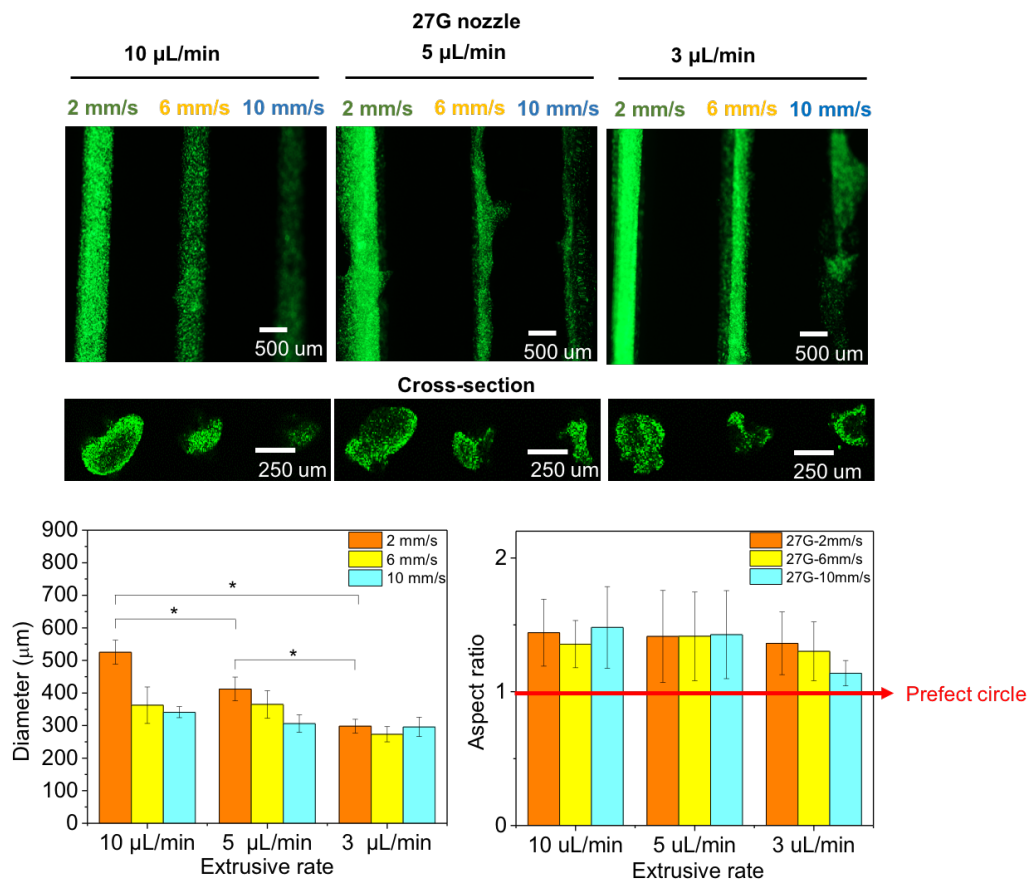


Figure 4.22: Visualization of the fiber continuity and quantification of the fiber diameter and the circularity of printed fibers for 27G nozzle.

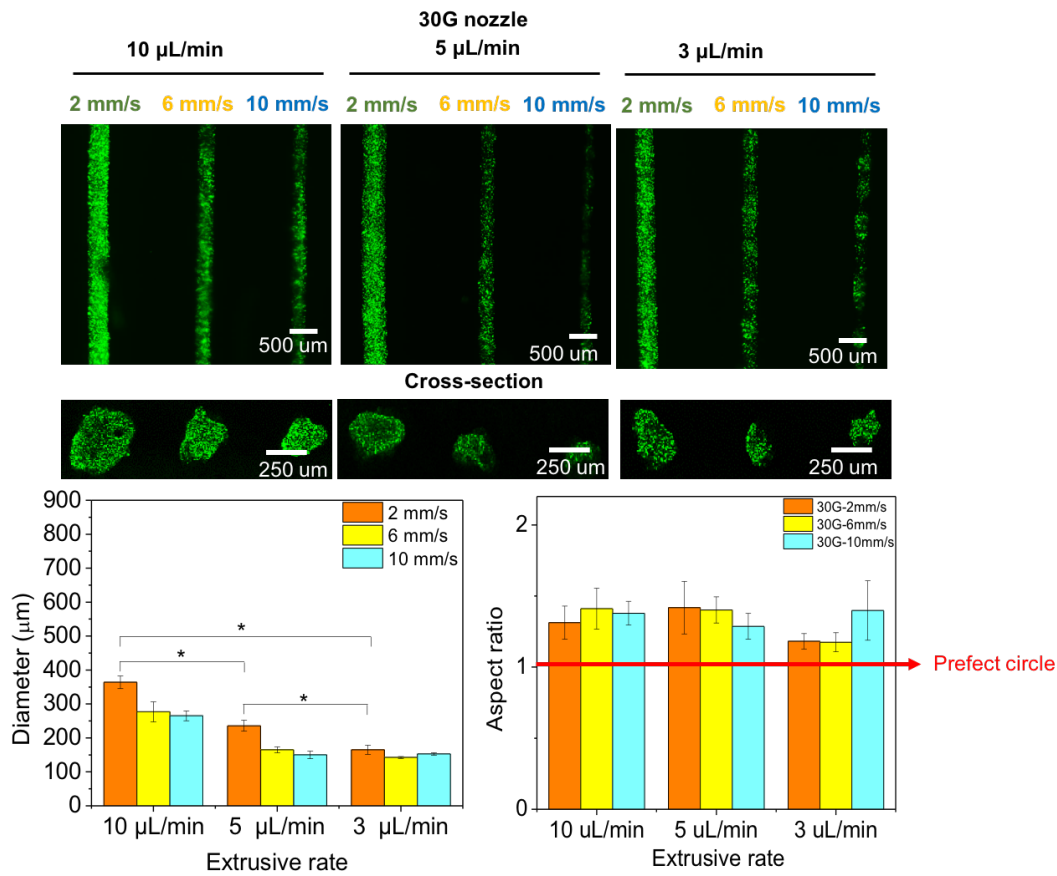


Figure 4.23: Visualization of the fiber continuity and quantification of the fiber diameter and the circularity of printed fibers for 30G nozzle. The fibers printed by 30 G nozzle at a printing rate of 3 $\mu\text{L}/\text{min}$ and with a nozzle moving rate of 2 mm/s could get the minimal diameter and obtain a fiber cross-section aspect ratio close to the one of a circle.

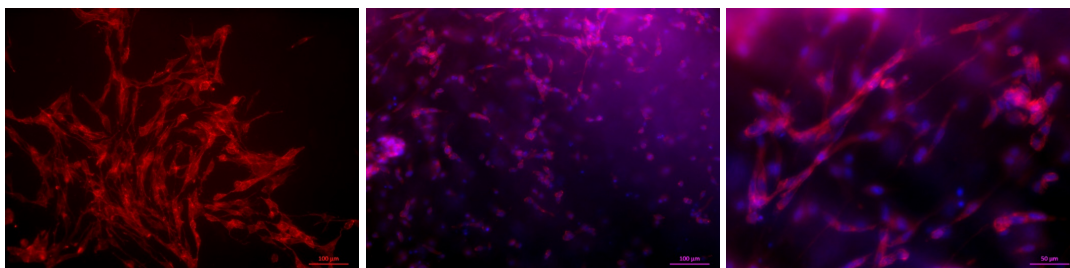


Figure 4.24: 3T3 cells spreading in the supporting bath. 5%wt GelMA, 0.25%wt PI, 800 mW/cm^2 UV power, 5 cm distance from source, 60s total UV exposure time, 8 million/ml cells (day 7). From the left: only Alexa Fluor 594 phalloidin[®] staining to observe cellular strands more accurately, then Alexa Fluor 594 phalloidin[®] / DAPI staining to include visualization of cell nuclei.



Figure 4.25: MCF-7 cells forming colonies in the supporting bath. 5%wt GelMA, 0.25%wt PI , 800 mW/cm² UV power, 5 cm distance from source, 60s total UV exposure time, 8 million/ml cells (day 7). Alexa Fluor 488 phalloidin[®]/ DAPI staining. The first two images are taken at different planes of focus to stress the fact that the cells were not in a 2D flat surface, but encapsulated in a 3D environment.

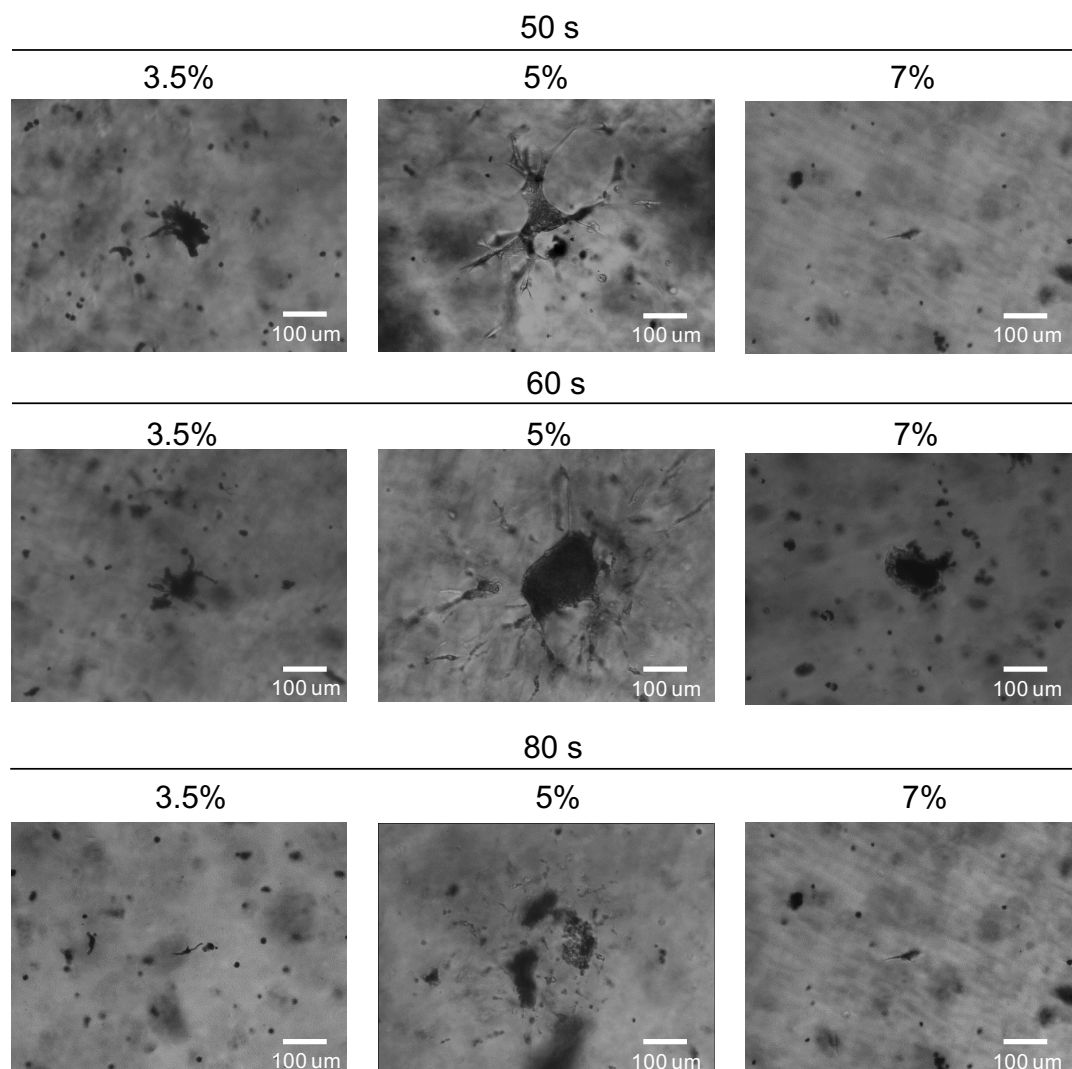


Figure 4.26: The morphologies of astrocyte in the 3.5%wt, 5%wt, and 7%wt GelMA gel with different UV exposed time after 14 days of incubation. It shows that the astrocytes could fully migrate and extend in 5%wt chemical GelMA hydrogel under 80 second of UV exposure time.

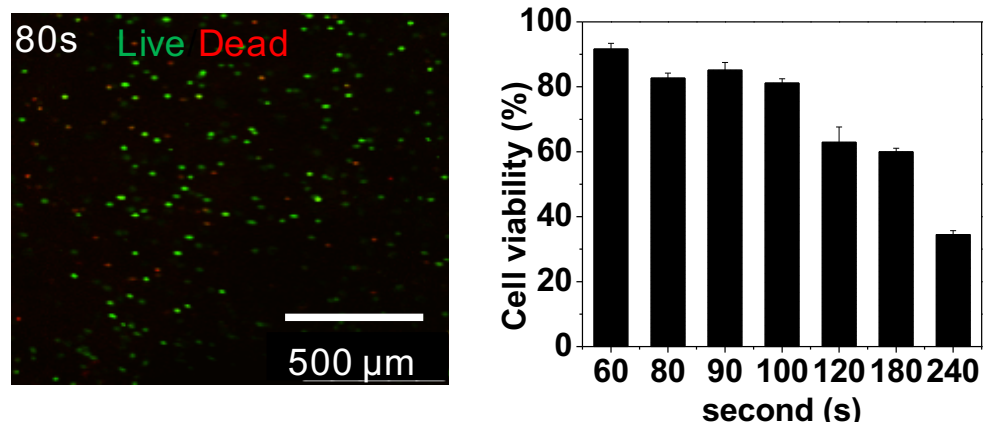


Figure 4.27: Live/Dead™ assay for 80 s UV exposure time and cell viability of astrocytes in the 5%wt GelMA supporting gel after UV treatment.

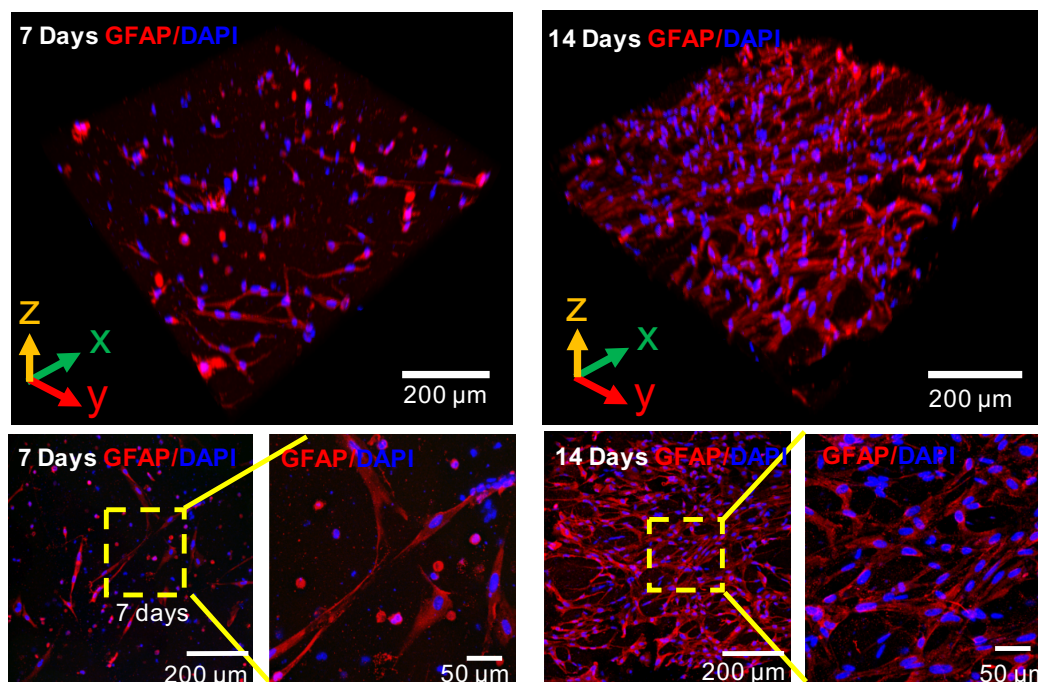


Figure 4.28: The cell viability and morphologies of astrocytes in the 5% GelMA supporting gel after 7 and 14 days of incubation. Figure shows that astrocytes could maintain a high viability, extend and form a network in the 5%wt GelMA supporting gel.

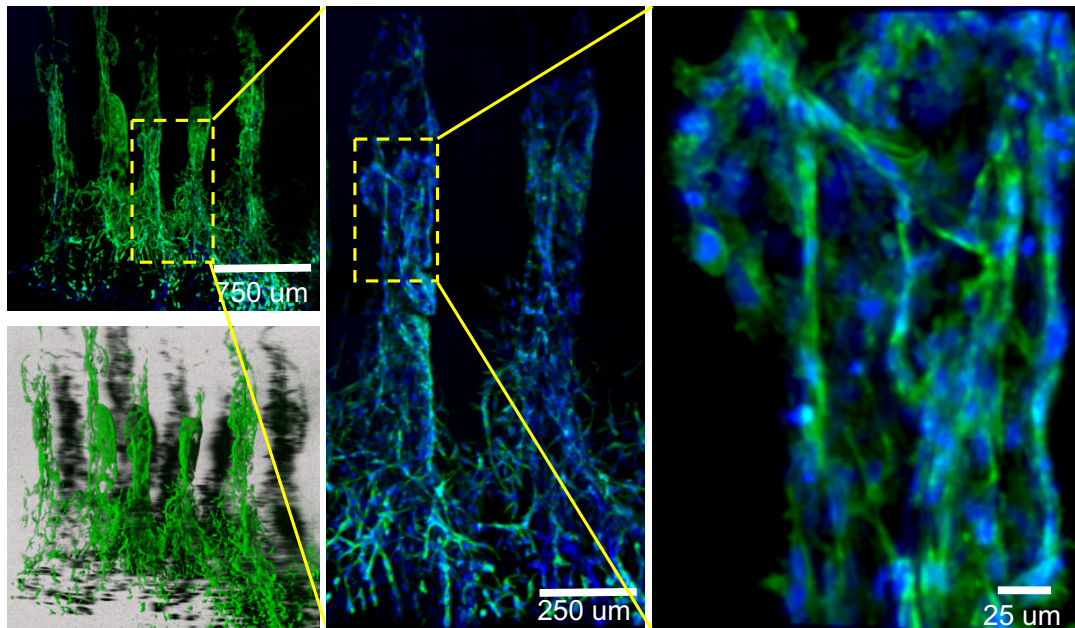


Figure 4.29: 3T3 cells encapsulated in 5%wt gelatin/2%wt alginate ink at treatment of 70 s UV after 7 days of incubation.

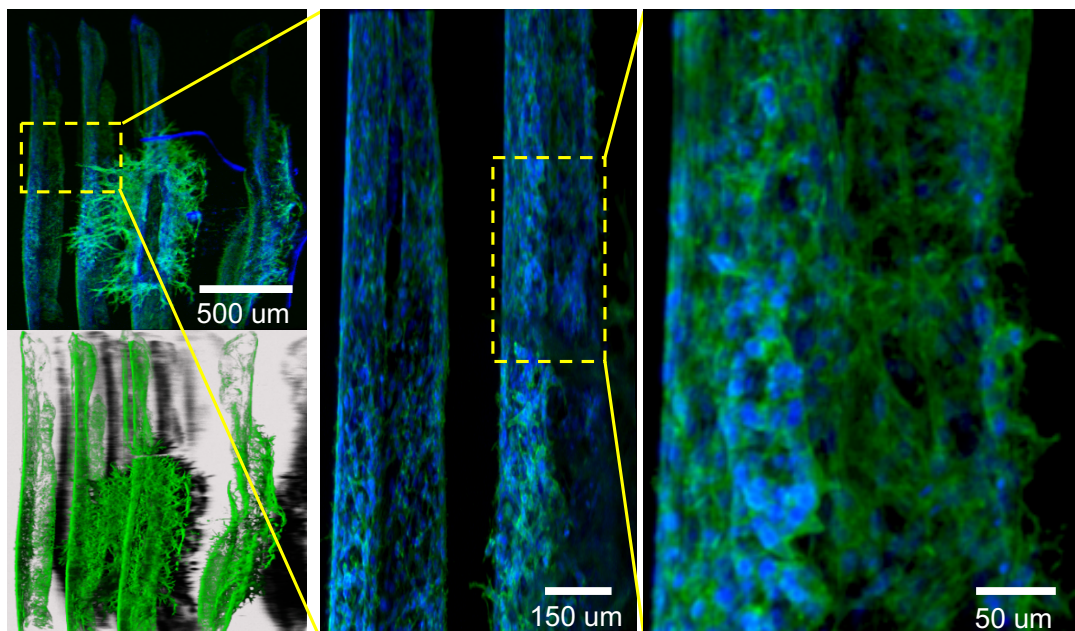


Figure 4.30: 3T3 cells encapsulated in 5%wt gelatin/2%wt alginate ink at treatment of 80 s UV after 7 days of incubation.

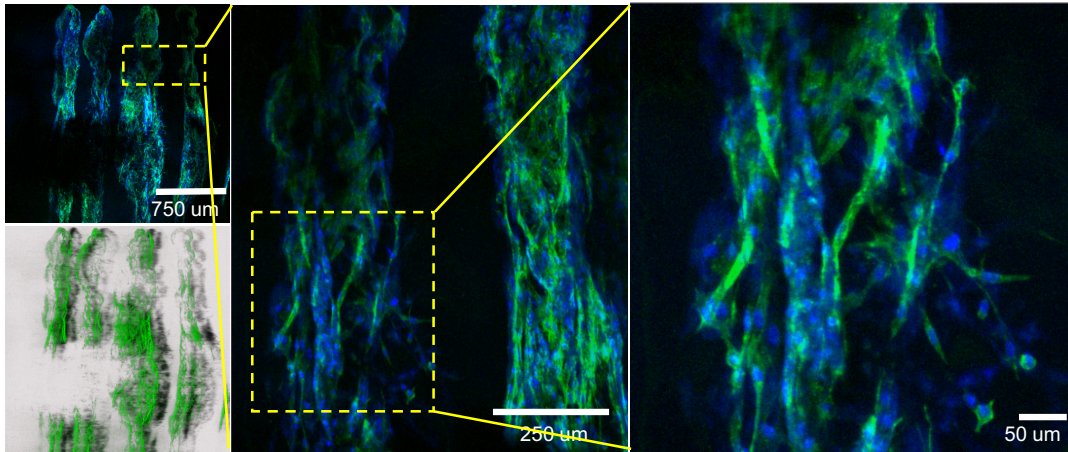


Figure 4.31: 3T3 cells encapsulated in 5%wt gelatin/2%wt alginate ink at treatment of 70 s UV after 14 days of incubation.

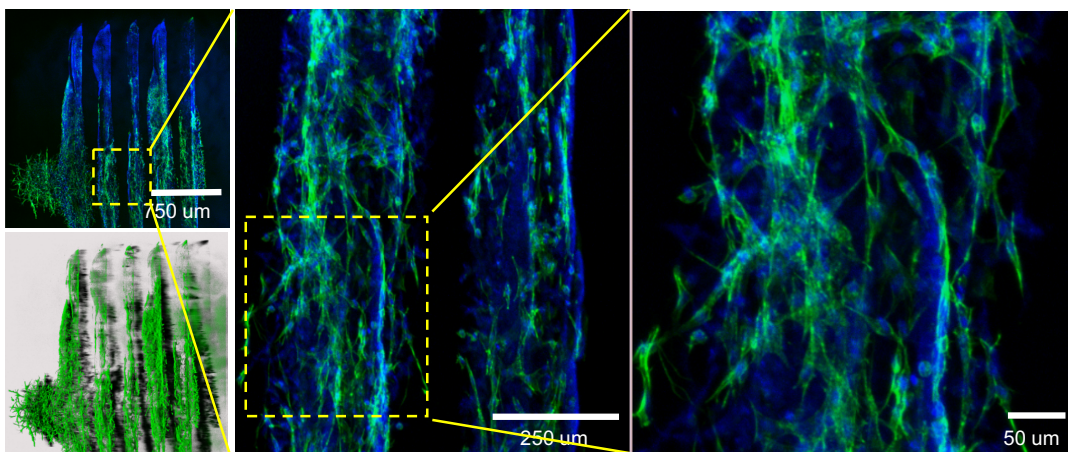


Figure 4.32: 3T3 cells encapsulated in 5%wt gelatin/2%wt alginate ink at treatment of 80 s UV after 14 days of incubation.

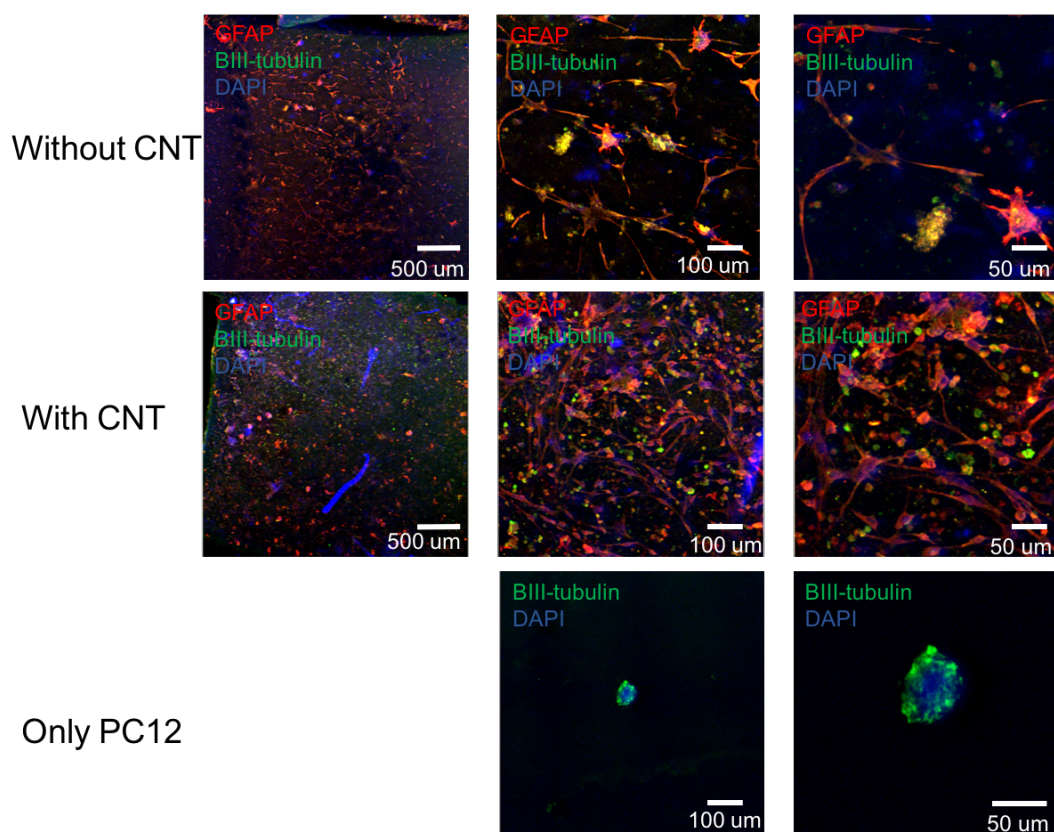


Figure 4.33: From top to bottom: co-cultures of astrocytes and PC12 cells in the absence (top) and presence (middle) of MWCNT, day 7. Imaging of PC12 aggregations (bottom), day 7.

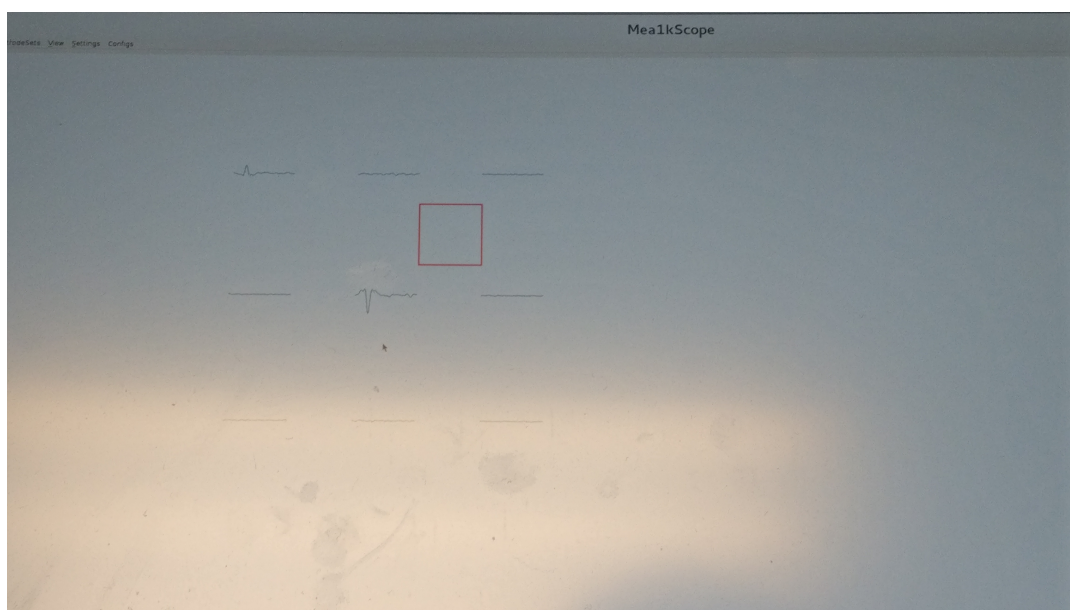


Figure 4.34: Axonal signal recorded through the HD-MEA.

Chapter 5

Conclusion and future work

A 3D bioprinted, self-standing, co-culture of astrocytes and neuronal cells was successfully developed. Materials development, testing, and optimization was fully achieved. Moreover, assessment of viability, development, proliferation, and phenotype expression for a series of cell types was carried out effectively, proving the structure to be an excellent platform for future studies on 3D neuronal networks, which addresses successfully a major set of limitations of previously developed 3D co-cultures (viability non-homogeneities, nutrient perfusion, microenvironment similarities with actual *in vivo* cellular microenvironment). In addition to that, the peculiarity of the developed structure and of the printing process, which allows for a precise and controlled disposition of cells in the network, suggests the possibility of using it for massively parallel and highly repeatable assays for drug discovery, testing, and cell behavior analyses. Nonetheless, this work must be seen in the framework of a bigger project, which still requires some additional steps to get to a conclusion. These steps are discussed in the following final paragraphs.

5.1 Future work

The next envisaged milestones for the project are here summarized:

- **Cell type:** in order to achieve a more significant *in vitro* model for the study of neurodegenerative disorders, primary neurons first, and human stem cells after will be used in the bioinks. At the same time, human-derived astrocytes will be integrated in the bath. This will provide higher quality results and more certainties when using this structure as an efficient translational model between *in vitro* and *in vivo* studies.
- **Assessment of astrocytes effect:** astrocytes are responsible for neurotransmission regulation, and avoid neurodegeneration in *in vitro* co-cultures (a condition that strongly affects single-cell type cultures). The hypothesis at the basis of the introduction of astrocytes in the 3D neuronal network is that they will remove the excess of glutamate produced during neurotransmission from the synaptic cleft, convert it to glutamine through the enzyme glutamine synthetase (GS), and providing the necessary substrate to the neurons for the production of new glutamate, therefore guaranteeing better neuronal functioning

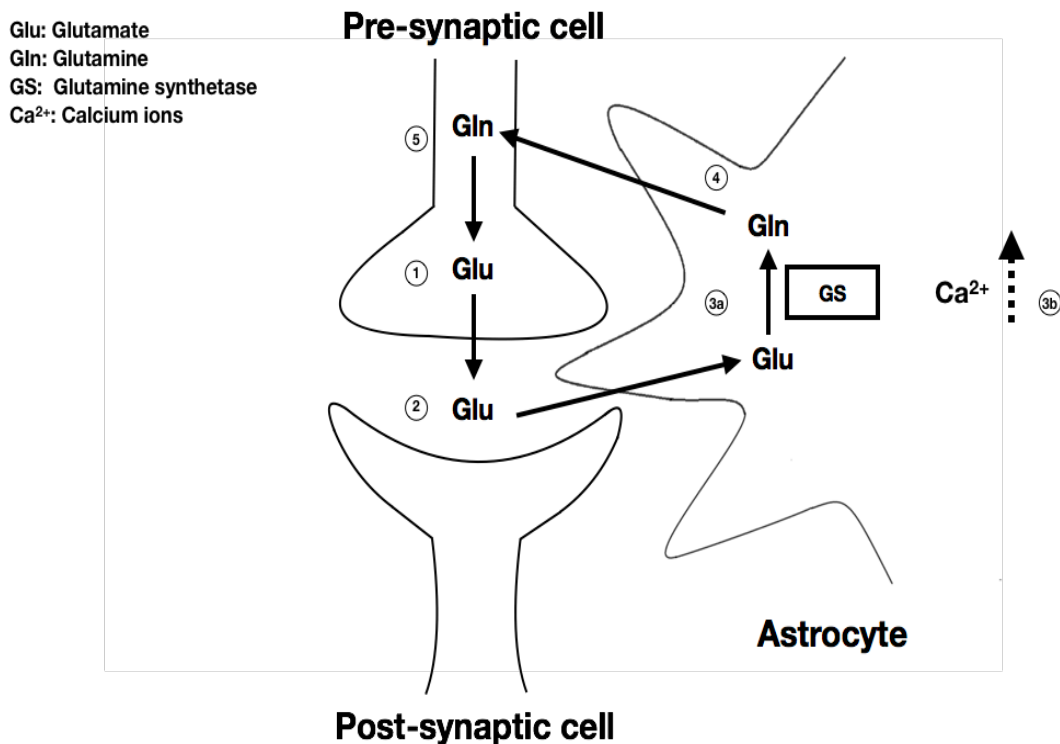


Figure 5.1: Astrocytes as regulators of the glutamate-glutamine cycle: during neurotransmission, glutamate produced by the pre-synaptic cell (1) is secreted into the synaptic cleft and interacts with the post-synaptic cell receptors (2). Astrocytes rapidly remove synaptically released glutamate, converting it into the amino acid glutamine by the enzyme glutamine synthetase (3a), and avoid excitotoxic damage of the cells. Glutamate uptake increases the calcium (Ca²⁺) intracellular concentration in astrocytes (3b), which triggers the release of glutamine into the extracellular space (4). Glutamine is then taken up by neurons, providing the necessary substrate for the synthesis of glutamate (5).

(See Fig. 5.1), and a more reliable environment on which drug discovery and testing could be performed.

- **Dexamethasone effects on glutamate-glutamine cycle:** in order to assess the effect of astrocytes on the 3D network functions, testing with dexamethasone will be performed. Dexamethasone, a synthetic glucocorticoid, is proven to have strong effects on the enzyme GS, enhancing glutamate uptake and reducing the risk of neurodegeneration [133] (See Fig. 5.2).

Since glutamate release by neurons is a calcium-dependent mechanism, Ca²⁺ imaging will be used to assess the effect of dexamethasone on the culture and, therefore, to assess how much the astrocytes presence affects positively the co-culture homeostasis (See Fig. 5.3).

- **Disease models:** if the previous tests will prove the developed neuronal network as a reliable testing platform, healthy neurons will be substituted with cells affected by Parkinson's and Alzheimer's, and testing will be performed

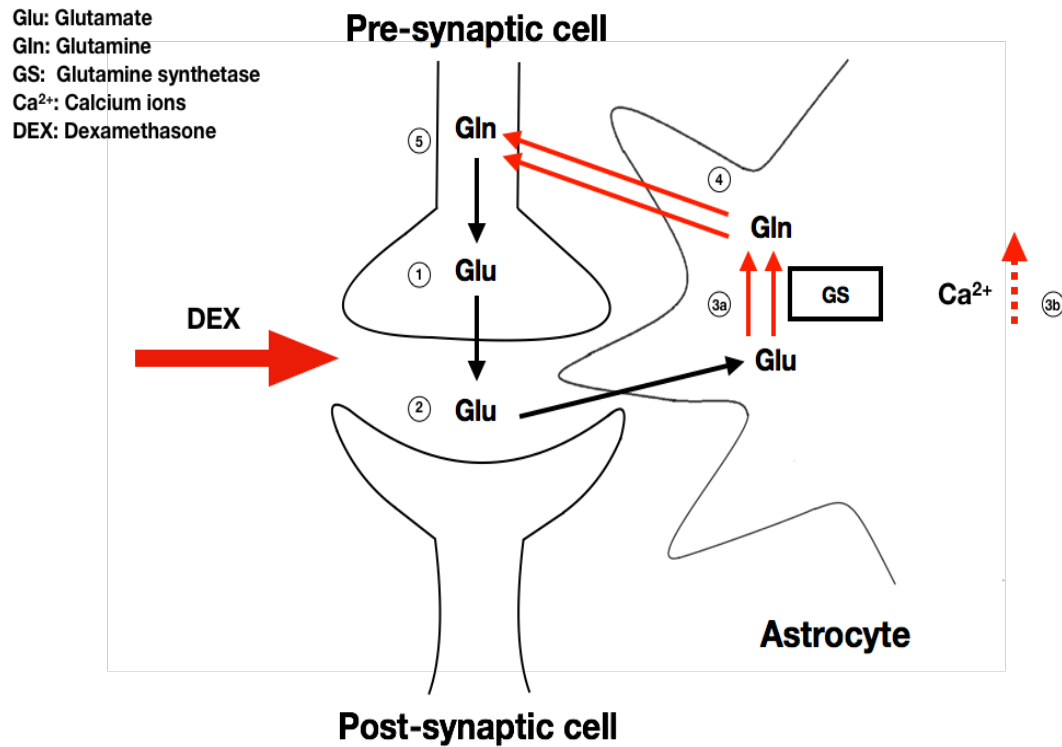


Figure 5.2: Effect of dexamethasone on the glutamate-glutamine cycle: rate of glutamate conversion to glutamine by astrocytes (3a) and glutamine release into the extracellular space (4) increase significantly. Increased glutamate uptake provokes a detectable increase in the Ca²⁺ intracellular concentration (3b).

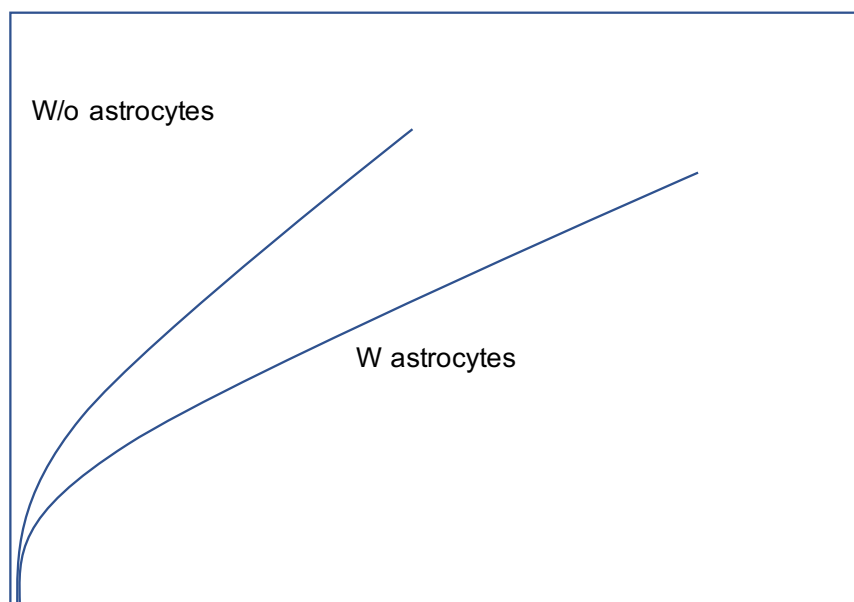


Figure 5.3: Glutamate assay with/without astrocytes (expected figure).

to assess the correlations between the 3D results in this particular setup with the already existing data, both *in vitro* (2D cultures, different 3D setups) and *in vivo*.

- **Tumor migration:** fibers will be modified in order to study the behavior of brain tumor initiating cells and metastases. This study will be part of a collaboration with Dr. Alfredo Quinones-Hinojosa laboratory (Mayo clinic, Jacksonville, Florida), and will study the particular tendency of brain tumor initiating cells to migrate along vascular tissue in the brain, and the way in which metastases move in brain tissue.
- **Electrical mapping of 3D neuronal network:** the hydrogels forming the bath and the ink will be made completely conductive and will be cultured on top of HD-MEAs at ETH-Z (Bio Engineering Laboratory), in order to conduct the first high-resolution electrophysiology studies on a complex 3D neuronal network. After this step is achieved, a series of disease models will be developed, and electrical characterization of neuronal behavior will be performed.

Appendix A

Supporting information

A.1 GelMA concentration

GelMA concentrations were tested in order to isolate the best conditions in terms of both material properties and cell viability, expression, and functionality. Limitations on UV exposure times were taken into consideration when performing these analyses [A.1](#).

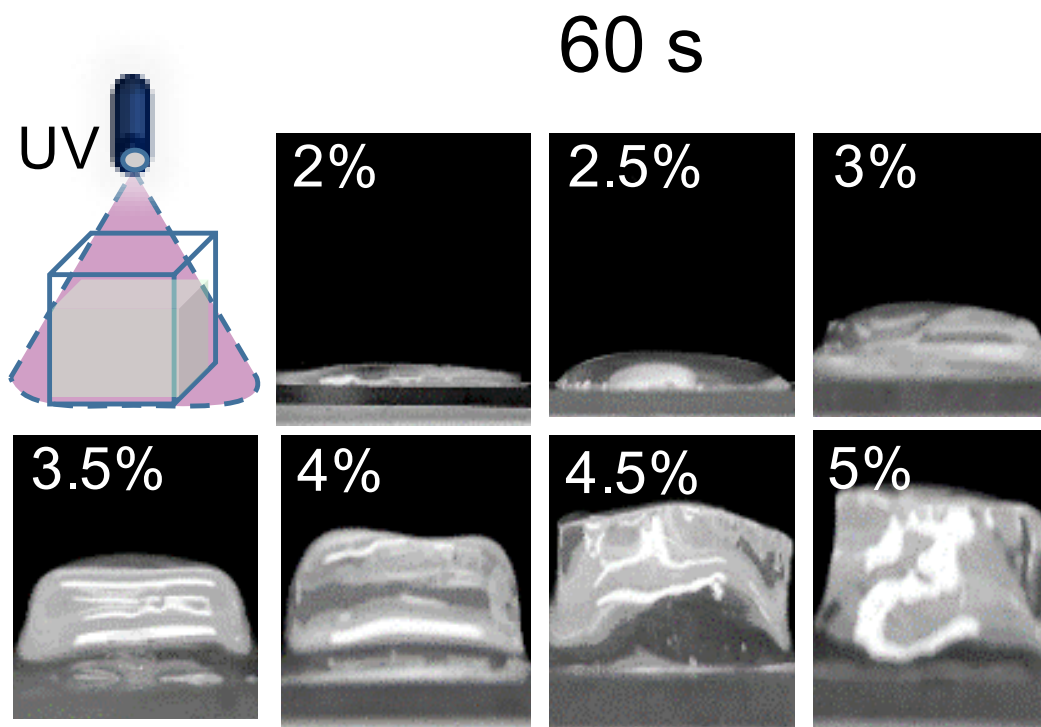


Figure A.1: Formation of a fully-crosslinked gel for different concentration of GelMA at 60 s UV exposure time.

A.2 The effect of CaCl_2 on shear-thinning behavior

Possible effects from the introduction of CaCl_2 were investigated, and it was found that no substantial difference derived either from the presence or the absence of it in

terms of shear-thinning behavior of the material [A.2](#), [A.3](#).

A.3 Bioink testing

Other bioink recipes were tested mechanically to assess their printability [A.4](#), [A.5](#), [A.6](#).

A.4 Astrocytes viability for different UV exposure times

Live/Dead™ assays were carried out for different exposure times to assess variations in viability [A.7](#).

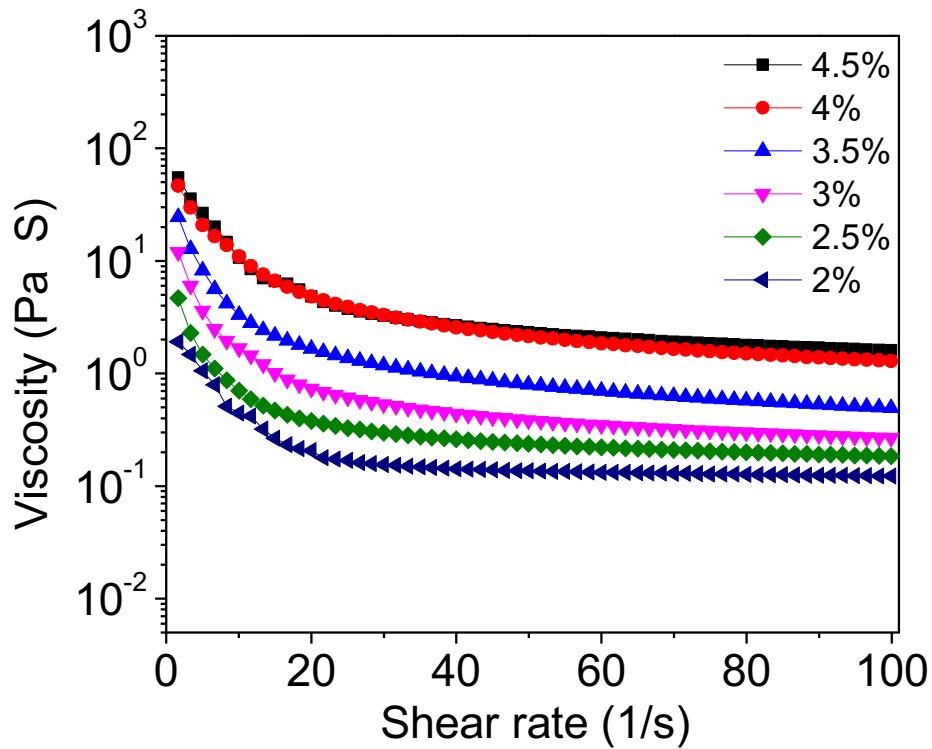


Figure A.2: Shear-thinning behavior for different concentrations of GelMA in the presence of CaCl₂.

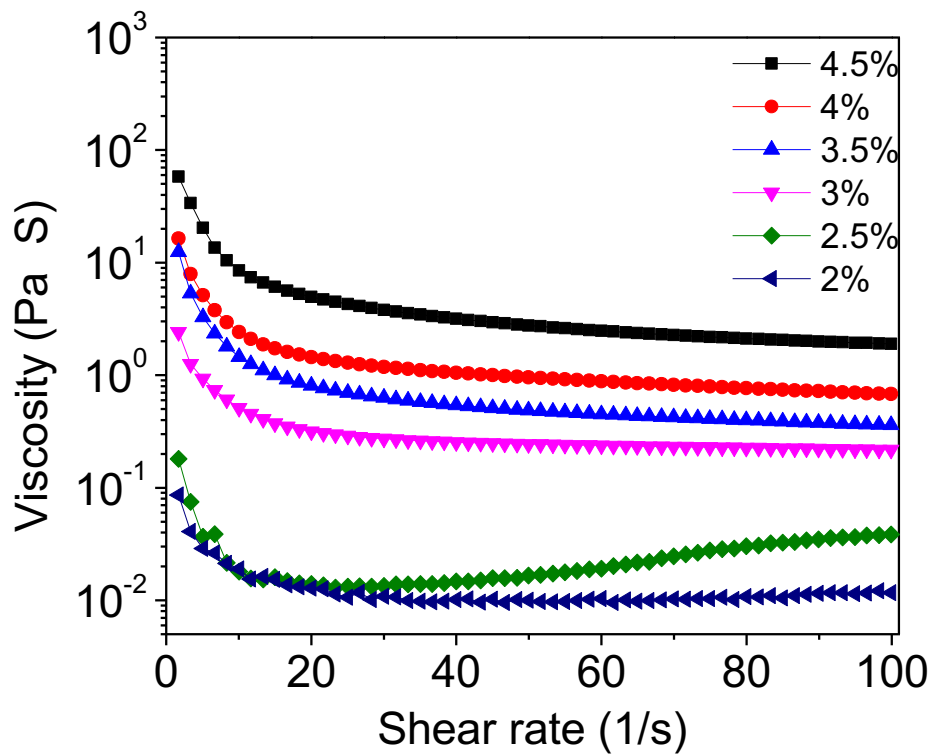


Figure A.3: Shear-thinning behavior for different concentrations of GelMA in the absence of CaCl₂.

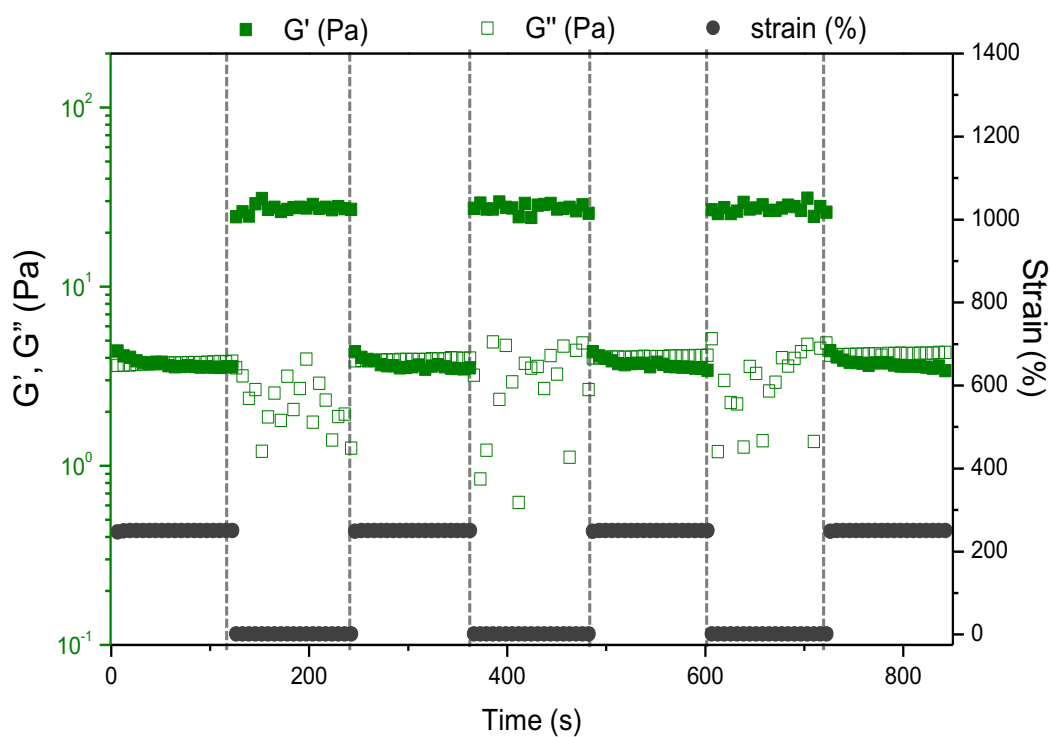


Figure A.4: Oscillatory strain sweep between low (1%) and high (250%) strain shows the rapid self-healing ability of 3% gelatin/ 2% alginate bioinks during the printing process.

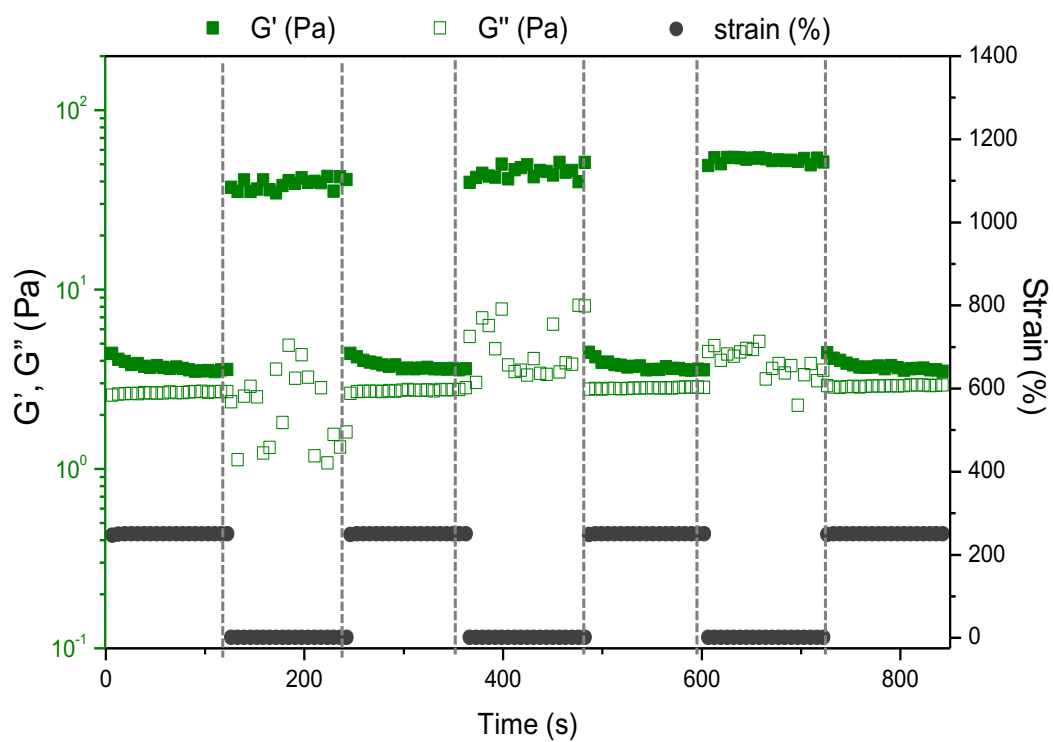


Figure A.5: Oscillatory strain sweep between low (1%) and high (250%) strain shows the rapid self-healing ability of 3.5% gelatin/ 2% alginate bioinks during the printing process.

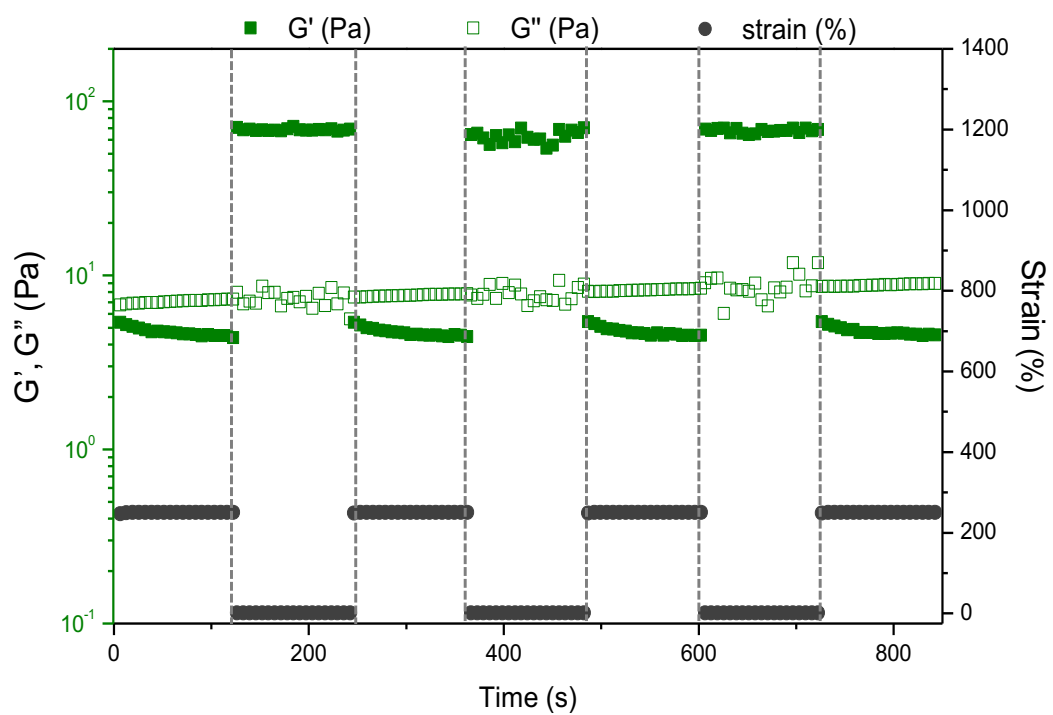


Figure A.6: Oscillatory strain sweep between low (1%) and high (250%) strain shows the rapid self-healing ability of 7% gelatin/ 2% alginate bioinks during the printing process.

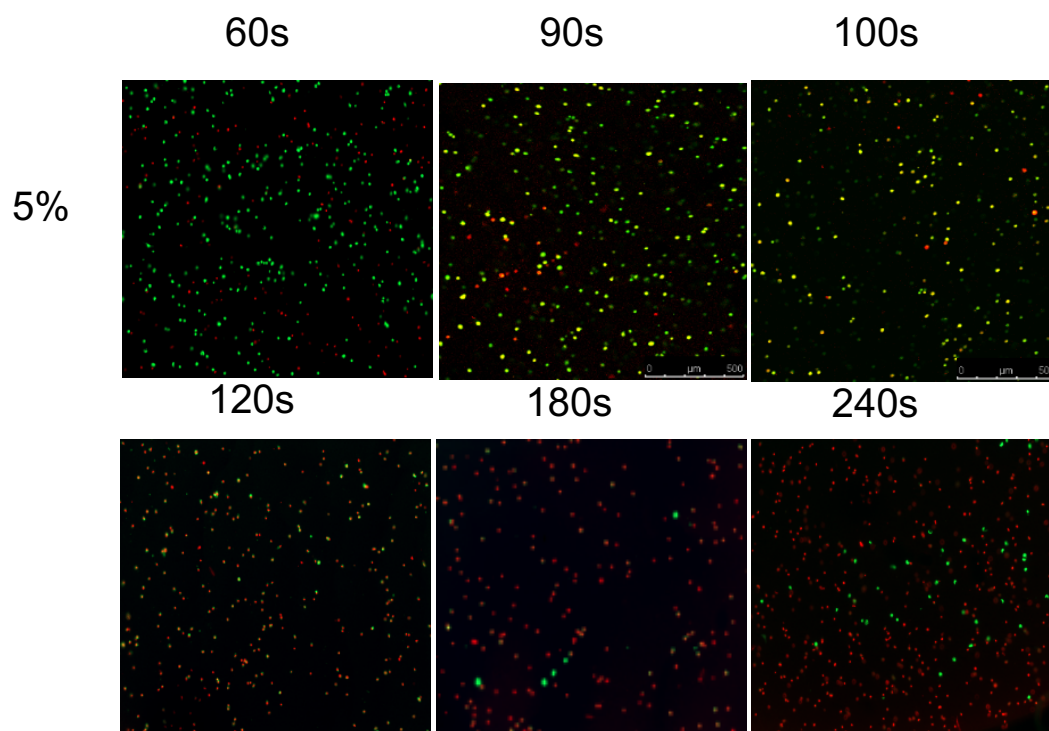


Figure A.7: The Live/Dead™ assay of astrocyte-laden 5% GelMA gel after different UV exposure times. It shows that astrocyte mortality will increase following the increase of UV exposure time.

Bibliography

- [1] Jason T Huse and Eric C Holland. "Targeting brain cancer: advances in the molecular pathology of malignant glioma and medulloblastoma". In: *Nature reviews. Cancer* 10.5 (2010), p. 319.
- [2] Debraj Mukherjee et al. "Disparities in access to neuro-oncologic care in the United States". In: *Archives of Surgery* 145.3 (2010), pp. 247–253.
- [3] Roger Stupp et al. "Radiotherapy plus concomitant and adjuvant temozolomide for glioblastoma". In: *New England Journal of Medicine* 352.10 (2005), pp. 987–996.
- [4] Kaisorn L Chaichana et al. "When gross total resection of a glioblastoma is possible, how much resection should be achieved?" In: *World neurosurgery* 82.1 (2014), e257–e265.
- [5] Kaisorn L Chaichana et al. "The butterfly effect on glioblastoma: is volumetric extent of resection more effective than biopsy for these tumors?" In: *Journal of neuro-oncology* 120.3 (2014), pp. 625–634.
- [6] Kaisorn L Chaichana et al. "Establishing percent resection and residual volume thresholds affecting survival and recurrence for patients with newly diagnosed intracranial glioblastoma". In: *Neuro-oncology* 16.1 (2013), pp. 113–122.
- [7] Matthew J McGirt et al. "Independent association of extent of resection with survival in patients with malignant brain astrocytoma". In: *Journal of neurosurgery* 110.1 (2009), pp. 156–162.
- [8] Quinn T Ostrom et al. "CBTRUS statistical report: Primary brain and central nervous system tumors diagnosed in the United States in 2006-2010". In: *Neuro-oncology* 15.suppl_2 (2013), pp. ii1–ii56.
- [9] Masahiko Tanaka et al. "Observation of the highly organized development of granule cells in rat cerebellar organotypic cultures". In: *Brain research* 641.2 (1994), pp. 319–327.
- [10] Hugo Guerrero-Cázares, Kaisorn L Chaichana, and Alfredo Quiñones-Hinojosa. "Neurosphere culture and human organotypic model to evaluate brain tumor stem cells". In: *Cancer Stem Cells: Methods and Protocols* (2009), pp. 73–83.

- [11] Kaisorn L Chaichana et al. "Preservation of glial cytoarchitecture from ex vivo human tumor and non-tumor cerebral cortical explants: a human model to study neurological diseases". In: *Journal of neuroscience methods* 164.2 (2007), pp. 261–270.
- [12] James O Hardin et al. "Microfluidic printheads for multimaterial 3D printing of viscoelastic inks". In: *Advanced materials* 27.21 (2015), pp. 3279–3284.
- [13] Carlos C Chang et al. "Direct-write bioprinting three-dimensional biohybrid systems for future regenerative therapies". In: *Journal of Biomedical Materials Research Part B: Applied Biomaterials* 98.1 (2011), pp. 160–170.
- [14] Bin Duan et al. "3D bioprinting of heterogeneous aortic valve conduits with alginate/gelatin hydrogels". In: *Journal of biomedical materials research Part A* 101.5 (2013), pp. 1255–1264.
- [15] Wouter Schuurman et al. "Bioprinting of hybrid tissue constructs with tailorable mechanical properties". In: *Biofabrication* 3.2 (2011), p. 021001.
- [16] Tao Xu et al. "Complex heterogeneous tissue constructs containing multiple cell types prepared by inkjet printing technology". In: *Biomaterials* 34.1 (2013), pp. 130–139.
- [17] Xiaofeng Cui et al. "Direct human cartilage repair using three-dimensional bioprinting technology". In: *Tissue Engineering Part A* 18.11-12 (2012), pp. 1304–1312.
- [18] Xiaofeng Cui et al. "Thermal inkjet printing in tissue engineering and regenerative medicine". In: *Recent patents on drug delivery & formulation* 6.2 (2012), pp. 149–155.
- [19] Kyle Christensen et al. "Freeform inkjet printing of cellular structures with bifurcations". In: *Biotechnology and bioengineering* 112.5 (2015), pp. 1047–1055.
- [20] Benjamin R Whatley et al. "Magnetic-directed patterning of cell spheroids". In: *Journal of biomedical materials research Part A* 102.5 (2014), pp. 1537–1547.
- [21] L Koch et al. "Laser assisted cell printing". In: *Current pharmaceutical biotechnology* 14.1 (2013), pp. 91–97.
- [22] Bertrand Guillotin et al. "Laser assisted bioprinting of engineered tissue with high cell density and microscale organization". In: *Biomaterials* 31.28 (2010), pp. 7250–7256.
- [23] Stefanie Michael et al. "Tissue engineered skin substitutes created by laser-assisted bioprinting form skin-like structures in the dorsal skin fold chamber in mice". In: *PloS one* 8.3 (2013), e57741.
- [24] Christopher B Highley, Christopher B Rodell, and Jason A Burdick. "Direct 3D printing of shear-thinning hydrogels into self-healing hydrogels". In: *Advanced Materials* 27.34 (2015), pp. 5075–5079.

- [25] Thomas J Hinton et al. "Three-dimensional printing of complex biological structures by freeform reversible embedding of suspended hydrogels". In: *Science advances* 1.9 (2015), e1500758.
- [26] Tapomoy Bhattacharjee et al. "Writing in the granular gel medium". In: *Science advances* 1.8 (2015), e1500655.
- [27] Michael Balls, Robert D Combes, and Nirmala Bhogal. *New Technologies for Toxicity Testing*. Vol. 745. Springer Science & Business Media, 2012.
- [28] Anna Birgersdotter, Rickard Sandberg, and Ingemar Ernberg. "Gene expression perturbation in vitro—a growing case for three-dimensional (3D) culture systems". In: *Seminars in cancer biology*. Vol. 15. 5. Elsevier. 2005, pp. 405–412.
- [29] Rasheena Edmondson et al. "Three-Dimensional Cell Culture Systems and Their Applications in Drug Discovery and Cell-Based Biosensors". In: *Assay and Drug Development Technologies* 12.4 (2014), pp. 207–218.
- [30] Kiran Bhadriraju and Christopher S Chen. "Engineering cellular microenvironments to improve cell-based drug testing". In: *Drug Discovery Today* 7.11 (2002), pp. 612–620. ISSN: 1359-6446.
- [31] Hossein Baharvand et al. "Differentiation of human embryonic stem cells into hepatocytes in 2D and 3D culture systems in vitro". In: *International Journal of Developmental Biology* 50.7 (2004), pp. 645–652.
- [32] Nilesh Gupta et al. "Microfluidics-based 3D cell culture models: Utility in novel drug discovery and delivery research". In: *Bioengineering & Translational Medicine* 1.1 (2016), pp. 63–81.
- [33] Hans-Jürgen Boxberger and Thomas F. Meyer. "A new method for the 3-D in vitro growth of human RT112bladder carcinoma cells using the alginate culture technique". In: *Biology of the Cell* 82.2 (1994), pp. 109–119. ISSN: 0248–4900.
- [34] Grace N Li et al. "Genomic and morphological changes of neuroblastoma cells in response to three-dimensional matrices". In: *Tissue engineering* 13.5 (2007), pp. 1035–1047.
- [35] Hug Aubin et al. "Directed 3D cell alignment and elongation in microengineered hydrogels". In: *Biomaterials* 31.27 (2010), pp. 6941–6951.
- [36] Ira Mellman and W James Nelson. "Coordinated protein sorting, targeting and distribution in polarized cells". In: *Nature Reviews Molecular Cell Biology* 9.11 (Nov. 2008), pp. 833–845.
- [37] E Farrell et al. "A comparison of the osteogenic potential of adult rat mesenchymal stem cells cultured in 2-D and on 3-D collagen glycosaminoglycan scaffolds". In: *Technology and Health Care* 15.1 (2007), pp. 19–31.
- [38] Xulang Zhang et al. "A novel 3-D model for cell culture and tissue engineering". In: *Biomedical microdevices* 11.4 (2009), pp. 795–799.

- [39] Chunnuan Chen, Kathryn Chen, and Shang-Tian Yang. "Effects of Three-Dimensional Culturing on Osteosarcoma Cells Grown in a Fibrous Matrix: Analyses of Cell Morphology, Cell Cycle, and Apoptosis". In: *Biotechnology progress* 19.5 (2003), pp. 1574–1582.
- [40] Jun Luo and Shang-Tian Yang. "Effects of Three-Dimensional Culturing in a Fibrous Matrix on Cell Cycle, Apoptosis, and MAb Production by Hybridoma Cells". In: *Biotechnology progress* 20.1 (2004), pp. 306–315.
- [41] Yu-Fen Lin et al. "Comparison of several radiation effects in human MCF10A mammary epithelial cells cultured as 2D monolayers or 3D acinar structures in matrigel". In: *Radiation research* 171.6 (2009), pp. 708–715.
- [42] June Rae Merwin et al. "Transforming growth factor beta1 modulates extracellular matrix organization and cell-cell junctional complex formation during in vitro angiogenesis". In: *Journal of cellular physiology* 142.1 (1990), pp. 117–128.
- [43] Yoshinori Imamura et al. "Comparison of 2D-and 3D-culture models as drug-testing platforms in breast cancer". In: *Oncology reports* 33.4 (2015), pp. 1837–1843.
- [44] Victor Sanjit Nirmalanandhan et al. "Activity of anticancer agents in a three-dimensional cell culture model". In: *Assay and drug development technologies* 8.5 (2010), pp. 581–590.
- [45] Jayme L Horning et al. "3-D tumor model for in vitro evaluation of anticancer drugs". In: *Molecular pharmaceuticals* 5.5 (2008), pp. 849–862.
- [46] Tomoaki Nakamura et al. "E-cadherin-dependent intercellular adhesion enhances chemoresistance". In: *International journal of molecular medicine* 12.5 (2003), pp. 693–700.
- [47] Ville Härmä et al. "A comprehensive panel of three-dimensional models for studies of prostate cancer growth, invasion and drug responses". In: *PloS one* 5.5 (2010), e10431.
- [48] Hagit Peretz et al. "Superior survival and durability of neurons and astrocytes on 3-dimensional aragonite biomatrices". In: *Tissue engineering* 13.3 (2007), pp. 461–472.
- [49] Bin Wang et al. "Phenotypical analysis of adult rat olfactory ensheathing cells on 3-D collagen scaffolds". In: *Neuroscience letters* 401.1 (2006), pp. 65–70.
- [50] V Chopra, TV Dinh, and EV Hannigan. "Three-dimensional endothelial-tumor epithelial cell interactions in human cervical cancers". In: *In Vitro Cellular & Developmental Biology-Animal* 33.6 (1997), pp. 432–442.
- [51] S Scaglione et al. "Engineering of osteoinductive grafts by isolation and expansion of ovine bone marrow stromal cells directly on 3D ceramic scaffolds". In: *Biotechnology and bioengineering* 93.1 (2006), pp. 181–187.

- [52] Claudia C Ceresa, Alan J Knox, and Simon R Johnson. "Use of a three-dimensional cell culture model to study airway smooth muscle-mast cell interactions in airway remodeling". In: *American Journal of Physiology-Lung Cellular and Molecular Physiology* 296.6 (2009), pp. L1059–L1066.
- [53] Jens M Kelm et al. "Method for generation of homogeneous multicellular tumor spheroids applicable to a wide variety of cell types". In: *Biotechnology and bioengineering* 83.2 (2003), pp. 173–180.
- [54] Andrea Ivascu and Manfred Kubbies. "Rapid generation of single-tumor spheroids for high-throughput cell function and toxicity analysis". In: *Journal of biomolecular screening* 11.8 (2006), pp. 922–932.
- [55] Juergen Friedrich et al. "Spheroid-based drug screen: considerations and practical approach". In: *Nature protocols* 4.3 (2009), pp. 309–324.
- [56] Hynda K Kleinman and George R Martin. "Matrigel: basement membrane matrix with biological activity". In: *Seminars in cancer biology*. Vol. 15. 5. Elsevier. 2005, pp. 378–386.
- [57] John W Haycock. "3D cell culture: a review of current approaches and techniques". In: *3D cell culture: methods and protocols* (2011), pp. 1–15.
- [58] Ibrahim Tarik Ozbolat. *3D Bioprinting: Fundamentals, Principles and Applications*. Academic Press, 2016.
- [59] Brian Derby. "Printing and prototyping of tissues and scaffolds". In: *Science* 338.6109 (2012), pp. 921–926.
- [60] Jens M Kelm et al. "A novel concept for scaffold-free vessel tissue engineering: self-assembly of microtissue building blocks". In: *Journal of biotechnology* 148.1 (2010), pp. 46–55.
- [61] Lenke Horváth et al. "Engineering an in vitro air-blood barrier by 3D bioprinting". In: *Scientific reports* 5 (2015), p. 7974.
- [62] Yin Yu et al. "Three-dimensional bioprinting using self-assembling scalable scaffold-free "tissue strands" as a new bioink". In: *Scientific reports* 6 (2016), p. 28714.
- [63] Francoise Marga et al. "Toward engineering functional organ modules by additive manufacturing". In: *Biofabrication* 4.2 (2012), p. 022001.
- [64] Yin Yu, Yahui Zhang, and Ibrahim T Ozbolat. "A hybrid bioprinting approach for scale-up tissue fabrication". In: *Journal of Manufacturing Science and Engineering* 136.6 (2014), p. 061013.
- [65] Yong He, Guang-huai Xue, and Jian-zhong Fu. "Fabrication of low cost soft tissue prostheses with the desktop 3D printer". In: *Scientific reports* 4 (2014).
- [66] Robert J Klebe. "Cytoscribing: a method for micropositioning cells and the construction of two-and three-dimensional synthetic tissues". In: *Experimental cell research* 179.2 (1988), pp. 362–373.

- [67] Sean V Murphy and Anthony Atala. "3D bioprinting of tissues and organs". In: *Nature biotechnology* 32.8 (2014), pp. 773–785.
- [68] Wei Zhu et al. "3D printing of functional biomaterials for tissue engineering". In: *Current opinion in biotechnology* 40 (2016), pp. 103–112.
- [69] Kalyani Nair et al. "Characterization of cell viability during bioprinting processes". In: *Biotechnology journal* 4.8 (2009), pp. 1168–1177.
- [70] Sean V Murphy, Aleksander Skardal, and Anthony Atala. "Evaluation of hydrogels for bio-printing applications". In: *Journal of Biomedical Materials Research Part A* 101.1 (2013), pp. 272–284.
- [71] EL Talbot et al. "Evaporation of picoliter droplets on surfaces with a range of wettabilities and thermal conductivities". In: *Physical Review E* 85.6 (2012), p. 061604.
- [72] Béla Hopp et al. "Femtosecond laser printing of living cells using absorbing film-assisted laser-induced forward transfer". In: *Optical Engineering* 51.1 (2012), pp. 014302–1.
- [73] Robert Chang, Jae Nam, and Wei Sun. "Effects of dispensing pressure and nozzle diameter on cell survival from solid freeform fabrication-based direct cell writing". In: *Tissue Engineering Part A* 14.1 (2008), pp. 41–48.
- [74] Béla Hopp et al. "Survival and proliferative ability of various living cell types after laser-induced forward transfer". In: *Tissue engineering* 11.11-12 (2005), pp. 1817–1823.
- [75] David F Williams. "On the mechanisms of biocompatibility". In: *Biomaterials* 29.20 (2008), pp. 2941–2953.
- [76] Jennifer L West and Jeffrey A Hubbell. "Polymeric biomaterials with degradation sites for proteases involved in cell migration". In: *Macromolecules* 32.1 (1999), pp. 241–244.
- [77] Dietmar W Hutmacher. "Scaffolds in tissue engineering bone and cartilage". In: *Biomaterials* 21.24 (2000), pp. 2529–2543.
- [78] Abhishek Ananthanarayanan et al. "Purpose-driven biomaterials research in liver-tissue engineering". In: *Trends in biotechnology* 29.3 (2011), pp. 110–118.
- [79] Suphasinee Limpanuphap and B Derby. "Manufacture of biomaterials by a novel printing process". In: *Journal of Materials Science: Materials in Medicine* 13.12 (2002), pp. 1163–1166.
- [80] Ulrich Hersel, Claudia Dahmen, and Horst Kessler. "RGD modified polymers: biomaterials for stimulated cell adhesion and beyond". In: *Biomaterials* 24.24 (2003), pp. 4385–4415.
- [81] Jeffrey M Karp et al. "Controlling size, shape and homogeneity of embryoid bodies using poly (ethylene glycol) microwells". In: *Lab on a Chip* 7.6 (2007), pp. 786–794.

- [82] Molly M Stevens and Julian H George. "Exploring and engineering the cell surface interface". In: *Science* 310.5751 (2005), pp. 1135–1138.
- [83] Richard O Hynes and Alexandra Naba. "Overview of the matrisome—an inventory of extracellular matrix constituents and functions". In: *Cold Spring Harbor perspectives in biology* 4.1 (2012), a004903.
- [84] David C Sullivan et al. "Decellularization methods of porcine kidneys for whole organ engineering using a high-throughput system". In: *Biomaterials* 33.31 (2012), pp. 7756–7764.
- [85] Kim Jong-Hoon et al. "Dopamine neurons derived from embryonic stem cells function in an animal model of Parkinson's disease". In: *Nature* 418.6893 (2002), p. 50.
- [86] Benjamin E Reubinoff et al. "Embryonic stem cell lines from human blastocysts: somatic differentiation in vitro". In: *Nature biotechnology* 18.4 (2000), p. 399.
- [87] Lisa Goers, Paul Freemont, and Karen M Polizzi. "Co-culture systems and technologies: taking synthetic biology to the next level". In: *Journal of The Royal Society Interface* 11.96 (2014), p. 20140065.
- [88] Christopher Moraes et al. "Organs-on-a-chip: a focus on compartmentalized microdevices". In: *Annals of biomedical engineering* 40.6 (2012), pp. 1211–1227.
- [89] Min-Hsien Wu, Song-Bin Huang, and Gwo-Bin Lee. "Microfluidic cell culture systems for drug research". In: *Lab on a Chip* 10.8 (2010), pp. 939–956.
- [90] Karine Alain and Joël Querellou. "Cultivating the uncultured: limits, advances and future challenges". In: *Extremophiles* 13.4 (2009), pp. 583–594.
- [91] Wael Sabra et al. "Biosystems analysis and engineering of microbial consortia for industrial biotechnology". In: *Engineering in Life Sciences* 10.5 (2010), pp. 407–421.
- [92] Richard Kitney and Paul Freemont. "Synthetic biology—the state of play". In: *FEBS letters* 586.15 (2012), pp. 2029–2036.
- [93] Larry Squire et al. *Fundamental neuroscience*. Academic Press, 2012.
- [94] Edward George Gray. "The fine structure of the insect ear". In: *Philosophical Transactions of the Royal Society of London B: Biological Sciences* 243.700 (1960), pp. 75–94.
- [95] Amanda Foust et al. "Action potentials initiate in the axon initial segment and propagate through axon collaterals reliably in cerebellar Purkinje neurons". In: *Journal of Neuroscience* 30.20 (2010), pp. 6891–6902.
- [96] Marie Engelen J Obien et al. "Revealing neuronal function through micro-electrode array recordings". In: *Frontiers in neuroscience* 8 (2014).

- [97] Jan Müller et al. "High-resolution CMOS MEA platform to study neurons at subcellular, cellular, and network levels". In: *Lab on a Chip* 15.13 (2015), pp. 2767–2780.
- [98] Micha E Spira and Aviad Hai. "Multi-electrode array technologies for neuroscience and cardiology". In: *Nature nanotechnology* 8.2 (2013), pp. 83–94.
- [99] Hristelina Ilieva, Magdalini Polymenidou, and Don W Cleveland. "Non-cell autonomous toxicity in neurodegenerative disorders: ALS and beyond". In: *The Journal of cell biology* 187.6 (2009), pp. 761–772.
- [100] Nicole Wallis et al. "Combined excitotoxic–oxidative stress and the concept of non-cell autonomous pathology of ALS: Insights into motoneuron axonopathy and astrogliosis". In: *Neurochemistry international* 61.4 (2012), pp. 523–530.
- [101] Chiara Di Malta et al. "Astrocyte dysfunction triggers neurodegeneration in a lysosomal storage disorder". In: *Proceedings of the National Academy of Sciences* 109.35 (2012), E2334–E2342.
- [102] Ludo Van Den Bosch and Wim Robberecht. "Crosstalk between astrocytes and motor neurons: what is the message?" In: *Experimental neurology* 211.1 (2008), pp. 1–6.
- [103] Bianca Marchetti et al. "Uncovering novel actors in astrocyte–neuron crosstalk in Parkinson's disease: the Wnt/ β -catenin signaling cascade as the common final pathway for neuroprotection and self-repair". In: *European Journal of Neuroscience* 37.10 (2013), pp. 1550–1563.
- [104] Pierre J Magistretti et al. "Neurotransmitters regulate energy metabolism in astrocytes: implications for the metabolic trafficking between neural cells". In: *Developmental neuroscience* 15.3-5 (1993), pp. 306–312.
- [105] Eric A Newman. "New roles for astrocytes: regulation of synaptic transmission". In: *Trends in neurosciences* 26.10 (2003), pp. 536–542.
- [106] Michael D Ehlers. "Synapse formation: astrocytes spout off". In: *Current Biology* 15.4 (2005), R134–R137.
- [107] Bruce R Ransom and Christopher B Ransom. "Astrocytes: multitasking stars of the central nervous system". In: *Astrocytes: Methods and Protocols* (2012), pp. 3–7.
- [108] Evangelina Avila-Muñoz and Clorinda Arias. "When astrocytes become harmful: functional and inflammatory responses that contribute to Alzheimer's disease". In: *Ageing research reviews* 18 (2014), pp. 29–40.
- [109] Marta Sidoryk-Wegrzynowicz et al. "Role of astrocytes in brain function and disease". In: *Toxicologic pathology* 39.1 (2011), pp. 115–123.
- [110] Phillip M Rappold and Kim Tieu. "Astrocytes and therapeutics for Parkinson's disease". In: *Neurotherapeutics* 7.4 (2010), pp. 413–423.

- [111] Giorgio Carmignoto, Lucia Pasti, and Tullio Pozzan. "On the role of voltage-dependent calcium channels in calcium signaling of astrocytes in situ". In: *Journal of Neuroscience* 18.12 (1998), pp. 4637–4645.
- [112] V Vedam-Mai et al. "Deep brain stimulation and the role of astrocytes". In: *Molecular psychiatry* 17.2 (2012), p. 124.
- [113] Sally Temple. "The development of neural stem cells". In: *Nature* 414.6859 (2001), p. 112.
- [114] Sally Temple. "Division and differentiation of isolated CNS blast cells in microculture". In: *Nature* 340.6233 (1989), pp. 471–473.
- [115] Brent A Reynolds, Samuel Weiss, et al. "Generation of neurons and astrocytes from isolated cells of the adult mammalian central nervous system". In: *science* 255.5052 (1992), pp. 1707–1710.
- [116] Ronald McKay. "Stem cells in the central nervous system". In: *Science* 276.5309 (1997), pp. 66–71.
- [117] Fred H Gage. "Mammalian neural stem cells". In: *Science* 287.5457 (2000), pp. 1433–1438.
- [118] Angela Gritti et al. "Multipotential stem cells from the adult mouse brain proliferate and self-renew in response to basic fibroblast growth factor". In: *Journal of Neuroscience* 16.3 (1996), pp. 1091–1100.
- [119] Chih-Huang Hung, Yi-Chen Li, and Tai-Horng Young. "Induction of neuronal differentiation of embryonic rat cortical neurospheres by nerve growth factor and fetal bovine serum on the nonadherent and adherent substrates". In: *Biomedical Engineering: Applications, Basis and Communications* 25.01 (2013), p. 1250053.
- [120] Hitomi Shirahama et al. "Precise tuning of facile one-pot gelatin methacryloyl (GelMA) synthesis". In: *Scientific reports* 6 (2016), p. 31036.
- [121] HD Soule et al. "A human cell line from a pleural effusion derived from a breast carcinoma 2". In: *Journal of the National Cancer Institute* 51.5 (1973), pp. 1409–1416.
- [122] RHS Westerink and AG Ewing. "The PC12 cell as model for neurosecretion". In: *Acta Physiologica* 192.2 (2008), pp. 273–285.
- [123] Kaberi P Das, Theresa M Freudenrich, and William R Mundy. "Assessment of PC12 cell differentiation and neurite growth: a comparison of morphological and neurochemical measures". In: *Neurotoxicology and teratology* 26.3 (2004), pp. 397–406.
- [124] Sebastian Schildge et al. "Isolation and culture of mouse cortical astrocytes". In: *Journal of visualized experiments: JoVE* 71 (2013).
- [125] Balázs V Varga et al. "Generation of diverse neuronal subtypes in cloned populations of stem-like cells". In: *BMC developmental biology* 8.1 (2008), p. 89.

- [126] Jingcheng Zhang et al. "Retinoic acid induces embryonic stem cell differentiation by altering both encoding RNA and microRNA expression". In: *PloS one* 10.7 (2015), e0132566.
- [127] Barbara Orsolits et al. "Retinoid machinery in distinct neural stem cell populations with different retinoid responsiveness". In: *Stem cells and development* 22.20 (2013), pp. 2777–2793.
- [128] Rachel Dreher and Binil Starly. "Biofabrication of Multimaterial Three-Dimensional Constructs Embedded With Patterned Alginate Strands Encapsulating PC12 Neural Cell Lines". In: *Journal of Nanotechnology in Engineering and Medicine* 6.2 (2015), p. 021004.
- [129] Eric A Appel et al. "Supramolecular polymeric hydrogels". In: *Chemical Society Reviews* 41.18 (2012), pp. 6195–6214.
- [130] Murat Guvendiren, Hoang D Lu, and Jason A Burdick. "Shear-thinning hydrogels for biomedical applications". In: *Soft matter* 8.2 (2012), pp. 260–272.
- [131] Jérôme Solon et al. "Fibroblast adaptation and stiffness matching to soft elastic substrates". In: *Biophysical journal* 93.12 (2007), pp. 4453–4461.
- [132] Yuhui Li et al. "An approach to quantifying 3D responses of cells to extreme strain". In: *Scientific reports* 6 (2016).
- [133] Edith Debroas, Carine Ali, and Dominique Duval. "Dexamethasone enhances glutamine synthetase activity and reduces N-methyl-D-aspartate neurotoxicity in mixed cultures of neurons and astrocytes". In: (2015).